EXCHANGE FORCES IN TRANSITION-METAL BONDING

Thesis by

Marvin Mark Goodgame

In Partial Fulfillment of the Requirements

for the Degree of

Doctor of Philosophy

California Institute of Technology

Pasadena, California

1984

(Submitted November 21, 1983)

ACKNOWLEDGMENTS

My time at Caltech has been a most rewarding experience. I am grateful for having had the opportunity to interact with so many quality people, and I shall always cherish the friendships that I have made here.

I thank Bill Goddard for his scientific guidance and support which helped me complete a very challenging research project.

Financial support from the National Science Foundation and the California Institute of Technology is gratefully acknowledged.

I thank all the members of the Goddard group for their friendship and scientific interaction. I am particularly grateful for having known Art Voter, Janet Allison, and Mark Brusich.

Finally, I thank my family for their support, encouragement, and love.

ABSTRACT

We have examined multiple bonds (σ, π, and δ) to transition metals and find that intra-atomic exchange forces on these metals are crucial for correct prediction of ground states and that a proper description of these terms is required for a quantitative understanding of bond energies.

Our calculations on models for bridged Fe porphyrin dimers show that intra-atomic exchange forces on the Fe's are critical to the explanation for the dramatic differences in the Fe-Fe coupling for μ-oxo and μ-nitrido bridged Fe porphyrin dimers. The qualitative bonding concepts obtained are used to predict properties of the μ-carbido bridged Fe porphyrin dimer.

In most cases, the interactions responsible for bonding lead to antiferromagnetic coupling between the d orbitals localized on adjacent centers, resulting in overall low-spin couplings. However, some extended metal systems (eg. metallic Ni) lead to net ferromagnetic interactions between d orbitals localized on different centers. In order to elucidate these effects, we have examined the direct and indirect $d-d$ couplings in the Ni_4 cluster as a function of bond distance. We find that ferromagnetic coupling dominates in a region of bond distance around the bulk Ni value of 2.5 Å with antiferromagnetic coupling dominating for short R (by 2.0 Å) and for long R (by 3.5 Å). The dominant interactions responsible for ferromagnetic coupling involve spin polarization of the conduction band (s-like), supporting a model for ferromagnetism in bulk metallic systems very similar to the Ruderman-Kittel model for magnetic impurities.

The dimers Cr_2 and Mo_2 provide the most dramatic illustration of the importance of exchange forces in bonding. With six unpaired

electrons on each atom, there is the potential for up to *six* covalent bonds. However, formation of $d-d$ covalent bonds requires a concomitant loss in intra-atomic $d-d$ exchange energy. The net result is a double well where the long-R minimum (3 Å) is dominated by $s-s$ pairing (no loss of intra-atomic $d-d$ terms) while the short-R minimum (1.7 to 1.9 Å) involves a strong quintuple bond of d orbitals plus an antibonding $s-s$ interaction. To properly handle the intra-atomic exchange terms during this transition from long R with local high-spin coupling to small R with dominant singlet pairing within bonding pairs presents a formidable challenge to *ab initio* computation. To carry out such studies, we have extended the GVB and related approaches of *ab initio* calculations and have also developed a simple approximate method of including the electron correlation missing in GVB wavefunctions that provides a quantitatively accurate description of these systems.

The effects studied here should be of comparable importance for multiple bonds involving transition metals, lanthanides, and actinides bonding to each other and to such ligands as CR_2, CR, O, N, and NR. Correlation terms beyond GVB are most important for the least electronegative ligands. Thus, the proper treatment of intra-atomic exchange and of interatomic $d-d$ coupling should be of considerable importance in studies of heterogeneous and homogeneous catalytic systems.

TABLE OF CONTENTS

Page

Introduction to Thesis

In this thesis, we examine several different chemical systems in which exchange forces are important. Each system involves a significant theoretical challenge. Even a qualitative understanding requires that we allow the unpaired d orbitals on an atom to be high-spin coupled (since this is optimal for the free atom). However, to describe the bond pairing of d orbitals on different atoms requires that we allow also low-spin coupling of orbitals on different centers. Thus, for an unbiased treatment of bonding, we must optimize the spin-coupling when solving for the various wavefunctions. For example, with two Mo atoms in the s^1d^5 ground state, there are 132 possible spin couplings corresponding to an overall singlet state! When I initially attacked these problems, our computer codes could treat the coupling of only six electrons (leading to five possible spin couplings for the singlet). In order to tackle the problems of interest, I developed a new series of algorithms and codes which allow the spin couplings of an arbitrary number of electrons to be treated (see Appendix A).

After developing the ability to fully optimize the spin coupling of our systems, we found that it was not accurate to use the orbitals from a GVB-PP calculation (our usual approach to calculating optimal orbitals), rather it is necessary to optimize the orbitals while simultaneously calculating the optimal spin coupling. In this, we made use of the recently developed general MCSCF program (GVB3) which allows one to optimize the orbitals for an arbitrary CI wavefunction. However, for the systems of interest, the data required to tell the program how to do this are prohibitively complicated to construct manually. Consequently, I developed programs (see Appendix B) to generate energy expressions (the data needed by GVB3) for wavefunctions having optimal spin coupling for any number

of electrons. Unfortunately, for cases with more than 250 configurations, these energy expressions were too lengthy for use in our MCSCF program (GVB3). Consequently, I developed a new series of programs (see Appendix C) to generate density matrices for these wavefunctions. This resulted in an efficient procedure for optimizing the orbitals for very complicated wavefunctions having up to 30,000 configurations and made the studies in this thesis possible.

This persistent attack on the theoretically challenging problem of metal-metal multiple bonds has resulted in significant advances in state-of-the-art *ab initio* methods of electronic structure theory. These advances are also proving useful for examining other systems in which the spin coupling among the valence electrons deviates significantly from perfect-pairing.

With these methods, we have been able to examine such systems as Cr_2 and Mo_2 in the limit where all possible ways to couple the s^1d^5 state of the atoms are optimized self-consistently in the molecule. At this level of description, we obtain excellent agreement with spectroscopic results on Mo_2 (R_e=1.93 Å and ω_e=477 cm^{-1} versus our values R_e=1.97 Å and ω_e=455 cm^{-1}) but very serious errors for Cr_2 (R_e=1.68 Å and ω_e=470 cm^{-1} versus our values R_e=3.06 Å and ω_e=110 cm^{-1}). Since the correlation terms included here would have been quite adequate for accurate treatment of bonds between non transition-metal atoms, we examined closely the electron correlation terms omitted in the current studies. The result is a simple procedure for correcting GVB wavefunctions based entirely upon correlation errors in the atoms. For such test systems as H_2 and N_2, this results in quantitatively accurate potential curves. For Cr_2, these calculations lead to the prediction of a *double well* in the ground-state

potential curve with the inner minimum at 1.63 Å (observed at 1.68 Å) and the outer minimum at 3.0 Å (as found in the uncorrelated results). This method of atomic correlation correction (GVB-ACC) provides the promise of quantitative accuracy from simple (GVB) wavefunctions and hence may be of quite general utility.

CHAPTER 1

Electronic States of Porphyrin Dimers

I. Introduction

The oxidation and spin states of the irons in $(FeTPP)_2N$ are experimentally ambiguous, despite numerous physical measurements, and seem to differ markedly from the properties of $(FeTPP)_2O$, a well characterized dimer. In order to obtain a qualitative understanding of the bonding in $(FeTPP)_2N$ and of why it differs so markedly from that of $(FeTPP)_2O$, I have examined both bridged porphyrin dimers using accurate *ab initio* wavefunctions on simple models, $[\ Fe{-}N{-}Fe\ ]^{4+}$ and $[\ Fe{-}O{-}Fe\ ]^{4+}$, with appropriate restrictions on electronic occupations to account for the ligand field effects of the porphyrins. The electronic description of the bonding which emerges provides a good quantitative description of the magnetic interactions in these dimers. Our simple model does not provide a precise description of the charge transfer in the real porphyrin dimers; however, it allows us to assign electronic configurations based on comparison to experimental properties and leads to a qualitative description of the bonding. The qualitative ideas obtained from these studies were used to predict the nature of the bonding in the dimer $(FeTPP)_2C$.

II. Summary of Results

A. Qualitative Description of Bonding

Ground-state Fe atom has the valence electron configuration $3d^6 4s^2$ with net spin $S=2$. In a ferrous Fe-heme complex,

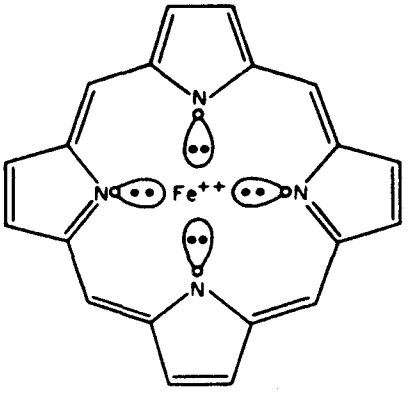

the $d_{x^2-y^2}$ orbital is greatly destabilized (due to overlap with the N lone pairs) while the d_{z^2} orbital is slightly destabilized. The remaining three orbitals (d_{xy}, d_{xz}, d_{yz}) have similar energy (with d_{xz} and d_{yz} degenerate). In denoting the orbital occupations of these states, we shall use a qualitative energy diagram of the form

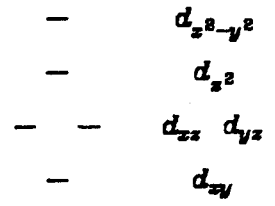

and dispense with the labels. The two lowest wavefunctions ($S=2$) are

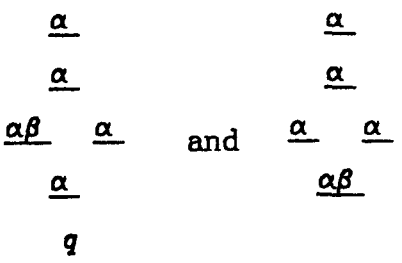

The left form is lower than the right and is also most favorable for bonding to various ligands. Consequently, we will discuss only this high-spin wavefunction (denoted q).

For the atom, intermediate- and low-spin wavefunctions such as

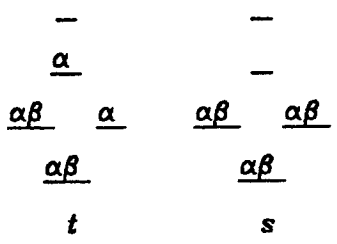

would be much higher than q (83 kcal for t and 113 kcal for s). However, the destabilization of $d_{x^2-y^2}$ and of d_{z^2} by the heme ameliorates these difficulties, leading to the spectrum (total energies)

$Fe^{II}s$	43
$Fe^{II}t$	13
$Fe^{II}q$	0

The factors dominating these energy differences are

	LIGAND FIELD	ATOMIC EXCHANGE	NET EXCITATION ENERGY
s	0	0	0
t	0	-30	-30
q	70	-113	-43

Thus, the ligand field factors strongly favor low spin, and high-spin configurations remain the ground states only because of the large exchange energies associated with high-spin coupling.

Covalent spin pairing of the d orbitals with open-shell orbitals on N and O ligands leads to a decrease in the atomic exchange terms and hence can lead to a change in the effective atomic spin configuration in the molecule. Thus, we will find that covalent interactions with bonding ligands can rearrange these levels so that q, t, and s are all candidates for the ground state in bridged dimers.

Similar considerations for Fe^{III} lead to three spatial configurations

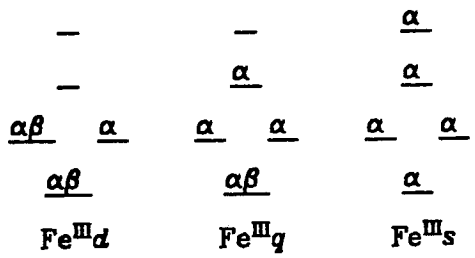

corresponding to low spin (S=1/2), intermediate spin (S=3/2), and high spin (S=5/2), respectively. Here the atomic separations are large

$Fe^{III}d$	191
$Fe^{III}q$	118
$Fe^{III}s$	0

Summarizing, in a ferrous Fe-heme complex, there are three configurations of the d electrons to consider:

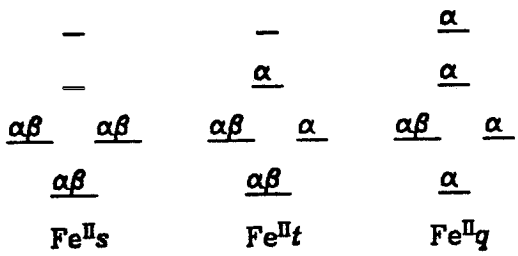

These all involve six electrons in d orbitals but differ in the net spin (S=0 for s, S=1 for t, and S=2 for q). Although these different states have atomic energies separated by up to 113 kcal, the ligand field effects due to the porphyrin put all these within 43 kcal. These same ligand field effects destabilize most other configurations for the Fe.

When the complex is oxidized, one of the two Fe's is ferric Fe which has three basic possibilities:

$\underline{\quad}$	$\underline{\quad}$	$\underline{\alpha}$
$\underline{\quad}$	$\underline{\alpha}$	$\underline{\alpha}$
$\underline{\alpha\beta}$ $\underline{\alpha}$	$\underline{\alpha}$ $\underline{\alpha}$	$\underline{\alpha}$ $\underline{\alpha}$
$\underline{\alpha\beta}$	$\underline{\alpha\beta}$	$\underline{\alpha}$
$Fe^{III}d$	$Fe^{III}q$	$Fe^{III}s$

We have considered dimers with the bridging atoms N and O. The structure of the dimer depends on pairing of the bridging atom with the two Fe atoms and can modify the relative positions of the s, t, q or d, q, s states. These effects of the bridging ligand should be thought of as spin coupling effects rather than as ligand field effects. The ground state of O atom has the configuration $2p^4$:

$$\underline{\alpha\beta} \quad \underline{\alpha} \quad \underline{\alpha}$$

O anion is

$$\underline{\alpha\beta} \quad \underline{\alpha\beta} \quad \underline{\alpha}$$

The ground state of N atom is $2p^3$:

$$\underline{\alpha} \quad \underline{\alpha} \quad \underline{\alpha}$$

while the N anion

$$\underline{\alpha\beta} \quad \underline{\alpha} \quad \underline{\alpha}$$

is not stable.

We have examined two possible coupling schemes for the case of two Fe-hemes bridged by a nitrogen atom. Assuming both Fe's to be high-spin, qq (the highest d orbital on each Fe is occupied), we find that the best state has the form

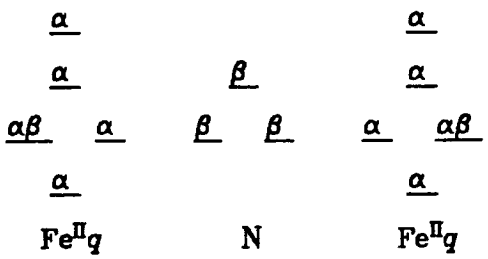

This diagram is to be interpreted as follows: There are three electrons in z orbitals: the left Fe has d_{z^2} with α spin, the right Fe has d_{z^2} with α spin, while the central N has p_z with β spin. Thus, there is spin pairing (bonding) of the N p_z with both Fe d_{z^2} orbitals, a three-center three-electron σ-bond. There are four electrons in x orbitals: the left Fe has two electrons in d_{xz} (with both α and β spins), while the right Fe has one electron in d_{xz} (α spin), and the N has one electron in p_x (β spin). The β-α spins on the two singly-occupied x orbitals indicate a two-electron π_x-bond between N and the right Fe. A similar situation prevails for the y orbitals, except that the π_y-bond is between the N and the left Fe. Because of the bonding effects, the spins of the two Fe's should each be opposite that of the N, and hence the Fe spins should be parallel. The result is that the d_{xy} and $d_{x^2-y^2}$ orbitals (δ-like with respect to the Fe-N-Fe axis) are coupled with their spins parallel, leading to a net $S=5/2$ state. This coupling is indirect, since the coupling results from intraatomic exchange to other Fe orbitals (σ and π) whose spins are coupled via the N. The net bonding is a three-electron three-center σ-bond plus two N-Fe π-bonds. The wavefunction shown is one of two equivalent resonance configurations. Assuming the Fe's are lower spin (the highest d orbital on each Fe is empty), the best state is tt:

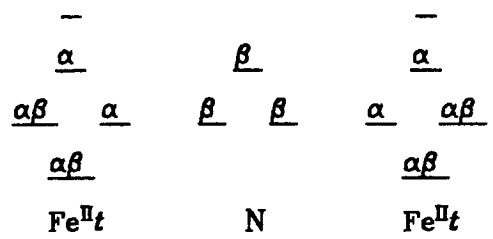

Here, there is a π_x-bond to the right, a π_y-bond to the left, plus a three-electron σ-bond (all just as in qq). However, the two low-lying (Fe-N-Fe) δ orbitals are each doubly-occupied, leading to a net $S=1/2$ state. Again, there are two resonance configurations.

The two states $Fe^{II}q-N-Fe^{II}q$ and $Fe^{II}t-N-Fe^{II}t$ each have two π-bonds plus a Fe-N-Fe three-electron σ-bond. Thus, since q is better than t, one might expect for $Fe^{II}q-N-Fe^{II}q$ to be the lower state. However, this ignores the changes in intraatomic exchange energies that necessarily accompany interatomic spin pairing (bonding). This is illustrated below:

	ENERGY CHANGES			
	INTRINSIC BOND ENERGY ($\sigma+2\pi$)	EXCITATION OF ISOLATED HEMES	CHANGE IN INTRAATOMIC EXCHANGE ENERGY	NET CHANGE IN ENERGY
$Fe^{II}q-N-Fe^{II}q$	-100	0	88	-12
$Fe^{II}t-N-Fe^{II}t$	-100	2×13	22	-42

Thus, even though the qq state is stable by 26 kcal with respect to tt for the separated dimer, the N-bridged dimer is expected to be t-N-t. This is because the spin pairing of three Fe d electrons with the three unpaired N p orbitals leads to a loss of 88 kcal of exchange for qq but only a 22 kcal loss for tt.

Similar considerations apply also to O, but the result is quite different. Assuming the tt state (with the highest d-orbital on each Fe empty), which we find to be optimal for the nitrogen bridge, we obtain

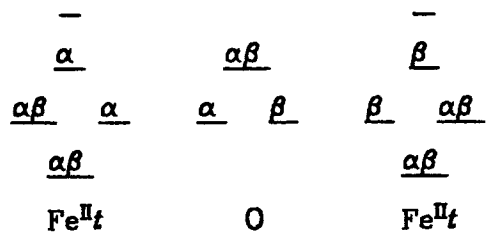

On the other hand, assuming the Fe's are high-spin, qq (highest d occupied), we find equivalent Fe's with resonance configurations like

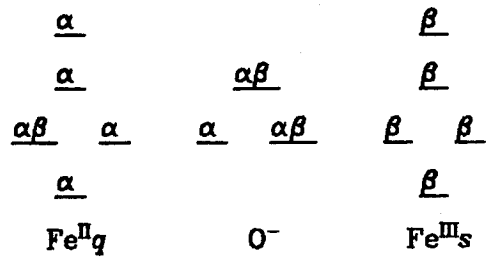

Our calculations show that the ground state of oxygen-bridged Fe-hemes is this [$q\,O^{-}s$] configuration. Unlike the nitrogen bridge, oxygen accepts an extra electron, and the Fe's are high-spin.

B. Charge Distribution and Spin Coupling

The dimer $(FeTPP)_2O$ has been well characterized experimentally and has usually been described as IIIs–O^{-2}–IIIs

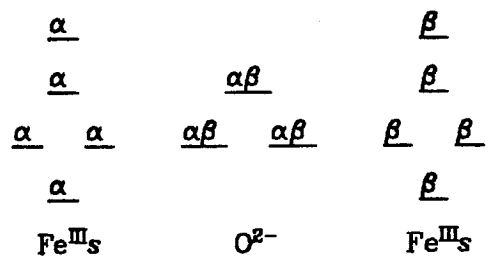

Our electronic structure [$q\,O^{-}s$] for this dimer is consistent with high-spin Fe's (highest d occupied). We also find two sets of five high-spin electrons coupled antiferromagnetically; however, one of the high-spin electrons is on the oxygen!

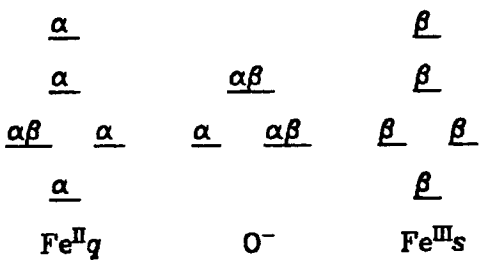

Thus, we conclude that the O-bridged Fe dimer usually formulated as $s O^{2-} s$ should instead be formulated as $[q O^{-} s]$.

The dimer $(FeTPP)_2N$ contains the only known μ-nitrido bridge between two first-row transition metals. Experiments have resulted in disagreement about the oxidation and spin states of the Fe's.[1-4] Currently, both Fe's are thought to be Fe^{III}. Some experiments indicate high-spin Fe's

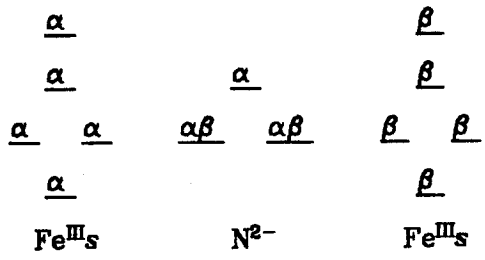

while other experiments indicate lower-spin Fe's, e.g.,

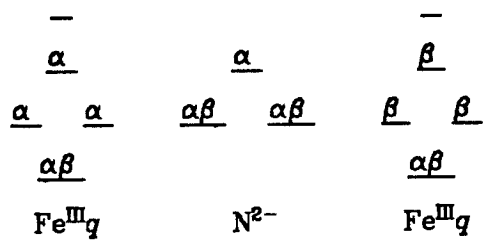

Our results indicate that the Fe's of this dimer are indeed lower-spin; however, we find that each Fe is best described as Fe^{II}, not Fe^{III}:

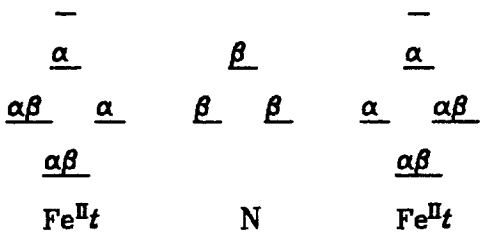

Although the coupling of the Fe's has been considered as strongly antiferromagnetic, we find that they are actually coupled ferromagnetically. However, the spin pairing with the N orbitals leads to a net singlet state.

C. High- Spin versus Lower- Spin Irons

In order to understand why the μ-oxo dimer has high-spin Fe's while the μ-nitrido dimer has lower-spin Fe's, we must understand the effects of spin pairing to open-shell ligands. Ligand field and crystal field arguments generally suppose closed-shell ligands, so that the effects on the metal can be described in terms of stabilization or destabilization of each metal orbital (indicated by the vertical ordering in the above diagrams). However, if there are singly-occupied orbitals on the ligands which spin pair to singly-occupied *d* orbitals on the metal, there can also be changes in the intraatomic exchange energy on the metal. Thus, for an atom with several high-spin electrons, bonds to that atom must lead to a loss in atomic exchange energies. The more high-spin electrons the atom has, the larger this effect of weakening the bond.

Consider first the μ-nitrido complex. The ground state of a four-coordinate Fe^{II}-heme is high-spin (q), but this state leads to weaker bonds than would the (excited) lower-spin states. Whether the ground-state configuration for Fe's in the μ-nitrido complex are high-spin or lower-spin depends on whether the increase in bond strength for the lower-spin states can make up for the excitation energy from the (ground) high-spin

states. Our calculations show that both Fe's are in excited, lower-spin states. Thus, the stronger bonds more than compensate for the excitation energy of both Fe's.

Let us now consider the magnitude of the exchange forces in the μ-nitrido dimer. Nitrogen can form three bonds, but to do so, it must lose 27 kcal ($\frac{3}{2}K_{pp}$) of exchange energy. If both Fe's are in the ground high-spin state, they must lose 88 kcal ($4K_{dd}$) of exchange energy to make three bonds to the nitrogen. If we excite one of the Fe's to a lower-spin state (a penalty of 13 kcal), the Fe's must lose only 44 kcal ($2K_{dd}$) to make the same bonds. If both Fe's are promoted to the excited state (costing 26 kcal), the Fe's need sacrifice only 22 kcal ($1K_{dd}$). Thus, assuming the same three bonds for each case, we find that the lowest energy is obtained when both Fe's are in excited lower-spin states.

Table 1. Estimated Full-Bond Spectrum (kcal) for Fe^{II} N Fe^{II}

Structure	Fe Excitation	Fe Exchange Loss	Total Energy Loss
$Fe^{II}t{=}N{-}Fe^{II}t$	26	22	48
$Fe^{II}t{=}N{-}Fe^{II}q$	13	44	57
$Fe^{II}q{=}N{-}Fe^{II}q$	0	88	88

The relative energies estimated above are not quantitative, because we assumed that bonds would be formed regardless of how much exchange energy must be lost. However, the system could choose not to make bonds and thus not have to sacrifice exchange energy. This extreme would result in relative energies approximately given by the excitation energies of the Fe's. The other extreme of making full bonds results in such a large loss of exchange energy that the order of states is

reversed. In the actual dimer, each state reaches a compromise by making partial bonds which require only a partial loss of exchange. The order of states depends on the compromise bond strengths. No matter what compromise is reached for each state, the Fe-N bonds are strongest when both Fe's are in excited lower-spin states, intermediate strength when only one Fe is excited, and weakest when neither Fe is excited. Our calculations show that the differential bond strength is large enough that both Fe's are excited in the ground state dimer.

Consider now the μ-oxo dimer. Our calculations indicate that both Fe's are in the ground high-spin state. Thus, the stronger bonds of the excited lower-spin state do not compensate for the excitation energy. The oxygen atom can make only two bonds, whereas nitrogen can make three. Perhaps the smaller bonding capacity of the μ-oxo group explains why the bonds of the excited lower-spin Fe's are not strong enough to stabilize this state relative to ground high-spin Fe's. Another important factor in the stability of the μ-oxo dimer with high-spin Fe's is that the oxygen is willing to accept an electron from the Fe's, allowing an Fe ferric center having five singly-occupied orbitals, with the concomitant large increase in exchange energy stabilization.

Let us now assume the μ-oxo dimer makes a full bond to each Fe. Oxygen can form two bonds at the expense of 11 kcal ($\frac{1}{2}K_{pp}$) exchange energy. If both Fe's are in the ground state, they must lose 66 kcal ($3K_{dd}$) to bond to the oxygen. If one Fe is excited, the Fe exchange loss is 44 kcal ($2K_{dd}$), and if both Fe's are excited, the exchange loss is 22 kcal ($1K_{dd}$).

Table 2. Estimated Full-Bond Spectrum (kcal) for Fe^{II} O Fe^{II}			
Structure	Fe Excitation	Fe Exchange Loss	Total Energy Loss
$Fe^{II}t$–O–$Fe^{II}t$	26	22	48
$Fe^{II}t$–O–$Fe^{II}q$	13	44	57
$Fe^{II}q$–O–$Fe^{II}q$	0	66	66

Our calculations show that the μ-oxo bond strengths are too small to yield the above predictions. In fact, we find that the ground state dimer chooses to be bridged by O^-, which can make only one bond. Counting exchange terms, we predict that it is more difficult to oxidize $Fe^{II}t$ to $Fe^{III}q$ than to oxidize $Fe^{II}q$ to $Fe^{III}s$ by 22 kcal ($1K_{dd}$). If $Fe^{II}t$ is making full bonds (such that the spins of the two open shells are randomly oriented), it is 44 kcal ($2K_{dd}$) more difficult to oxidize $Fe^{II}t$ than $Fe^{II}q$. Our calculations show that the μ-oxo group does oxidize $Fe^{II}q$ but not $Fe^{II}t$. The ability of the μ-oxo group to accept an extra electron adds to the stability of the ground state of μ-oxo dimer with high-spin Fe's because of the additional exchange stabilization of ionic configurations for high-spin Fe's relative to lower-spin Fe's.

Let us now consider the best ionic configurations with O^- which result from the possible combinations of high-spin and lower-spin Fe's. If both Fe's are high-spin, then the oxidation of one of the Fe's will break the Fe-O bond to the other Fe. The remaining Fe-O bond requires no exchange loss from O^-, but the oxidized Fe must lose 44 kcal ($2K_{dd}$) to make the bond. If one Fe is lower-spin, then the high-spin Fe will oxidize to break the Fe-O bond to the lower-spin Fe. This state is higher by the excitation energy (13 kcal) to the lower-spin Fe. Note that if the lower-spin Fe were to oxidize and break the Fe-O bond to the high-spin Fe, the

oxidized lower-spin bond must lose only 22 kcal ($1K_{dd}$) to make the bond. However, it is at least 22 kcal ($1K_{dd}$) more difficult to oxidize $Fe^{II}t$ to $Fe^{III}q$ than to oxidize $Fe^{II}q$ to $Fe^{III}s$. Thus, the high-spin Fe will oxidize. If both Fe's are lower-spin, then the oxidation of one of the Fe's will break the Fe-O bond to the other Fe. The remaining Fe-O bond requires only 22 kcal ($1K_{dd}$) exchange loss on the oxidized Fe. The excitation energy for this state includes the 13 kcal for exciting each Fe to lower-spin plus the additional exchange loss of at least 22 kcal ($1K_{dd}$) for oxidizing a lower-spin relative to a high-spin Fe.

Table 3. Estimated Full-Bond Spectrum (kcal) for Fe^{II} O^- Fe^{III}

Structure	Fe Excitation	Fe Exchange Loss	Total Energy Loss
$Fe^{II}t$ O^-–$Fe^{III}q$	26+22	22	70
$Fe^{II}t$ O^-–$Fe^{III}s$	13	44	57
$Fe^{II}q$ O^-–$Fe^{III}s$	0	44	44

Thus, we see that strong bonding cannot stabilize excited-state Fe's. Both Fe's must be high-spin.

III. Calculational Details

A. The Model

Our model is the simplest possessing the features required in a qualitative picture of the bonding in bridged porphyrin dimers. For both $(FeTPP)_2O$ and $(FeTPP)_2N$, the symmetry is approximately D_{4d}. We remove the porphyrins, leaving only the $[\ Fe{-}O{-}Fe\ ]^{4+}$ and $[\ Fe{-}N{-}Fe\ ]^{4+}$ units to be included explicitly. However, the orbital occupations are restricted in such a way as to account for the effects of the porphyrins.

The main effect the porphyrin ligand has on Fe^{2+} is to break the five-fold degeneracy of the d orbitals (only the d_π degeneracy remains). The biggest ligand field effect is to destabilize one of the two d_δ orbitals ($d_{x^2-y^2}$). We include this effect by considering only the specific electronic configurations that would be allowed in the full porphyrin dimer. Since each state has a fixed number of electrons of each orbital type, ligand-field energy corrections are simple to apply.

a. Symmetry Considerations

Before proceeding, we must consider a complication arising from the difference in symmetry between the prophyrin dimer and our model. Our model leads to $D_{\infty h}$ symmetry; however, the real system will have D_{4h} for the eclipsed dimer and D_{4d} for the staggered dimer. In the case of D_{4h}, there is no problem, because each orbital symmetry of $D_{\infty h}$ maps into a separate symmetry in D_{4h}. The orbital symmetries correlate as follows:

$D_{\infty h}$	D_{4h}
σ_g^+	a_{1g}
σ_u^+	a_{2u}
π_g^+	e_g^+
π_u^+	e_u^+
π_g^-	e_g^-
π_u^-	e_u^-
δ_g^+	b_{1g}
δ_u^+	b_{2u}
δ_g^-	b_{2g}
δ_u^-	b_{1u}

However, for D_{4d}, there is a problem. The following table shows how the orbital symmetries correlate:

$D_{\infty h}$	D_{4d}	Couplings
σ_g^+	a_1	
σ_u^+	b_2	
π_g^+	e_3^+	
π_u^+	e_1^+	
π_g^-	e_3^-	
π_u^-	e_1^-	
δ_g^+	e_2^+	←┐
δ_u^+	e_2^+	←┘
δ_g^-	e_2^-	←┐
δ_u^-	e_2^-	←┘

where the superscript + or - indicates the parity of reflection in the xz plane of D_{4d}. The important point to notice here is that the ligand field of

the two porphyrins allows the mixing of orbitals δ_g^+ with δ_u^+ and of δ_g^- with δ_u^-.

With two high-spin Fe's, each Fe has two singly-occupied δ-orbitals, leading to two δ-bonds. The D_{4d} ligand field of the two porphyrins destabilizes one of the δ-orbitals in each δ-bond. This can cause some transfer of charge from the destabilized orbital in each bond, resulting in one δ-bond partially localized on the left Fe and the other δ-bond partially localized on the right. In the case that the δ-bonds are fully localized, each Fe has one doubly-occupied and one empty δ-orbital, so that the system has converted the two high-spin Fe's into lower-spin Fe's. Electronic configurations with symmetric δ-bonds (high-spin Fe's) should not interact strongly with configurations having fully localized δ-bonds (lower-spin Fe's). Thus, we expect the states of a porphyrin dimer to have either nearly symmetric or fully localized δ-bonds.

In our model, we can calculate a state with two high-spin Fe's very cleanly. In the absence of the porphyrins, our δ-bonds are perfectly symmetric, so we can use δ_g and δ_u orbitals. However, a state with two lower-spin Fe's cannot be obtained straightforwardly, because we do not have the ligand field of the porphyrins to keep the δ-bonds localized. To solve this problem, we have chosen to put all four electrons in one δ-space, leaving the other δ-space empty. This is equivalent to rotating the porphyrins to an eclipsed configuration, resulting in D_{4h} symmetry. This change results in slightly more repulsion between the δ-electrons on opposite Fe's; however, all other interactions in our model are left invariant. The σ- and π-orbitals cannot distinguish between the D_{4d} and D_{4h} fields.

b. Spin States

Our wavefunctions have Fe's which are very cleanly either high-spin or lower-spin. To compare states of a dimer having Fe's with different spins, we must determine the relative ligand-field stabilization energy for each type of Fe. To do this, we calculate the energy of an isolated Fe ion having each d-configuration. Knowing the relative energies of the corresponding Fe-heme states, we can determine the relative stabilization energy for placing each type of Fe ion in a heme. This is only a one-center correction at each Fe. Thus, it cannot be used to compare dimers with different bridging ligands or even to compare the same dimer at different geometries. However, it is sufficient to correct the energies of different states of the same dimer at the same geometry, and this is all we need to determine the ground state of each dimer.

Let us now consider how our model should differ from the full system with porphyrins included. Adding the negatively charged porphyrin ligands around the Fe's would modify the electronic charge distribution, making the bridging ligands more negative. Since the porphyrins partially neutralize the Fe's, the d-orbitals should become larger. This would make d–d exchange integrals smaller and make d-bonds stronger. Thus, adding the porphyrins would have a tendency to favor lower-spin versus high-spin Fe's. Recall too that our model has a slight bias against lower-spin Fe's because we treat their δ-electrons as if the porphyrins were eclipsed. However, the dominant effect is probably that the porphyrins would promote oxidation of the Fe's. Exchange forces make high-spin Fe's more easily oxidized than lower-spin Fe's. Thus, the net effect of adding the porphyrins would be to favor high-spin Fe's.

B. Geometries

Our geometries are based upon crystal structures for $(FeTPP)_2O$[5] and $(FeTPP)_2N$.[2] The Fe-O bond length is 1.763 Å, while the Fe-N bond length is 1.661 Å. We have calculated both systems as linear, though the crystal structure for $(FeTPP)_2O$ has an Fe-O-Fe angle of 174.5°. The crystal structure for $(FeTPP)_2N$ has a linear Fe-N-Fe bridge.

One interesting question about the geometry of these systems is why the Fe-N-Fe bridge is linear while the Fe-O-Fe bridge is slightly bent. This difference has been rationalized with Walsh diagrams;[6] however, the prediction is not unambiguous, requiring assumptions about relative energetics. The same analysis for a nitrogen bridge could also lead to a bent geometry (depending on assumptions about relative energetics). Thus, this simple MO analysis does not lead to a qualitative prediction of geometry.

One way to rationalize a linear Fe-N-Fe bridge would be if the nitrogen made double bonds to each Fe. Although explaining the linear bond (N^+ orbitals the same as in diazomethane or as the C in CO_2), this would require transferring an electron from the nitrogen $2p_\sigma$ to an iron $3d_\delta$! However, the result would be a spin distribution inconsistent with experiment, and hence we conclude that the linearity of the Fe-N-Fe bridge requires new quantitative and qualitative theoretical investigation.

Another interesting geometrical question is why the nitrido bridge is symmetric, i.e. equal Fe-N bond lengths. Numerous asymmetrical as well as symmetrical M-N-M bridges exist. The factors responsible for the formation of a symmetrical vs. asymmetrical bridge are not understood.

Related to the question of a symmetric nitrido bridge is the very existence of the bridge. Why is this the only known example of a nitrido

bridge between two first-row transition metals?

Geometric parameters from crystal structures of $(FeTPP)_2O$ and $(FeTPP)_2N$ indicate the forces on the atoms of the Fe-O-Fe and Fe-N-Fe bridges. For both the oxygen and the nitrogen bridge, each iron is displaced from the mean plane of the porphinato nitrogens toward the bridging ligand. The bridging ligand obviously exerts an attractive force on each iron. Why is each iron pulled out of the heme? For the nitrogen bridge, the porphyrins are too far apart to repel each other significantly. Nonbonded repulsions between the bridging nitrogen and the porphinato nitrogens must be responsible for the irons being pulled out of the hemes. For the oxygen bridge, the porphyrins are even farther apart. Nonbonded repulsions between the bridging oxygen and the porphinato nitrogens must be pulling the irons out of the hemes.

The nitrogen bridge is found to exert more force on the irons than the oxygen bridge exerts. This is predicted by the capacity of nitrogen to make more bonds than oxygen. This is supported by the smaller distance observed between the bridging nitrogen and each iron than between the bridging oxygen and each iron. However, why the oxygen ligand pulls each iron 0.50 Å out of the mean plane of the porphinato nitrogens while the stronger nitrogen ligand pulls each iron only 0.32 Å out of the plane has heretofore not been explained.

Our results show that the irons of the μ-oxo dimer are different from the irons of the μ-nitrido dimer. We find that the δ-orbital pointed toward the porphinato nitrogens is singly-occupied in each iron of the μ-oxo dimer but empty in each iron of the μ-nitrido dimer. When this orbital is occupied, the iron is easier to pull out of the heme plane. Thus, the weaker oxygen bridge can pull each of its high-spin irons 0.50 Å out of the

plane, but the stronger nitrogen bridge can pull each of its lower-spin irons only 0.32 Å out of the plane. Structural evidence for our theoretical electronic structures includes the hole size of each porphyrin. The width of the mean plane of porphinato nitrogens is larger in the μ-oxo dimer than in the μ-nitrido dimer. This difference in hole size is due to the occupation of the iron δ-orbital pointed toward the porphinato nitrogens. When this orbital is occupied, the porphyrin hole expands.

It is interesting to note that the structural data for $(FeTPP)_2N$ have been considered inconclusive regarding the character of each iron. Confusion has arisen because the porphyrin hole size and out-of-plane displacement of the iron in $(FeTPP)_2N$ are consistent with both low-spin d^5 and high-spin d^4 configurations. Thus, whether the irons in $(FeTPP)_2N$ are high-spin or low-spin has been considered unanswered from structural data. Notice that the consistent d-configurations each have the δ-orbital pointed toward the porphinato nitrogens empty. We find that the occupation of this orbital is a dominant factor in determining hole size and out-of-plane displacement. The structural data for $(FeTPP)_2N$ clearly indicate that this orbital is empty in each iron.

C. Wavefunctions

a. Basis Sets

The Ar core of each Fe atom is replaced by an *ab initio* effective potential. The basis is constructed from the Wachters Fe basis.[7] Of the 14 s gaussians, 10 core functions are removed, and the remaining four valence s primitives are contracted DZ (3,1). All p functions are eliminated, but a single p gaussian (ζ=0.1) is added to allow polarization of the valence s-space. The five d gaussians are contracted DZ (4,1). Each

Fe basis is $(4s\,1p\,5d\,/\,2s\,1p\,2d)$.

Each bridging ligand, N and O, is described with Dunning's $(3s\,2p)$ contraction of Huzinaga's $(9s\,5p)$ basis set.[8] To allow the bridging ligand to become negatively charged, we also add negative ion functions. To N, we add a diffuse s gaussian (ζ=.066) and a diffuse p gaussian (ζ=.045). To O, we also add a diffuse s gaussian (ζ=.088) and a diffuse p gaussian (ζ=.060). Each bridging ligand basis is $(10s\,6p\,/\,4s\,3p)$.

b. Symmetries

Each dimer model, Fe-N-Fe and Fe-O-Fe, has a total of 47 contracted Cartesian gaussian functions. For $[Fe{-}N{-}Fe]^{4+}$, 19 electrons are explicitly included (six from each Fe^{2+} and seven from N). For $[Fe{-}O{-}Fe]^{4+}$, 20 electrons are explicitly included. In all cases, the $1s$ and $2s$ core electrons of the bridging ligand are uncorrelated but solved for self-consistently. All wavefunctions have at least D_{4h} symmetry, and symmetry orbitals are used in the MCSCF. The configurations in each MCSCF include all symmetry-allowed (D_{2h}) products of full CI's in each symmetry. In all cases, each π-space has four electrons in three orbitals. For two high-spin irons, each δ-space has two electrons in two orbitals. For two lower-spin irons, one δ-space has four electrons in two orbitals, and the other δ-space is empty. For the nitrogen ligand, the σ-space has three electrons in three orbitals. For the oxygen ligand, the σ-space has four electrons in three orbitals.

The completeness of our wavefunctions can be seen from the lower states.

Table 4. $Fe^{II}q$–N–$Fe^{II}q$ Wavefunctions		
Spin S	Spatial Configs	Spin Eigenfns
$\frac{5}{2}$	640	3678
$\frac{3}{2}$	992	8380
$\frac{1}{2}$	1132	8764

Table 5. $Fe^{II}q$–O–$Fe^{II}q$ Wavefunctions		
Spin S	Spatial Configs	Spin Eigenfns
1	968	7414
0	976	4137

IV. Results and Discussion

In order to describe the spin states of the bridged dimers, it is necessary to use a more precise description of spin coupling than contained in the simple orbital diagrams with α's and β's. To do this, we employ Young tableaux which permit a quantitative discussion of orbital couplings.

A. $Fe^{II}q-N-Fe^{II}q$

a. Analysis with High- Spin Coupling on Each Atom

Consider first the μ-nitrido dimer. What are the lowest states at long Fe^{II}–N–Fe^{II} separation? Each Fe^{II} would be in its ground $S=2$ state, and nitrogen would be in its ground $S=\frac{3}{2}$ state. The optimum coupling of the N with either Fe should have their spins *opposite* (leading to $S=\frac{1}{2}$), and hence the state with maximum bond coupling between nitrogen and each iron occurs when the coupling between the irons is high spin (ferromagnetic), leading to a net total spin of $S=\frac{5}{2}$.

Next, we will use diagrams to examine exactly this case of Fe^{II}–N–Fe^{II} at long separation. We shall use l=left, r=right, and c=center to represent the singly-occupied orbitals on the left and right irons and center nitrogen. The states with total spin $S=\frac{11}{2}$, $\frac{9}{2}$, and $\frac{7}{2}$ have the form:

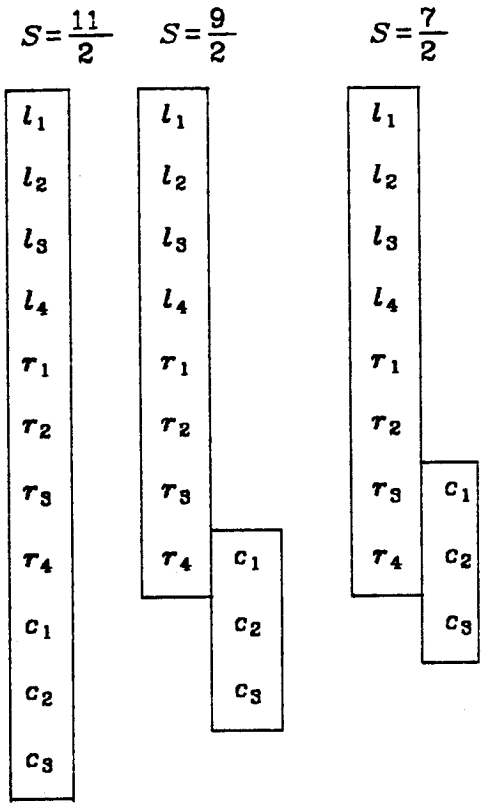

where sequential orbitals in the same column are coupled high-spin. The total spin S is just half the number of rows with one element, so that the first diagram has total spin of $S=\frac{11}{2}$. The other two diagrams have one or two rows with two orbitals in the same row. This indicates spin pairing of the two columns to yield a net spin corresponding to half the number of rows having one entry. This way of using tableaux is nonstandard and is described further in Appendix I. The state with $S=\frac{5}{2}$, expected (*vide supra*) to be the lowest in energy, can be written three ways, all with equivalent meanings:

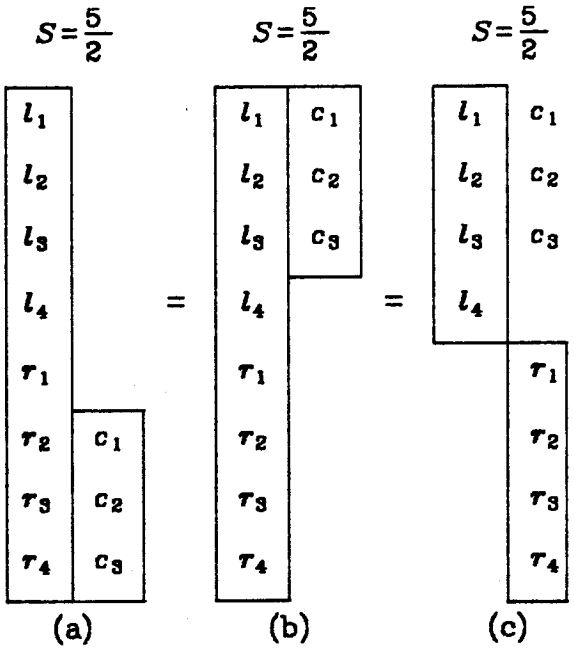

The first tableau (a) is a natural way to represent this state, similar to the representation of the states of higher total spin. The second tableau (b) is the standard representation (see Appendix I). The third tableau is of the form we will find useful for representing states of lower total spin. The corresponding states with $S=\frac{3}{2}$ and $\frac{1}{2}$ are:

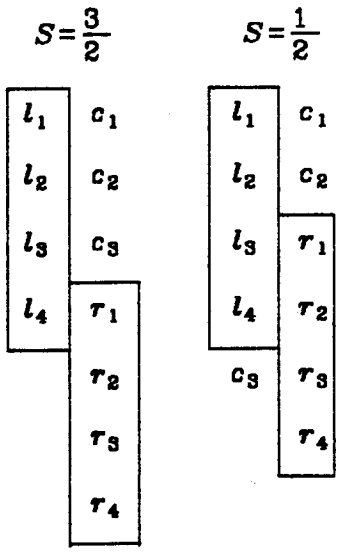

Using the same Fe and N orbitals for all spin states, the energies

of the above states can all be evaluated in terms of permutational matrix elements U_{ij} that are implied by the form of the tableau (see Appendix I). The result is

$$\begin{aligned} E-E_0 &= U_{lr}E_{lr} + U_{lc}E_{lc} + U_{rc}E_{rc} \\ &= U_{lr}E_{lr} + 2U_{lc}E_{lc} \end{aligned}$$

where $U_{lc}=U_{rc}$ and $E_{lc}=E_{rc}$ and where E_0 is some constant while the E_{ij} include various one- and two-electron exchange energies. The U_{ij} may range from -1 (high-spin coupling) to +1 (low-spin or bond coupling), and for the cases of interest here they are

Table 6. Long-R U_{ij}'s

S	U_{lr}	$U_{lc}=U_{rc}$
$\frac{11}{2}$	-1	-1
$\frac{9}{2}$	-1	$-0.54\overline{16}$
$\frac{7}{2}$	-1	$-0.1\overline{6}$
$\frac{5}{2}$	-1	+0.125
$\frac{3}{2}$	-0.5	0
$\frac{1}{2}$	-0.125	-0.125

The E_{lc} term dominates and is negative so that maximum U_{lc} is best for bonding (corresponding to maximal antiparallel coupling of the l and c orbitals). Thus, from Table 6, we expect the energy ordering $S=\frac{5}{2}$ lowest, $S=\frac{3}{2}$, $S=\frac{1}{2}$, $S=\frac{7}{2}$, $S=\frac{9}{2}$, $S=\frac{11}{2}$ (highest). Indeed, this is exactly the ordering found for high-spin irons, even at the short experimental geometry of $(FeTPP)_2N$, as indicated in Table 7:

Table 7. Calculated $Fe^{II}q$–N–$Fe^{II}q$ Spectrum	
S	E(cm^{-1})
$\frac{9}{2}$	14212
$\frac{7}{2}$	5978
$\frac{5}{2}$	0
$\frac{3}{2}$	379
$\frac{1}{2}$	1905

b. Analysis of Maximal Bonding Interactions

Although this analysis predicts the proper spectrum of spin states, the assumption that the coupling on each center remains high-spin after including Fe-N bonding is not valid. For maximum bonding we would want S=0 for the two electrons in each bond pair, and this necessarily means that the spins on an atom are no longer high-spin. The stronger the bonding, the greater this effect. Thus, there is a compromise in the spin coupling between low-spin for inter atomic (bond pairing) and high-spin for intra atomic.

We will analyze this effect for the σ, π, and δ spaces separately. Consider first the sigma orbitals σ_l, σ_r, and σ_c. The high-spin coupling of these orbitals

$^4\Sigma_g^+$

leads to a very high energy corresponding to an antibond between the N and each Fe. When possible, these orbitals will couple into the doublet

$^2\Sigma_g^+$

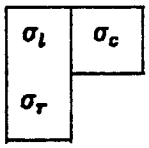

since this leads to σ_c having the opposite spin from σ_l and σ_r ($U_{lc}=U_{rc}=+\frac{1}{2}$, $U_{lr}=-1$). There is a second doublet

$^2\Sigma_u^+$

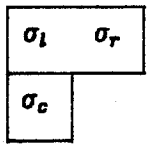

(which singlet couples σ_l and σ_r). But this has $U_{lc}=U_{rc}=-\frac{1}{2}$, $U_{lr}=+1$ so that it maximizes high-spin character between N and the Fe's and consequently is very bad energetically; it is never a major contributor to any low-lying state. Thus, the σ-space exerts a ferromagnetic force between the irons.

Consider next the δ-space. With four singly-occupied δ orbitals, there are three possible couplings:

$^5\Sigma_g^+$

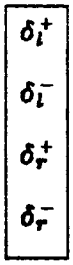

$^3\Sigma_u^+$

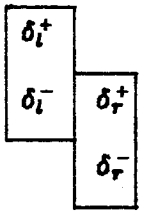

and

$^1\Sigma_g^+$

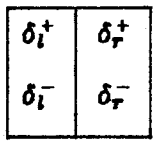

Considering only the direct $\delta_l-\delta_r$ interactions, there are overlap terms favoring $S=0$ and two-electron exchange terms favoring $S=2$ with the $S=0$ expected to be slightly lower. Thus, the δ-space is weakly antiferromagnetic. However, these interatomic couplings in the δ-space are much smaller than the intraatomic couplings keeping the spins in the δ orbitals on each Fe high-spin coupled to the σ and π orbitals on the same center. Thus, the $\delta-\delta$ coupling is dominated by indirect interactions through the σ- and π-spaces, leading to a net ferromagnetic interaction.

Finally, we consider the π-space. This is more complicated because we must consider resonance of two spatial configurations. The two cases are

I: $(\mathrm{Fe}_l d_{xz})^2(\mathrm{N}p_x - \mathrm{Fe}_r d_{xz})$
$(\mathrm{Fe}_l d_{yz} - \mathrm{N}p_y)(\mathrm{Fe}_r d_{yz})^2$

with a N–Fe_r π_x-bond and a N–Fe_l π_y-bond and

II: $(\mathrm{Fe}_l d_{xz} - \mathrm{N}p_x)(\mathrm{Fe}_r d_{xz})^2$
$(\mathrm{Fe}_l d_{yz})^2(\mathrm{N}p_y - \mathrm{Fe}_r d_{yz})$

with a N–Fe_l π_x-bond and a N–Fe_r π_y-bond. Thus, there are two resonance states

$$\mathrm{I} \pm \mathrm{II}$$

and ignoring for the moment the doubly-occupied d orbitals, we might write the pairing for I+II for $S=0$ as

$^1\Sigma_g^+$

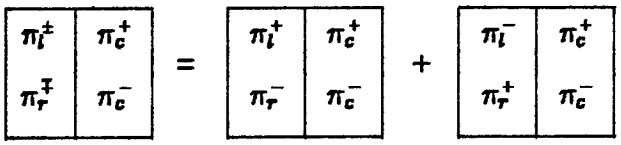

which we collect into one diagram as indicated on the left. Similarly for $S=1$ and $S=2$ we obtain

$^3\Sigma_u^+$

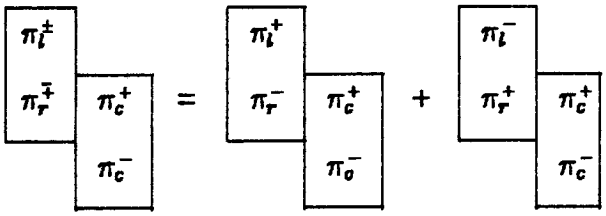

and

$$^5\Sigma_g^+$$

$$\begin{bmatrix} \pi_l^{\pm} \\ \pi_r^{\mp} \\ \pi_c^{+} \\ \pi_c^{-} \end{bmatrix} = \begin{bmatrix} \pi_l^{+} \\ \pi_r^{-} \\ \pi_c^{+} \\ \pi_c^{-} \end{bmatrix} + \begin{bmatrix} \pi_l^{-} \\ \pi_r^{+} \\ \pi_c^{+} \\ \pi_c^{-} \end{bmatrix}$$

Maximal bonding occurs, of course, with $S=1$ leading to two π-bonds.

Summarizing, to maximize Fe-N bonding the σ and π interactions lead to ferromagnetic coupling of the spins on the two Fe's, while the δ interactions favor antiferromagnetic coupling. However, the former dominate, so that the net coupling of the Fe spins is ferromagnetic.

c. Analysis of the Optimal Coupling

We are now ready to analyze the actual spin couplings at the experimental geometry. To maximize bonding, the high-spin state ($S=\frac{11}{2}$) is the product (properly antisymmetrized)

$$(^4\overset{\sigma}{\Sigma}_g^+)(^5\overset{\pi}{\Sigma}_g^+)(^5\overset{\delta}{\Sigma}_g^+) \rightarrow {}^{12}\Sigma_g^+$$

leading to an overall $^{12}\Sigma_g^+$ state

σ_l

σ_r

σ_c

$\pi_l^{\pm}$

$\pi_r^{\mp}$

π_c^{+}

π_c^{-}

δ_l^{+}

δ_l^{-}

δ_r^{+}

δ_r^{-}

with $U_{lc}=U_{rc}=-1$ and $U_{lr}=-1$.

For the lowest $S=\frac{9}{2}$ state, we maximize the σ-bonding with a concomitant sacrifice of intraatomic exchange and π-bonding. The σ-space is a nearly pure gerade doublet:

$$(^2\overset{\sigma}{\Sigma}_g^+)(^5\overset{\pi}{\Sigma}_g^+)(^5\overset{\delta}{\Sigma}_g^+) \rightarrow {}^{10}\Sigma_g^+$$

σ_l	σ_c
σ_r	
$\pi_l^{\pm}$	
$\pi_r^{\mp}$	
π_c^{+}	
π_c^{-}	
δ_l^{+}	
δ_l^{-}	
δ_r^{+}	
δ_r^{-}	

leading to $U_{lc}=U_{rc}=+\frac{1}{2}$ and $U_{lr}=-1$ for the σ orbitals and $U_{ij}=-1$ for non σ orbitals. If the σ orbitals were coupled to the π and δ orbitals so as to avoid any loss of intraatomic exchange, the σ- and π-bond couplings between iron and nitrogen would have been $U_{lc}=-0.541\overline{6}$. Instead, each σ-bond coupling approaches the maximum of +0.5, while the π-bond couplings go to the minimum of -1.0. The exchange coupling between the nitrogen p_σ and p_π's goes from -1.0 to $-0.\overline{3}$, and the coupling between each iron d_σ and the other iron d's goes from -1.0 to $-0.8\overline{3}$. The σ-bonding is so important that it has been maximized at the expense of π-bonding and intraatomic exchange.

For a net spin of $S=\frac{7}{2}$, we can have

$$(^2\overset{\sigma}{\Sigma}_g^+)(^3\overset{\pi}{\Sigma}_u^+)(^5\overset{\delta}{\Sigma}_g^+)$$

leading to an increased amount of π-bonding along with the σ-bonding

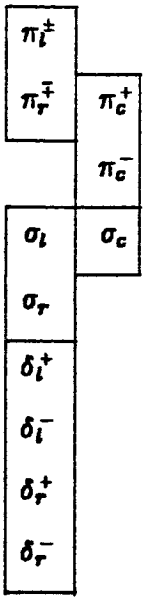

For $S=\frac{5}{2}$, the system can now have the maximum bonding in both the σ and π spaces

$$(^2\overset{\sigma}{\Sigma}_g^+)(^1\overset{\pi}{\Sigma}_g^+)(^5\overset{\delta}{\Sigma}_g^+)$$

leading to

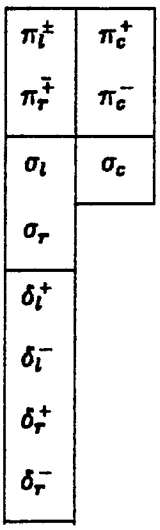

This maximal σ- and π-bonding can be retained in the remaining lower spin states. The lowest $S=\frac{3}{2}$ state begins to increase the δ-bonding:

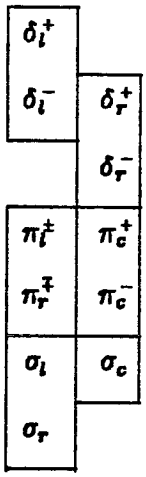

This increase in δ-bonding frustrates the indirect ferromagnetic interactions through the σ- and π-spaces. These indirect interactions are energetically more important than the direct δ-bonding, so the $S=\frac{3}{2}$ state is higher in energy. Finally, we come to the $S=\frac{1}{2}$ state, which maximizes the δ-bonding:

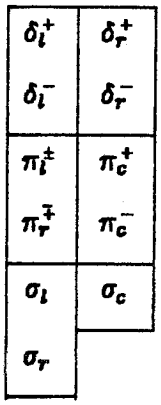

This state further frustrates the indirect ferromagnetic interactions through the σ- and π-spaces, and hence is even higher in energy.

The above analysis sets the stage for considering the actual spin coupling computed from the optimal wavefunctions of this system. To do this analysis, we have evaluated the net spins in the σ, π, and δ spaces by evaluating $\langle\hat{S}^2\rangle$ for the electrons in each space (see Appendix D). If the

electrons in a given space are coupled to form an eigenfunction of spin, then $\langle\hat{S}^2\rangle = S(S+1)$. In the σ-space, the value of $\langle\hat{S}^2\rangle_\sigma$ can be as small as 0.75 for $S=\frac{1}{2}$ or as large as 3.75 for $S=\frac{3}{2}$. The value of $\langle\hat{S}^2\rangle_\sigma$ gives the density of each spin in the σ-space, so that, for example, a state where the σ-space is half $S=\frac{1}{2}$ and half $S=\frac{3}{2}$ would yield $\langle\hat{S}^2\rangle_\sigma=2.25$. Hence, a value below 2.25 means the σ-space is mostly doublet, while a larger value means the σ-space is mostly quartet.

In the π-space or δ-space, the value of $\langle\hat{S}^2\rangle$ can be as small as 0 for $S=0$ or as large as 6 for $S=2$. For a pure $S=1$ state, we obtain $\langle\hat{S}^2\rangle=2$. Unfortunately, the value of $\langle\hat{S}^2\rangle$ does not give the density of each spin in the π-space or δ-space. Thus, a value smaller than 1 means the space must be mostly $S=0$, while a value larger than 4 means the space must be mostly $S=2$. Unfortunately, for $\langle\hat{S}^2\rangle$ between 1 and 4, we can not rigorously distinguish (in this analysis) between a state that is mostly $S=1$ and a state with no $S=1$ character but an appropriate average of $S=0$ and $S=2$. However, in all cases for which we have found values in this range, an analysis of the total spatial and spin symmetries indicates that the net spin is clearly mostly $S=1$.

Table 8. Calculated $Fe^{II}q$–N–$Fe^{II}q$ Spin Coupling									
TOTAL	EXPECTATION VALUES			DOMINANT SPIN			DEDUCED SYMMETRY		
S	$\langle\hat{S}^2\rangle_\sigma$	$\langle\hat{S}^2\rangle_\pi$	$\langle\hat{S}^2\rangle_\delta$	S_σ	S_π	S_δ	σ	π	δ
$\frac{11}{2}$	3.75	6.00	6.00	$\frac{3}{2}$	2	2	$^4\Sigma_g^+$	$^5\Sigma_g^+$	$^5\Sigma_g^+$
$\frac{9}{2}$	0.83	5.97	6.00	$\frac{1}{2}$	2	2	$^2\Sigma_g^+$	$^5\Sigma_g^+$	$^5\Sigma_g^+$
$\frac{7}{2}$	0.82	2.50	5.58	$\frac{1}{2}$	1	2	$^2\Sigma_g^+$	$^3\Sigma_u^+$	$^5\Sigma_g^+$
$\frac{5}{2}$	0.83	0.74	5.14	$\frac{1}{2}$	0	2	$^2\Sigma_g^+$	$^1\Sigma_g^+$	$^5\Sigma_g^+$
$\frac{3}{2}$	0.80	0.69	2.45	$\frac{1}{2}$	0	1	$^2\Sigma_g^+$	$^1\Sigma_g^+$	$^3\Sigma_u^+$
$\frac{1}{2}$	0.79	0.68	0.97	$\frac{1}{2}$	0	0	$^2\Sigma_g^+$	$^1\Sigma_g^+$	$^1\Sigma_g^+$

Besides obtaining the dominant spin of each space, we can also obtain the bond couplings. These tell us even more about the spin coupling.

Table 9. $Fe^{II}q$–N–$Fe^{II}q$ Bond Couplings		
S	U_π	U_δ
$\frac{11}{2}$	-1.00	-1.00
$\frac{9}{2}$	-0.99	-1.00
$\frac{7}{2}$	-0.13	-0.89
$\frac{5}{2}$	+0.63	-0.79
$\frac{3}{2}$	+0.64	-0.11
$\frac{1}{2}$	+0.63	+0.26

The values of U_π are approximately what our tableaux would predict:

U_π=−1 for $S=\frac{9}{2}$, U_π=0 for $S=\frac{7}{2}$, and $U_\pi=\frac{1}{2}$ for $S=\frac{5}{2}$, $\frac{3}{2}$, and $\frac{1}{2}$. For $S=\frac{5}{2}$, $\frac{3}{2}$, and $\frac{1}{2}$, the value of U_π slightly exceeds $\frac{1}{2}$, because the π-space has a little valence-bond (G1) S=0 character:

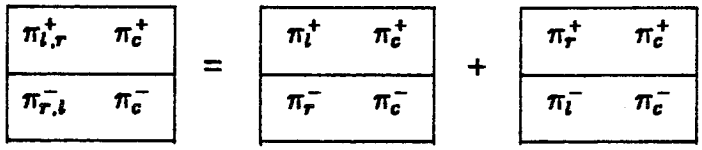

For $S=\frac{7}{2}$, the value given for U_π is actually the average of U_{π^+}=−0.05 and U_{π^-}=−0.22. The two π-bond couplings are slightly different because the π-space has a little G1 S=1 character:

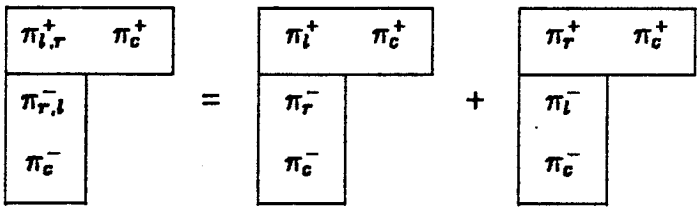

When this G1 S=1 coupling contributes, the π^+ and π^- orbital shapes become inequivalent.

The values of U_δ are close to what our tableaux would predict: U_δ=−1 for $S=\frac{9}{2}$, $\frac{7}{2}$, and $\frac{5}{2}$, U_δ=0 for $S=\frac{3}{2}$, and $U_\delta=\frac{1}{2}$ for $S=\frac{1}{2}$. Because bonding interactions are very weak in the δ-space, G1 character is negligible. The largest deviation from our tableaux occurs with U_δ=+0.26 for $S=\frac{1}{2}$. Because of indirect ferromagnetic interactions, the δ-space does not want to be singlet. The value of $\langle\hat{S}^2\rangle_\delta$ = 0.97 indicates a significant deviation from S_δ=0.

B. $Fe^{II}t-N-Fe^{II}t$

a. Analysis with High- Spin Coupling on Each Atom

Consider now forming stronger bonds between the nitrogen and each iron. Exciting each iron from its ground high-spin state to the excited lower-spin state, we obtain much larger bond couplings. Examining just the singly-occupied orbitals on the left and right irons and center nitrogen, consider the lowest state for each total spin at large distances:

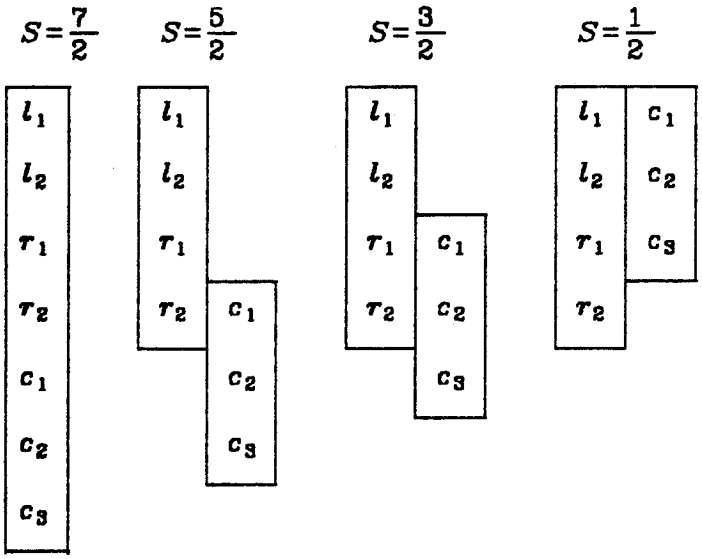

The bond couplings between the nitrogen and each iron should dominate the relative energies of these states.

Table 10. Long-R t–N–t U_{ij}'s		
S	U_{lr}	$U_{lc}=U_{rc}$
$\frac{7}{2}$	-1	-1
$\frac{5}{2}$	-1	$-0.41\bar{6}$
$\frac{3}{2}$	-1	0
$\frac{1}{2}$	-1	+0.25

At long distances, we would expect twice as much bonding in the $S=\frac{1}{2}$ ground state of $Fe^{II}t$–N–$Fe^{II}t$ as in the $S=\frac{5}{2}$ ground state of $Fe^{II}q$–N–$Fe^{II}q$. For these states, $U_{lc}=U_{rc}$ is the reciprocal of the total number of high-spin d-electrons, of which there are eight for high-spin irons but only four for lower-spin irons.

At the short experimental geometry of $(FeTPP)_2N$, we find that this coupling does indeed predict the correct ordering of states.

Table 11. Calculated $Fe^{II}t$–N–$Fe^{II}t$ Spectrum	
S	E(cm^{-1})
$\frac{7}{2}$	54897
$\frac{5}{2}$	26450
$\frac{3}{2}$	12544
$\frac{1}{2}$	0

However, the actual spin coupling shows that the bonding is stronger.

b. Analysis of the Optimal Coupling

Table 12. Calculated $Fe^{II}t$–N–$Fe^{II}t$ Spin Coupling

TOTAL	EXPECTATION		DOMINANT	
S	$\langle\hat{S}^2\rangle_\sigma$	$\langle\hat{S}^2\rangle_\pi$	S_σ	S_π
$\frac{7}{2}$	3.75	6.00	$\frac{3}{2}$	2
$\frac{5}{2}$	0.81	5.94	$\frac{1}{2}$	2
$\frac{3}{2}$	0.77	2.03	$\frac{1}{2}$	1
$\frac{1}{2}$	0.77	0.05	$\frac{1}{2}$	0

The σ- and π-spaces are each almost pure eigenfunctions of spin. When possible, the σ-orbitals couple into an almost pure doublet. The character of the π-bonds is given by the bond couplings:

Table 13. $Fe^{II}t$–N–$Fe^{II}t$ Bond Couplings

S	U_{π^+}	U_{π^-}
$\frac{7}{2}$	-1	-1
$\frac{5}{2}$	-0.99	-0.99
$\frac{3}{2}$	+0.93	-0.96
$\frac{1}{2}$	+0.96	+0.96

Clearly, G1 character now dominates. We can accurately represent each state as a single tableau. The $S=\frac{7}{2}$ state is the high-spin product of a gerade $S=\frac{3}{2}$ σ-space and the gerade resonance of a $S=2$ π-space:

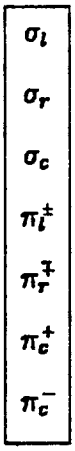

The $S=\frac{5}{2}$ state maximizes the σ-bonding at the expense of intraatomic exchange and π-bonding. The σ-space is an almost pure gerade doublet:

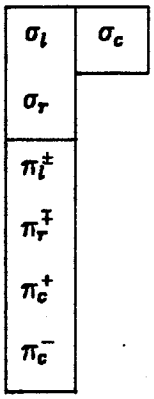

The maximal σ-bonding is retained for all lower spin states. The $S=\frac{3}{2}$ state increases the π-bonding with the ungerade resonance of a G1 $S=1$ π-space:

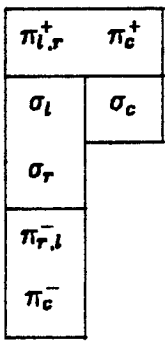

The $S=\frac{1}{2}$ state maximizes the π-bonding with the gerade resonance of a

G1 $S=0$ π-space:

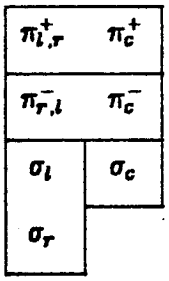

This is the ground state.

The high-spin irons of $Fe^{II}q$–N–$Fe^{II}q$ have a great deal of exchange stabilization energy which must be sacrificed to make strong bonds. The σ-bonding interaction is so strong that the σ-space is always an almost pure doublet when the total spin allows. The π-bonding interaction is weaker than the σ-interaction but strong enough that the π-space attains the lowest spin allowed, given that the σ-space is first allowed to couple low-spin. The π-bonding interaction is strong enough to have a little G1 character. The δ-bonding interactions are so weak that G1 character is negligible.

The lower-spin irons of $Fe^{II}t$–N–$Fe^{II}t$ have less exchange stabilization energy than high-spin irons, so stronger bonds can be made. The δ-electrons on each iron are coupled singlet, so no energy of exchange with the δ-orbitals is sacrificed to make strong σ- and π-bonds. As with high-spin irons, the σ-space attains maximal bonding when possible. The π-space again couples into the lowest spin allowed. However, the π-bonds now have almost pure G1 character, so the lower-spin irons attain maximal π-bonding.

c. Examination of the π- Resonance

We will now examine the role resonance plays in the π-bonding. There are both favorable and unfavorable resonances:

Table 14. Relative Energies (cm^{-1}) of the Resonant and Antiresonant States of $Fe^{II}t-N-Fe^{II}t$

S	Resonant State	Antiresonant State	$\Delta E(cm^{-1})$
$\frac{7}{2}$	54897	55614	717
$\frac{5}{2}$	26450	29253	2803
$\frac{3}{2}$	12544	19066	6522
$\frac{1}{2}$	0	13248	13248

The net spin in each space is the same, as indicated in Table 15.

Table 15. Calculated $Fe^{II}t-N-Fe^{II}t$ Spin Coupling

TOTAL	FAVORABLE		UNFAVORABLE	
S	$\langle\hat{S}^2\rangle_\sigma$	$\langle\hat{S}^2\rangle_\pi$	$\langle\hat{S}^2\rangle_\sigma$	$\langle\hat{S}^2\rangle_\pi$
$\frac{7}{2}$	3.75	6.00	3.75	6.00
$\frac{5}{2}$	0.81	5.94	0.89	5.85
$\frac{3}{2}$	0.77	2.03	0.84	2.08
$\frac{1}{2}$	0.77	0.05	0.79	0.55

The bond couplings are the same for $S=\frac{7}{2}$ and $\frac{5}{2}$ but quite different for $S=\frac{3}{2}$ and $\frac{1}{2}$, as indicated in Table 16.

Table 16. $Fe^{II}t$–N–$Fe^{II}t$ Bond Couplings				
TOTAL	FAVORABLE		UNFAVORABLE	
S	U_{π^+}	U_{π^-}	U_{π^+}	U_{π^-}
$\frac{7}{2}$	-1	-1	-1	-1
$\frac{5}{2}$	-0.99	-0.99	-0.96	-0.96
$\frac{3}{2}$	+0.93	-0.96	-0.02	-0.02
$\frac{1}{2}$	+0.96	+0.96	+0.67	+0.66

The favorable and unfavorable states for $S=\frac{7}{2}$ and $\frac{5}{2}$ differ only in the spatial symmetry of the π-space. The spin symmetries are the same. The unfavorable $S=\frac{7}{2}$ state is the product of a gerade $S=\frac{3}{2}$ σ-space and the ungerade resonance of a $S=2$ π-space:

$$\begin{vmatrix} \sigma_l \\ \sigma_r \\ \sigma_c \\ \pi_l^{\pm} \\ \pi_r^{\mp} \\ \pi_c^{+} \\ \pi_c^{-} \end{vmatrix}$$

The unfavorable $S=\frac{5}{2}$ state has an almost pure gerade doublet σ-space:

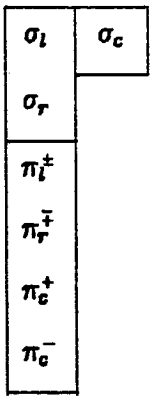

The unfavorable π-resonance does not favor strong π-bonding. The unfavorable $S=\frac{3}{2}$ state is accurately represented by the gerade resonance of a $S=1$ π-space:

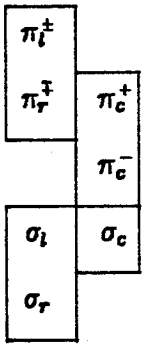

Unlike the favorable $S=\frac{3}{2}$ state, the π-space of this state has negligible G1 character. The unfavorable $S=\frac{1}{2}$ state is dominantly the ungerade resonance of a $S=0$ π-space:

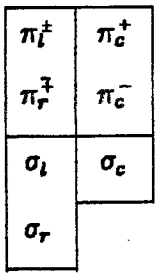

Unlike the favorable $S=\frac{1}{2}$ state, the π-space of this state has only a little G1 character.

C. Fe–O–Fe

a. Analysis Assuming High- Spin Coupling on Each Atom

1. $Fe^{II}q$–O–$Fe^{II}q$

Consider now the μ-oxo dimer. At long Fe^{II}–O–Fe^{II} separation, the lowest states would have each Fe^{II} in its ground S=2 state and the oxygen in its ground S=1 state. The lowest states with S=5 and 4 have the form:

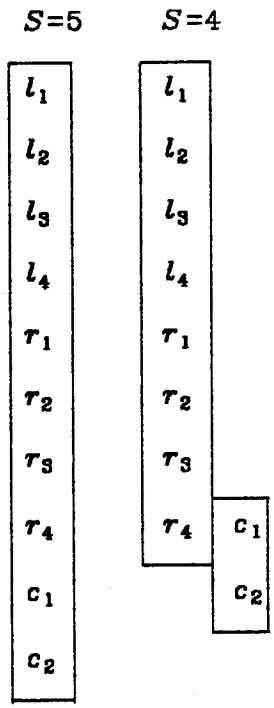

The state with S=3 should be the lowest in energy:

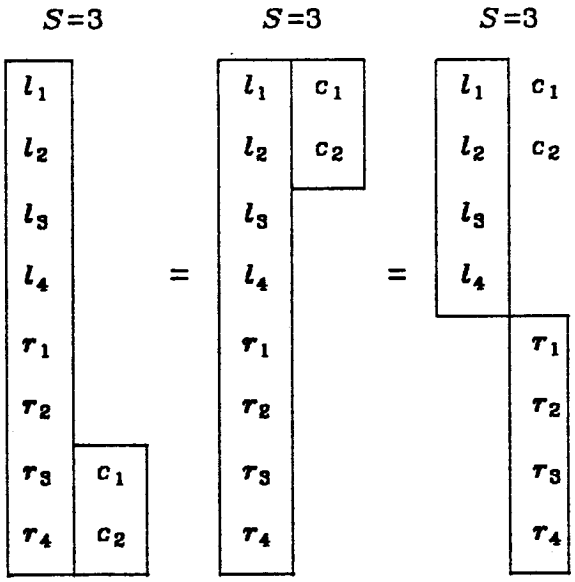

The states with S=2, 1, and 0 are:

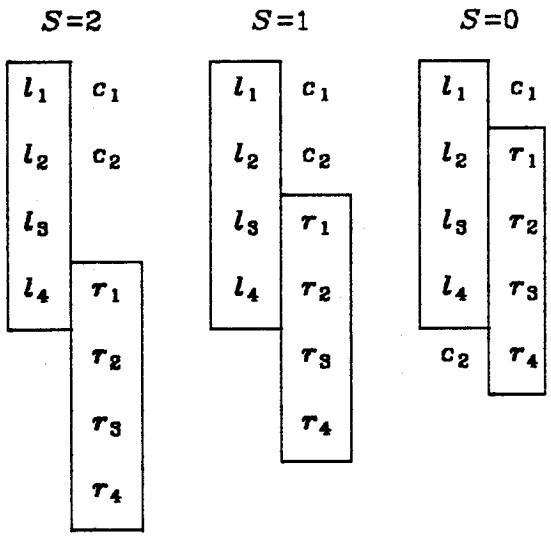

The relative energies of these long-distance states should be dominated by the bond couplings between the oxygen and each iron.

Table 17. Long-R q–O–q U_{ij}'s		
S	U_{lr}	$U_{lc}=U_{rc}$
5	-1	-1
4	-1	-0.375
3	-1	+0.125
2	-0.5	0
1	-0.125	-0.125
0	+0.125	-0.25

2. $Fe^{II}t$–O–$Fe^{II}t$

Consider a case in which stronger bonds can be formed between the oxygen and each iron. Larger bond couplings can be obtained if we excite each iron from its ground high-spin state to its excited lower-spin state. At long distances, the lowest states for S=3, 2, 1, and 0 are:

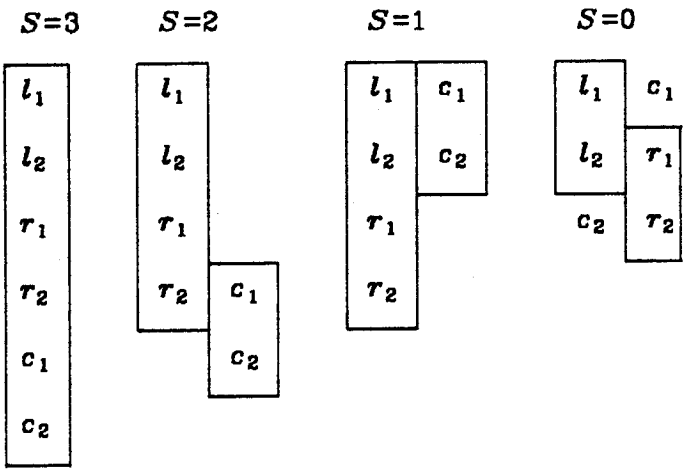

The bond couplings between the oxygen and each iron dominate the relative energies of these states.

Table 18. Long-R t–O–t U_{ij}'s		
S	U_{lr}	$U_{lc}=U_{rc}$
3	-1	-1
2	-1	-0.25
1	-1	+0.25
0	0	0

At long separation, we expect twice the bonding in the S=1 ground state of $Fe^{II}t$–O–$Fe^{II}t$ than in the S=3 ground state of $Fe^{II}q$–O–$Fe^{II}q$. The bonding should be proportional to $U_{lc}=U_{rc}$, which for these states is the reciprocal of the total number of high-spin d-electrons. There are eight high-spin d-electrons in $Fe^{II}q$–O–$Fe^{II}q$ but only four in $Fe^{II}t$–O–$Fe^{II}t$.

b. Analysis of the Optimal Coupling

At the short experimental geometry of $(FeTPP)_2O$, the character of bonding is completely different. Even the ordering of the states has changed from our long-distance predictions for both $Fe^{II}q$–O–$Fe^{II}q$ and $Fe^{II}t$–O–$Fe^{II}t$.

1. $Fe^{II}t$–O–$Fe^{II}t$

Consider first the simpler case of $Fe^{II}t$–O–$Fe^{II}t$. The lowest state is not S=1, as we had predicted for long separation, but rather S=0.

Table 19. Calculated $Fe^{II}t-O-Fe^{II}t$ Spectrum	
S	E(cm^{-1})
3	11104
2	7164
1	2957
0	0

Let us now look at the actual spin coupling computed for this system. In the σ-space, we now have four electrons. The dominant configuration has σ_c doubly-occupied with σ_l and σ_r singly-occupied. The singlet coupling of these orbitals is gerade,

σ_l	σ_r

while the triplet coupling of these orbitals is ungerade.

σ_l
σ_r

The value of $\langle\hat{S}^2\rangle_\sigma$ is 0 for $S=0$ and 2 for $S=1$. The value of $\langle\hat{S}^2\rangle_\sigma$ gives the density of each spin in the σ-space. When the σ-space is half $S=0$ and half $S=1$, $\langle\hat{S}^2\rangle_\sigma = 1$.

Table 20. Calculated $Fe^{II}t$–O–$Fe^{II}t$ Spin Coupling				
TOTAL	EXPECTATION		DOMINANT	
S	$\langle\hat{S}^2\rangle_\sigma$	$\langle\hat{S}^2\rangle_\pi$	S_σ	S_π
3	2.00	6.00	1	2
2	0.68	4.65	0	2
1	0.39	1.69	0	1
0	0.14	0.14	0	0

The σ and π spaces are not very pure eigenfunctions of spin for the states of total S=1 and 2. We can now look at the bond coupling between the singly-occupied σ-orbitals. The π-bond couplings give a more complete description of the spin coupling.

Table 21. $Fe^{II}t$–O–$Fe^{II}t$ Bond Couplings		
S	U_σ	U_π
3	-1	-1
2	+0.32	-0.70
1	+0.61	+0.14
0	+0.86	+0.82

The S=3 state is the high-spin product of an ungerade S=1 σ-space and the gerade resonance of a S=2 π-space:

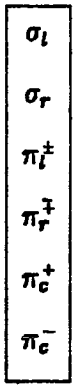

The S=2 state is 66%

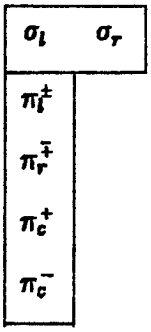

with 34% long-distance character.

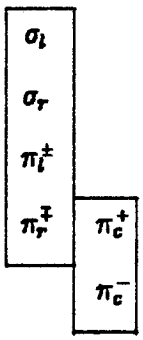

This mixture matches the observed U_σ=+0.32,

$$+0.32 = +1(.66) - 1(.34)$$

and predicts U_π=−0.74,

$$-0.74 = -1(.66) - 0.25(.34)$$

which is close to the observed U_π=−0.70.

The S=1 state is 80%

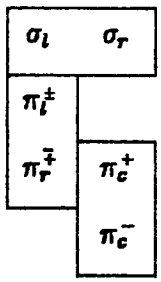

with 20% long-distance character.

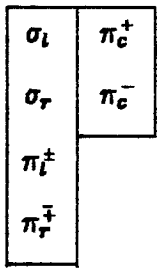

This mixture matches the observed U_σ=+0.61,

$$+0.60 = +1(.80) -1(.20)$$

and predicts U_π=+0.05,

$$+0.05 = 0(.80) +0.25(.20)$$

which is close to the observed U_π=+0.14.

The S=0 state is dominantly

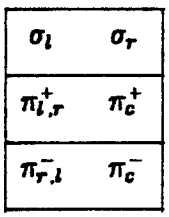

with some long-distance character.

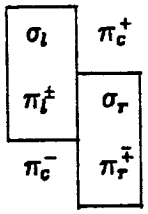

This mixture would predict equal U_σ and U_π, and the observed values are almost equal. The observed U_σ=+0.86 is only slightly larger than the observed U_π=+0.82 because of a very small amount of

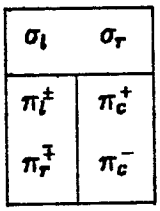

These three tableaux overlap, so no quantitative decomposition of the S=0 wavefunction will be given.

2. $Fe^{II}q-O-Fe^{II}q$

Consider the actual spin coupling of $Fe^{II}q-O-Fe^{II}q$ at the experimental geometry of $(FeTPP)_2O$. The lowest state is not $S=3$, as predicted for long distances, but rather $S=0$. In fact, the spectrum of states at long separation (see Table 17) looks completely different from the spectrum at the experimental distance:

Table 22. Calculated $Fe^{II}q-O-Fe^{II}q$ Spectrum (Energies in cm^{-1})

Spin S	Short-R Spectrum (Fe-O 1.763 Å)	Heisenberg Spectrum ($J=-200\ cm^{-1}$)
5	4919	6000
4	3684	4000
3	2347	2400
2	1203	1200
1	402	400
0	0	0

This spectrum looks very much like the Heisenberg coupling between two sets of five high-spin electrons, where the relative energies are given by

$$E_S = E_0 - JS(S+1)$$

with total spins of $S=0, 1, 2, 3, 4, 5$. A simple check on the validity of this formula is to evaluate the Heisenberg coupling constant J for each $S>0$ using

$$J_S = (E_0-E_S)/(S^2+S)$$

Table 23. Heisenberg Coupling Constant for $Fe^{II}q-O-Fe^{II}q$	
S	$J_S(cm^{-1})$
5	-164
4	-184
3	-196
2	-200
1	-201

Alternatively, as indicated in Table 22, we can calculate an excellent fit to the entire spectrum using $J=-200\ cm^{-1}$. This description in terms of two $S=\frac{5}{2}$ Fe^{III}'s antiferromagnetically coupled through a bridging O^{2-} is quite compelling and is the model most often used to describe the spin states of the oxo-bridged Fe dimer.

Our computed Heisenberg constant is comparable to experimentally determined exchange parameters.† A least-squares fit to the temperature dependence of a Knight shift yields an exchange constant of $-155\pm25\ cm^{-1}$ for $(FeTPP)_2O$ and $-168\pm25\ cm^{-1}$ for $(FeTpMPP)_2O$.[9] In Table 24, we compare our best value of J with experimental values.

Table 24. Comparison of J Values	
SOURCE	$J(cm^{-1})$
THEORY $Fe^{II}-O-Fe^{II}$	-201
EXPER. $(FeTPP)_2O$	-155±25
EXPER. $(FeTpMPP)_2O$	-168±25

The agreement with experiment, 25%, is excellent given that the calcula-

† The experimental constants are defined to correspond to twice our value. Thus, the values quoted are divided by two.

tion is purely *ab initio* and on a model in which the porphyrins are eliminated! In addition to any effects on J due to excluding the porphyrins from our model, we have also chosen Fe-O-Fe to be linear, which should lead to a larger exchange constant. [The real system has an Fe-O-Fe bond angle of 174.5°.]

Compelling as is the above interpretation, we find that the charge distribution in the oxo-bridged dimer does not correspond to O^{2-} but rather to O^{-}. Still, the spin coupling would appear to be the same as that expected for O^{2-}, as we shall see. The spin analysis in Table 25 demonstrates that the total coupling cannot be qualitatively described as the product of separate σ, π, and δ couplings.

Table 25. Calculated Spin Coupling for $Fe^{II}q-O-Fe^{II}q$

TOTAL	EXPECTATION			DOMINANT		
S	$\langle\hat{S}^2\rangle_\sigma$	$\langle\hat{S}^2\rangle_\pi$	$\langle\hat{S}^2\rangle_\delta$	S_σ	S_π	S_δ
5	2.00	6.00	6.00	1	2	2
4	1.58	4.23	4.61	1	2	2
3	1.22	2.84	3.41	1	1	1
2	0.94	1.90	2.35	0	1	1
1	0.75	1.31	1.56	0	1	1
0	0.67	1.03	1.14	0	1	1

Note in Table 25 that for S=4, 1, and 0, the dominant spins of each space do *not* sum to the total spin. This rule was never violated in the cases we examined previously. The violation in this case occurs because the total coupling is qualitatively the product of two sets of high-spin electrons, each spanning the σ, π, and δ spaces. The calculated bond couplings are shown in Table 26

Table 26. $Fe^{II}q$–O–$Fe^{II}q$ Bond Couplings				
S	U_σ	U_π	U_δ	Heisenberg Coupling
5	-1	-1	-1	-1
4	-0.58	-0.56	-0.65	-0.6
3	-0.22	-0.19	-0.35	-0.28
2	+0.06	+0.08	-0.09	-0.04
1	+0.25	+0.26	+0.11	+0.12
0	+0.33	+0.34	+0.22	+0.2

where we see that for each spin, the σ- and π-bond couplings are almost equivalent, while the δ-bond couplings are smaller (either less positive or more negative). Pure Heisenberg coupling would be as indicated in Table 26. For $S>0$, the σ- and π-bond couplings are larger and the δ-bond couplings are smaller than the Heisenberg bond couplings. For $S=0$, even the δ-bond couplings are larger than the Heisenberg bond couplings. We shall see later that these deviations are to be expected. Thus, it appears that the spin coupling is dominantly Heisenberg coupling, although the charge distribution seems inconsistent with this coupling.

c. Charge Distribution versus Spin Coupling

As discussed above, the charge distribution for $Fe^{III}\,O^{2-}\,Fe^{III}$ is expected to yield two sets of $S=\frac{5}{2}$ spins coupled to yield an antiferromagnetic Heisenberg spectrum of states. However, the charge distribution indicates O^- rather than O^{2-}. For example, Mulliken populations for our wavefunctions show that for high-spin irons, the bridging oxygen is O^-, and the populations of p_x, p_y, and p_z are nearly equal. In each of the σ, π^+, and π^- spaces, four electrons are distributed as follows: $d_i(1.2)$, $p(1.5)$, $d_r(1.2)$. Note that this population analysis of the ground state ($S=0$)

yields about half a negative charge on the bridging oxygen. The same analysis of the highest excited state (S=5) yields a full negative charge. Thus, we shall next explore the spin couplings to be expected of Fe^{II}–O^{-}–Fe^{III}. Here, of course, we must include the resonance of Fe^{II}–O^{-}–Fe^{III} with Fe^{III}–O^{-}–Fe^{II}. Looking now at just the σ and π spaces, we can view this system as the resonance of six equally contributing configurations:

σ	$\underline{\alpha\beta}$	$\underline{\alpha}$	$\underline{\beta}$	$\underline{\alpha}$	$\underline{\beta}$	$\underline{\alpha\beta}$
π^{+}	$\underline{\alpha}$	$\underline{\alpha\beta}$	$\underline{\beta}$	$\underline{\alpha}$	$\underline{\alpha\beta}$	$\underline{\beta}$
π^{-}	$\underline{\alpha}$	$\underline{\alpha\beta}$	$\underline{\beta}$	$\underline{\alpha}$	$\underline{\alpha\beta}$	$\underline{\beta}$
σ	$\underline{\alpha}$	$\underline{\alpha\beta}$	$\underline{\beta}$	$\underline{\alpha}$	$\underline{\alpha\beta}$	$\underline{\beta}$
π^{+}	$\underline{\alpha\beta}$	$\underline{\alpha}$	$\underline{\beta}$	$\underline{\alpha}$	$\underline{\beta}$	$\underline{\alpha\beta}$
π^{-}	$\underline{\alpha}$	$\underline{\alpha\beta}$	$\underline{\beta}$	$\underline{\alpha}$	$\underline{\alpha\beta}$	$\underline{\beta}$
σ	$\underline{\alpha}$	$\underline{\alpha\beta}$	$\underline{\beta}$	$\underline{\alpha}$	$\underline{\alpha\beta}$	$\underline{\beta}$
π^{+}	$\underline{\alpha}$	$\underline{\alpha\beta}$	$\underline{\beta}$	$\underline{\alpha}$	$\underline{\alpha\beta}$	$\underline{\beta}$
π^{-}	$\underline{\alpha\beta}$	$\underline{\alpha}$	$\underline{\beta}$	$\underline{\alpha}$	$\underline{\beta}$	$\underline{\alpha\beta}$
	Fe^{II}	O^{-}	Fe^{III}	Fe^{III}	O^{-}	Fe^{II}

Assuming all configurations are equal in each of the σ, π^{+}, and π^{-} symmetries, the doubly-occupied orbital would have the character of $\frac{2}{3}p_c$, $\frac{1}{6}d_l$, and $\frac{1}{6}d_r$ for all three symmetries (σ, π^{+}, and π^{-}). In addition, one singly-occupied orbital would have the character $\frac{5}{6}d_l$ and $\frac{1}{6}p_c$, while the

other singly-occupied orbital would be $\frac{5}{6}d_\tau$ and $\frac{1}{6}p_c$. Because each singly-occupied orbital is dominantly d_l or d_τ, this $Fe^{II}-O^{-}-Fe^{III}$ resonance case would yield a Heisenberg coupling similar to that expected for $Fe^{III}\,O^{2-}\,Fe^{III}$. Thus, the observed Heisenberg spectrum does *not* distinguish between these descriptions. However, the *strength* of the Heisenberg coupling is sensitive to the charge distribution. Our computed coupling constant appears to be slightly too strong. Adding porphyrins with the negatively charged porphine nitrogens will tend to reduce the Fe (less positive charge), which should in turn allow more charge to transfer onto the oxygen by localizing the doubly-occupied orbitals more on the oxygen. This would localize the singly-occupied orbitals more on the irons, making the interactions between the singly-occupied orbitals weaker. Thus, for our model system, we expect a coupling constant slightly too large. The states with S=5, 4, and 3 look like:

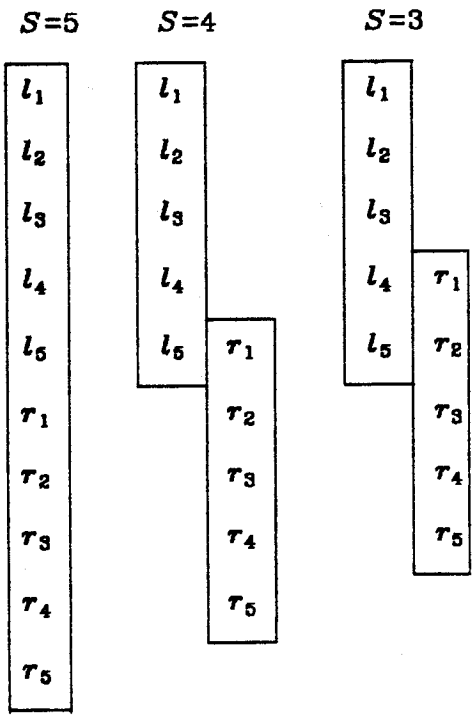

The states with S=2, 1, and 0 look like:

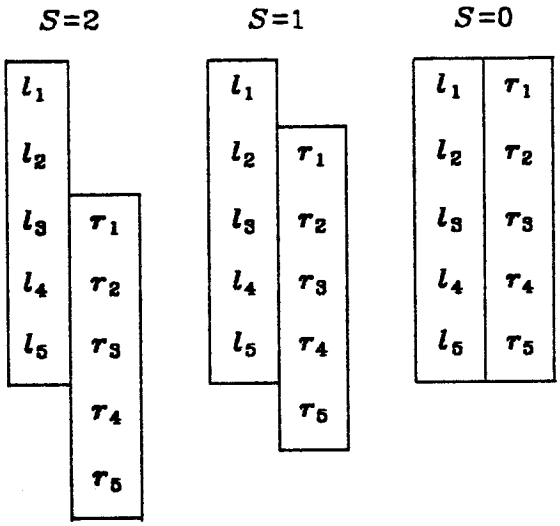

We are now in a position to understand why our bond couplings deviate from ideal Heisenberg bond couplings. For $Fe^{II}t$–O–$Fe^{II}t$, the spin coupling is dominated by strong σ- and π-bonding. However, for $Fe^{II}q$–O–$Fe^{II}q$, the spin coupling is dominated by exchange interactions on the irons. This exchange energy makes $Fe^{II}q$ easier to ionize than $Fe^{II}t$, which results in the reduced bridge O^-. Reducing the oxygen bridge localizes the singly-occupied orbitals on the irons, which makes the Heisenberg coupling more favorable. Even though Heisenberg coupling dominates, we should expect some contribution from strong σ- and π-bonding. Suppose that in each configuration, the singly-occupied O^- p-orbital were strongly bonded to the overlapping Fe d-orbital. We shall illustrate for S=0:

$\sigma_{l,r}$	σ_c
π_l^+	π_r^+
π_l^-	π_r^-
δ_l^+	δ_r^+
δ_l^-	δ_r^-

+

$\pi_{l,r}^+$	π_c^+
σ_l	σ_r
π_l^-	π_r^-
δ_l^+	δ_r^+
δ_l^-	δ_r^-

+

$\pi_{l,r}^-$	π_c^-
σ_l	σ_r
π_l^+	π_r^+
δ_l^+	δ_r^+
δ_l^-	δ_r^-

For this coupling, U_δ=0.25, but the magnitude of U_σ=U_π is not easily determined, because the tableaux overlap. A crude estimate is U_σ=U_π=0.5, which we obtain by assuming

$$0.5 = \frac{2}{3}(0.25) + \frac{1}{3}(+1)$$

We shall not attempt a quantitative analysis, because these tableaux overlap not only each other but also the S=0 Heisenberg tableau.

For all S<5, we should expect some contribution from strong σ- and π-bonding. For each spin, we can write this contribution as a linear combination of tableaux, each with strong bonding in one of the σ, π^+, or π^- spaces. For S=4 and 3, these tableaux are:

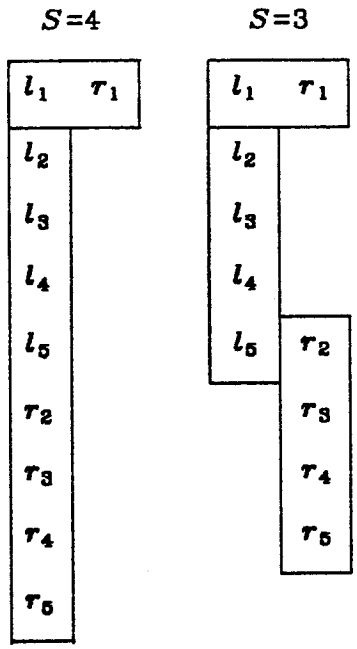

For S=2, 1, and 0, the tableaux become:

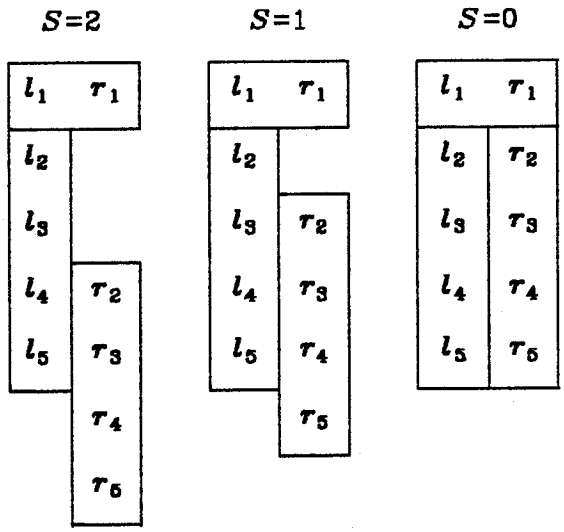

Using the same analysis as we illustrated for S=0, we estimate the following bond couplings for strong σ- and π-bonding:

Table 27. Strong Bond Couplings

S	$U_\sigma = U_\pi$	U_δ	Heisenberg Coupling
5	-1	-1	-1
4	$-0.\overline{3}$	-1	-0.6
3	0	-0.5	-0.28
2	+0.25	-0.125	-0.04
1	$+0.41\overline{6}$	+0.125	+0.12
0	+0.5	+0.25	+0.2

Note that for $S<5$, all $U_\sigma = U_\pi$ are larger and most U_δ are smaller than for Heisenberg coupling. The exceptions are that U_δ for $S=1$ is almost equal to and that U_δ for $S=0$ is larger than the corresponding Heisenberg couplings. The contribution of these configurations with strong σ- and π-bonds explains the deviations of our calculated bond couplings from the ideal Heisenberg couplings.

V. Conclusion

From these studies of bridged porphyrin dimers, we have learned that the well-characterized dimer $(FeTPP)_2O$ has the Heisenberg spin coupling expected for two ferric high-spin ($S=\frac{5}{2}$) centers antiferromagnetically coupled through a bridging O^{2-}. However, we find the charge distribution corresponds to O^{-}.

Contrary to some previous studies, we have found that the iron centers in $(FeTPP)_2N$ are *less* oxidized than in the oxygen-bridged dimer. The system is qualitatively best described as two ferrous centers bridged by a *neutral* nitrogen.

The spin-state of the Fe's in the nitrogen-bridged dimer is neither low-spin nor high-spin. Instead, we find that each iron is *intermediate-spin* ($S=1$) yielding a net spin of $S=\frac{1}{2}$ for the complex (in agreement with experiment). The remarkable difference between the oxygen-bridged dimer with high-spin Fe's and the nitrogen-bridged dimer with intermediate-spin Fe's arises from the difference in occupation of the $d_{z^2-y^2}$ orbital.

The Fe-Fe coupling for the nitrido coupled dimer is not strongly antiferromagnetic, as had been assumed. Each iron is coupled antiferromagnetic to the bridging nitrogen, so the Fe-Fe coupling is actually *ferromagnetic!* Indeed, we find that were the Fe's in a high-spin state, the bridging nitrogen would couple the Fe's to yield a total spin of $S=\frac{5}{2}$.

References

(1) D.A. Summerville and I.A. Cohen, *J. Am. Chem. Soc.* **1976,** *98,* 1747-1752.

(2) W.R. Scheidt, D.A. Summerville, and I.A. Cohen, *J. Am. Chem. Soc.* **1976,** *98,* 6623-6628.

(3) K.M. Kadish, L.A. Bottomley, J.G. Brace, and N. Winograd, *J. Am. Chem. Soc.* **1980,** *102,* 4341-4344.

(4) G.A. Schick and D.A. Bocian, *J. Am. Chem. Soc.* **1980,** *102,* 7982-7984.

(5) A.B. Hoffman, D.M. Collins, V.W. Day, E.B. Fleischer, T.S. Srivastava, and J.L. Hoard, *J. Am. Chem. Soc.* **1972,** *94,* 3620-3626.

(6) K. Tatsumi and R. Hoffmann, *J. Am. Chem. Soc.* **1981,** *103,* 3328-3341.

(7) A.J.H. Wachters, *J. Chem. Phys.* **1970,** *52,* 1033-1036.

(8) T.J. Dunning, Jr., *J. Chem. Phys.* **1970,** *53,* 2823.

(9) P.D.W. Boyd and T.D. Smith, *Inorg. Chem.* **1971,** *10,* 2041.

CHAPTER 2

Origin of Ferromagnetism in Nickel

I. Introduction

In this investigation, we shall seek to understand the exchange forces responsible for ferromagnetism. Of the magnetic elements, we have selected nickel for this study, because of its relative simplicity. However, the electronic structure of nickel is not simple. Theoretical methods disagree on the atomic configuration of Ni in the metal. The most common assumption by solid-state theorists is that the average configuration is $d^{9.4}$, so that 0.6 electrons per Ni are free to be ferromagnetically coupled. This is thought to explain the observed moment/atom $\mu_m = 0.6\,\mu_B$ at 0°K. However, our calculations on small clusters indicate that all of the atoms have d^9 configurations. Even so, we find that this too agrees with the oberved moment/atom, because half our d^9 centers are nonmagnetic. We have elucidated the exchange forces responsible for both magnetic and nonmagnetic d^9 centers.

Starting with Slater,[1] the exchange forces responsible for ferromagnetism in the elements have been illustrated in a plot of the energy of magnetization kT_C (Boltzmann constant times Curie temperature) versus the ratio R/r (atomic separation / diameter of unfilled shell). For small R/r (Sc to Mn), the exchange coupling is negative. For larger R/r, the coupling becomes positive at Fe, reaches a maximum at Co, decreases at Ni, and finally approaches zero as $R/r \to \infty$. Our calculations lead to a quite similar plot for Ni. We find that the exchange coupling versus R (atomic separation) is negative for small R, positive for R near the optimal value of 2.5 Å, and *negative* for large R. This change at large

R is a consequence of the Mott transition, and it serves as strong evidence for the model we shall propose for the exchange forces responsible for ferromagnetism.

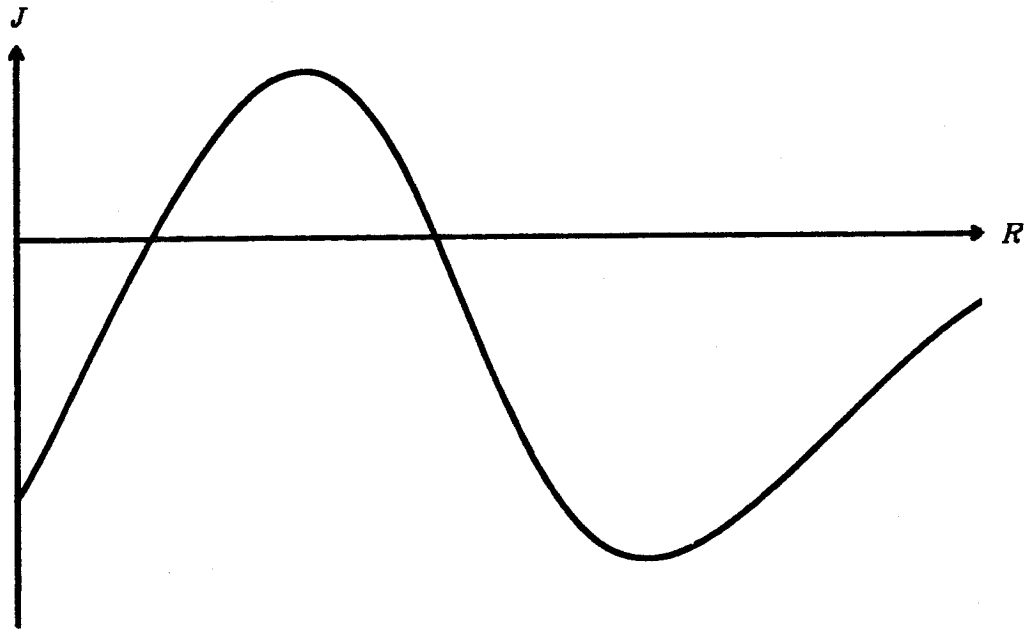

Figure 1. J (exchange coupling) versus R (atomic separation).

II. Preliminary Investigation of Iron

A. Discussion

In our quest for an understanding of ferromagnetism, we quite naturally turned first to iron. Our goal is to identify and understand the exchange forces responsible for magnetism. We generated a model for the interactions in solid iron, and reached some definitive conclusions regarding the origins of ferromagnetism.

Our model shows conclusively that direct $d-d$ exchange interactions are very weak for iron and are *antiferromagnetic*. Therefore, the magnetism of iron must be due to *indirect* exchange interactions. Our model supports the observation that magnetism in transition metals occurs only on the right side of the first row. This is because the direct $d-d$ interactions must be much smaller than the indirect interactions, thus favoring the case where d's are smallest with respect to the s's. Our model supports the idea that a ferromagnetic system should become antiferromagnetic at shorter R since the direct $d-d$ interactions will become much more important. In addition, we find that the system becomes antiferromagnetic at large R (corresponding to the Mott metal-insulator transition).

Our model has also led to some general conclusions about transition-metal dimers. We find that for dimers like Fe_2, indirect $s-d$ interactions dominate over direct $d-d$ interactions. The indirect interactions can be ferromagnetic or antiferromagnetic. When there is an odd number of s electrons, the interaction is ferromagnetic. When the number of s electrons is even, the interaction is antiferromagnetic. If the ground state of Fe_2 is made of an excited s^1d^7 state and a ground s^2d^6 state, then the dimer should be ferromagnetic. However, if the ground

state of Fe_2 is made of two excited s^1d^7 states, as is likely, then the dimer should be antiferromagnetic.

Our conclusions regarding the origin of magnetism have shown that a dimer is unlikely to provide an accurate model of ferromagnetism. We must examine larger clusters to see what magnetic forces are dominating in the solid. Because of the large number of unpaired spins in Fe, we have chosen to examine a larger cluster of Ni to identify these magnetic forces.

B. Calculational Details

Solid iron has *bcc* symmetry. Each atom is in a site of O_h symmetry with eight nearest neighbors and six next-nearest neighbors. The *d* orbitals of each atom are split into two e_g orbitals (e.g., $d_{x^2-y^2}$ and d_{z^2}) and three destabilized t_{2g} orbitals (e.g., d_{xy}, d_{xz}, d_{yz}). Cluster calculations on nickel lead us to believe that each iron contributes one conduction *s* electron, leaving a d^7 configuration. The lowest d^7 state is ^4F. In an O_h field, the seven components of this state split into $^4T_{1g}$ ($e_g^{2.2}t_{2g}^{4.8}$), $^4T_{2g}$ ($e_g^3t_{2g}^4$), and $^4A_{2g}$ ($e_g^4t_{2g}^3$). Since the t_{2g} orbitals are destabilized, the $^4A_{2g}$ state is best.[2]

In *bcc* iron, each nearest-neighbor dimer is in a site of D_{3d} symmetry. For each atom, we can choose any combination of the e_g doubly-occupied orbitals and any combination of the t_{2g} high-spin orbitals without changing the state. Since the internuclear axis of our dimer is a C_3 axis, we shall choose *d* orbitals with C_3 quantization. We shall denote the parity of reflection in one of the three σ_d planes with a + or -. An orbital which is sigma with respect to the internuclear axis is labeled with a 0. On each center, we have t_0, t_+, t_-, e_+, and e_-. Plus and minus combinations of orbitals of the same local symmetry yield orbitals of D_{3d} symmetry:

localized orbs	D_{3d} orbs
$t_0 \pm t_0$	a_{1g} , a_{2u}
$t_+ \pm t_+$	e_g^+ , e_u^+
$t_- \pm t_-$	e_g^- , e_u^-
$e_+ \pm e_+$	e_g^+ , e_u^+
$e_- \pm e_-$	e_g^- , e_u^-

We have optimized orbitals for a GVB wavefunction having the above D_{3d} orbital symmetries. The s orbitals were coupled into a singlet pair, and all singly-occupied d orbitals were coupled high spin. The A_{1g} and A_{2u} symmetries each contain a singly-occupied combination of sigma d's and a natural orbital of the s-pair. The self-consistent mixing of these orbitals yields little $s-d$ hybridization. Each of the four E symmetries contains one doubly-occupied orbital and one singly-occupied orbital. The self-consistent mixing of these orbitals yields an almost pure doubly-occupied combination of e's and an almost pure singly-occupied combination of t's.

A clever aspect of this model is how we obtain a $^4A_{2g}$ ($e_g^4 t_{2g}^3$) configuration at each atom without having an O_h field about that atom. Our model has $D_{\infty h}$ symmetry, but we use D_{3d} orbital symmetries. This allows the π and δ orbitals to mix. Given our occupation of these orbitals, they do mix, and our wavefunction has D_{3d} symmetry, not $D_{\infty h}$. This reduction in symmetry occurs because of *intraatomic* forces. Only one combination of π and δ orbitals in each of the four E symmetries of D_{3d} will yield pure ^4F symmetry on both atoms. Any other combination will mix in an excited ^4P state.

We have performed various CI calculations with these orbitals.

Since the orbitals have only D_{3d} symmetry, the largest abelian subgroup we can use is C_{2h}. The symmetries correlate as follows:

D_{3d}	C_{2h}
A_{1g} , E_g^+	A_g
A_{2g} , E_g^-	B_g
A_{1u} , E_u^-	A_u
A_{2u} , E_u^+	B_u

C. Results

Our model is capable of giving quantitatively the direct $d-d$ exchange interactions in bulk iron. Since the s electrons will be delocalized in bulk iron, the indirect exchange effects we calculate will be applicable only to the dimer. We can eliminate any indirect exchange interactions by keeping the s electrons coupled singlet. We have accomplished this by simply freezing the PP s-bond from the SCF. The six high-spin orbitals from the SCF are used as natural orbitals for (3/6)RCI's.

The nearest-neighbor distance in bulk iron is 2.5 Å. We find that the direct $d-d$ exchange between nearest neighbors is *antiferromagnetic*. For a Heisenberg spectrum of states, the energy of each excited state of spin S is determined by a single constant J:

$$E_S = E_0 - JS(S+1)$$

We can test the validity of this formula by determining the value of J for each excited state:

$$J = (E_0 - E_S)/(S^2+S)$$

At 2.5 Å, the value is constant.

Table 1. Direct Exchange @ 2.5 Å

S	E(cm^{-1})	J(cm^{-1})
3	277	-23
2	134	-22
1	44	-22
0	0	

The value of this coupling constant can be applied simultaneously to each of the eight nearest neighbors. We have shown not only that the

d-configuration at each iron is $e_g^4 t_{2g}^3$ but also that the spin coupling retains local $S=3/2$ character in each atomic d-shell. Thus, the interaction is isotropic. The direct $d-d$ exchange is definitely antiferromagnetic. The energy for $S=3$ is simply the SCF energy. Optimizing the orbitals for the other states would increase the magnitude of the coupling constant. Moreover, additional correlation would differentially favor the lower spin states.

At longer R, the coupling remains antiferromagnetic but falls off rapidly:

Table 2. Direct Exchange @ 3.0 Å

S	E(cm^{-1})	J(cm^{-1})
3	44.1	-3.7
2	21.9	-3.7
1	7.2	-3.6
0	0	

The value of J is expected to have exponential behavior:

$$J = ae^{-bR}$$

We find $a=-213000\ cm^{-1}$ and $b=3.65\ Å^{-1}$. At shorter R, the coupling becomes strongly antiferromagnetic:

Table 3. Direct Exchange @ 2.0 Å		
S	E(cm^{-1})	J(cm^{-1})
3	1974	-164
2	808	-135
1	241	-121
0	0	

At this short distance there is significant deviation from Heisenberg coupling. Using our exponential parameters, we would have predicted $J=-144\ cm^{-1}$.

These calculations show conclusively that direct $d-d$ exchange interactions in bulk iron are antiferromagnetic. Thus, the magnetism of iron must be due to indirect exchange. We have looked at indirect exchange in the dimer by allowing the s-bond to spin polarize. The energies were obtained from (4/8)RCI's.

Table 4. Dimer Exchange @ 2.5 Å		
S	E(cm^{-1})	J(cm^{-1})
3	1280	-107
2	591	-99
1	188	-94
0	0	

The exchange we see here is the sum of direct and indirect effects. Indirect exchange is obviously antiferromagnetic and larger in magnitude than direct exchange at this distance. Allowing the s-pair to spin polarize has caused a deviation from Heisenberg coupling. If the s-pair had remained singlet or if the s-pair had spin polarized sufficiently that each

s orbital had coupled high-spin to its *d*-shell, Heisenberg coupling would have resulted. The valence *s* orbitals are more diffuse than the *d* orbitals. At this distance, the *s*–*s* overlap is sufficiently large to cause substantial singlet coupling of the *s*-pair. However, the *s*-pair will never be perfectly singlet coupled, because the atomic *s*–*d* exchange is large. Thus, Heisenberg coupling will be observed only at larger distance.

III. Calculational Details

The model we have chosen is perhaps the simplest possible to show the origins of magnetism in nickel. Ni_2 has localized *s* orbitals and so does not serve to model a metallic system. Ni_3 can have delocalized orbitals in the triangular geometry, but the *s* electrons can lead to spin polarization without indirect exchange. Hence, this system does not offer a useful model for magnetic coupling in metallic systems. However with Ni_4 we do find delocalized *s* orbitals coupled dominantly into a singlet. These bonding electrons correspond to the *s* band of metallic nickel. The geometry we have selected is a section of the *fcc* bulk. It is a rhombus having all four edges and the shorter diagonal equal to the bulk nearest-neighbor distance of 2.5 Å. McAdon and Goddard[3] have shown from extensive studies on Li_4 (and other metal clusters up to Li_{13}) that the bonding orbitals localize *between* atoms favoring a rhombic structure in order to maximize singlet pairing of these orbitals. We expect it also to be the best for Ni_4, because the *s* orbitals dominate the bonding, and indeed the final wavefunctions

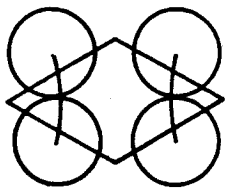

resemble those of Li_4. Thus, this model represents not only a section of the *fcc* bulk but also the best symmetry for Ni_4. In fact, it represents nearly the optimal geometry for Ni_4. Optimizing the scale of this cluster (uniform expansion) leads to an optimal nearest-neighbor distance of 2.5 Å, quite close to the value of bulk Ni (2.49 Å).

In our rhombohedral Ni_4 (D_{2h}) cluster, the spin coupling of the *s* electrons is singlet. The one-electron bond orbitals are coupled in singlet

pairs *parallel* to the shorter diagonal. This coupling induces strong indirect antiferromagnetic coupling between the d-holes across the shorter diagonal, but not between the d-holes across the longer diagonal. Consequently, the ground state at the optimal geometry for Ni_4 is triplet, which makes this cluster an ideal model for studying the origin of magnetism in nickel.

The assumption of d^9 character on each Ni is based on results of a series of calculations by the Goddard group, Ni_2,[4] $NiCH_2$,[5] and Ni(110) and Ni(111)[6] where clusters up to Ni_{18} show d^9 character on each metal. These ideas have also been confirmed by others, e.g. Basch, Newton, and Moskowitz[7] on square Ni_4. It should be noted that our basis is biased in favor of d^{10}(*vide infra*), yet the Ni_4 cluster still has d^9 character.

We find that the optimum four MO's for describing the s-space are (a_g, b_{1g}, b_{2u}, b_{3u}), which span the four irreducible representations expected from four bond functions, whereas (a_g, a_g, b_{2u}, b_{3u}) would be expected from a linear combination of s-orbitals. The antibonding orbital b_{1g} must be dominantly p. Because all the MO's are describing linear combinations of bond functions, each MO has appreciable p character, resulting in $4p$ orbitals being important to cluster cohesion energy.

For Ni_4 (D_{2h}), we find that the optimal d-holes span the symmetries (a_g, b_{3g}, a_u, b_{2u}).† We find that a single SCF with no symmetry restrictions can predict the optimal d-holes. The s-electrons are described with two GVB pairs, and the d-electrons are described with four average-field Hamiltonians, each having five orbitals. Each set of five orbitals becomes the five d's localized on a single nickel atom. The

† Basch, Newton, and Moskowitz found that the d-holes span the same irreducible representations as the s-orbitals for certain nickel clusters, specifically for Ni_4 (D_{4h}). However, we find that for our cluster, this is not true.

Hamiltonians correspond to the quintet coupling of the four d-holes in the average of all 5^4=625 configurations. The highest occupied eigenvector of each average-field Hamiltonian is taken to be the optimal d-hole on that nickel atom. The optimal d-holes across the shorter diagonal are d_{xz} so that they are δ with respect to that axis and antisymmetric upon reflection in the plane of the nuclei. These d-holes span the irreducible representations B_{3g} and A_u for D_{2h}. The optimal d-holes across the longer diagonal are $d_{x^2-y^2}$ so that they are δ with respect to that axis and symmetric upon reflection in the plane of the nuclei. These d-holes span the irreducible representations A_g and B_{2u}.

Table 5. Symmetries of MO's for Ni_4 (D_{2h})

orbitals	irreducible representations spanned			
s's	a_g	a_g	b_{2u}	b_{3u}
one-electron bonds	a_g	b_{1g}	b_{2u}	b_{3u}
optimal d-holes	a_g	b_{3g}	a_u	b_{2u}

We use several types of self-consistent muti-configurational wavefunctions. The best is often termed a Complete Active Space SCF (CASSCF). Here all eight active electrons (2 per nucleus) are described with a full CI in eight orbitals, and these orbitals are then calculated self-consistently. Four of these orbitals describe sp-like one-electron bonds between each metal (a_g,b_{1g},b_{2u},b_{3u}), and the other four orbitals describe localized d-holes, one on each metal, (a_g,b_{3g},a_u,b_{2u}). The other d-orbitals are taken as doubly-occupied but are solved for self-consistently along with the other orbitals. These CASSCF's give us our most reliable state energies. However, we would like wavefunctions with greater interpretability. We have found that very little energy penalty is paid to restrict all

configurations in our MCSCF to have four electrons in the four orbitals describing the one-electron bonds, two electrons in the two orbitals describing the d-holes across the shorter diagonal, and two electrons in the two orbitals describing the d-holes across the longer diagonal. This reduces the CASSCF wavefunction to the GVB form, allowing us to interpret the wavefunction. This permits us to evaluate quantitatively the spin-polarization of the s-space, as well as all transposition U_{ij}'s among the four d electrons. This interpretable wavefunction allows us not only to measure spin-polarization in the s-space but also to restrict the wavefunction to eliminate this spin coupling and hence evaluate its effect.

We should comment here on orthogonality restrictions. Orthogonality of orbitals that are doubly-occupied in all configurations of a wavefunction is justified by the Pauli Principle. However, one cannot in general require orthogonality of the orbitals unless a *complete* CI among these orbitals is included. Thus for the CASSCF, including as one does all allowed configurations among the non-doubly-occupied orbitals, orthogonality between the eight active orbitals is no restriction. However, when using only a subset of these CI configurations, the orthogonality of our orbitals can become a restriction. Thus when viewing our wavefunction in terms of one-electron orbitals, one might ask what orthogonality restrictions are being imposed on these one-electron orbitals. Fortunately, in the case of interest the symmetry is such that the d orbitals have no orthogonality restrictions. For the sp-bond space we include the full set of configurations, so we avoid possible orthogonality restrictions. The only restrictions remaining are between the d orbitals and the bond orbitals. These arise because we impose orthogonality between two a_g MO's (one d-like, one sp-bond like) and between two b_{2u} MO's (one d-like,

one sp-bond like). Thus, we artificially restrict the one-electron bonds to be orthogonal to the d-holes on the atoms defining the longer diagonal.

We should point out that at long distances, the s electrons localize on the atoms. This is seen in our calculations when a_g is preferred to b_{1g} as the antibonding MO. It is very important to choose the optimal antibonding MO, for it can completely alter the spectrum of states. We obtain totally different results at 3.5 Å with the two different antibonding MO's.

The Ar core of each Ni atom is replaced by an *ab initio* effective potential.[8] We use $4s$ and $4p$ basis sets contracted DZ (3,1) from four gaussians. These basis sets have previously been used with the nickel one-electron modified effective potential.[9] We use a d basis contracted MBS for d^{10} from five gaussians.[10] This basis favors the d^{10} state. The experimental splitting from the ground s^1d^9 state to the d^{10} state is 1.86 eV,[11] while the computed splitting with our basis is 1.79 eV. This good agreement is the result of our MBS d contraction for the d^{10} state. Numerical Hartree-Fock gives a splitting of 4.19 eV.[12] In our basis, the Hartree-Fock energy of ground-state Ni s^1d^9 is -38.9488788 h_0. Thus, the limit at infinite separation for our Ni_4 cluster is -155.795515 h_0.

IV. Results

A. State Energies

Prior to testing the optimal *d*-hole occupations, we followed the general findings of Basch, Newton, and Moskowitz. We assumed the *d*-holes to span the same irreducible representations as the *s*'s. For a general survey, we used a simple $^5B_{1g}$ SCF in which the MO's for the *d*-holes (a_g, a_g, b_{2u}, b_{3u}) were singly-occupied and the MO's for the one-electron bonds ($a_g, b_{1g}, b_{2u}, b_{3u}$) were given all symmetry-allowed occupations of four electrons. These eight MO's were used for CI calculations having all symmetry-allowed occupations of eight electrons in eight orbitals. These results are listed below:

Table 6. Preliminary SCF Energies (+155 h_0)

State	2.0 Å	2.5 Å	3.0 Å	3.5 Å
$^5B_{1g}$	-.849680	-.956066	-.866981	-.792058

Table 7. Preliminary CI Energies (+155 h_0)

State	2.0 Å	2.5 Å	3.0 Å	3.5 Å
$^1B_{1g}$	-.852085	-.956792	-.868555	-.793849
$^3B_{1g}$	-.851533	-.956948	-.868720	-.793980
$^3B_{3u}$	-.850892	-.957097	-.868884	-.794105
$^5B_{1g}$	-.850398	-.957257	-.869049	-.794232
^1A_g	-.852177	-.957710	-.869927	-.795445
$^3B_{2u}$	-.852247	-.957715	-.869927	-.795445

We obtained MCSCF wavefunctions corresponding to the above CI's:

Table 8. Preliminary SCF Energies (+155 h_0)				
State	2.0 Å	2.5 Å	3.0 Å	3.5 Å
$^1B_{1g}$	-.852679	-.957256	-.868627	-.793907
$^3B_{1g}$	-.851818	-.957459	-.868790	-.794047
$^3B_{3u}$	-.850974	-.957667	-.868953	-.794182
$^5B_{1g}$	-.850424	-.957889	-.869117	-.794317
^1A_g	-.852301	-.958517	-.870135	-.795722
$^3B_{2u}$	-.852368	-.958522	-.870135	-.795716†

Using the same MO's for the d-holes (a_g,a_g,b_{2u},b_{3u}), we tried using bonding MO's not for one-electron bonds but for localized s orbitals (a_g,a_g,b_{2u},b_{3u}). For all geometries, we optimized an MCSCF for ^5A_g with all symmetry-allowed occupations of eight electrons in eight orbitals. CI calculations for other symmetries were also obtained. We find that for distances as large as 3 Å, the six lowest-lying states correspond to one-electron bonds coupled ^1A_g. These are lower than the lowest state computed with MO's consistent with localized s orbitals. However, by 3.5 Å, we find that the six lowest-lying states correspond to localized s orbitals coupled $^1B_{1g}$. We show these six calculations at all distances:

† Note that the last entry in Table 8 is not fully converged. The converged energy should be -.795722, as evidenced by the preliminary CI energies in Table 7.

Table 9. s-Orbital CI Energies (+155 h_0)				
State	2.0 Å	2.5 Å	3.0 Å	3.5 Å
$^1B_{1g}$	-.824098	-.931062	-.852263	-.816672
$^3B_{2u}$	-.825176	-.931273	-.852694	-.817406
$^3B_{3u}$	-.823359	-.931788	-.852930	-.818295
^5A_g	-.822146	-.929325	-.856847	-.819115
^3A_g	-.816743	-.924978	-.856250	-.820840
^1A_g	-.825114	-.932099	-.855838	-.821573

Were it not for the bonding transition between 3.0 and 3.5 Å from delocalized one-electron bond orbitals to localized s orbitals, the cluster would remain ferromagnetic at large distances. However, with localized orbitals, the ground state is singlet. Unfortunately, our attempts at describing localized s orbitals at small distances have resulted in significant one-electron bond character.

At 2.5 Å, we used an average-field SCF to determine that the optimal d-holes do not span the same irreducible representations as the s orbitals. The optimal d-holes across the shorter diagonal span the irreducible representations B_{3g} and A_u. The optimal d-holes across the longer diagonal span the irreducible representations A_g and B_{2u}. We have performed three different MCSCF calculations for each of the six low-lying states at 2.5 Å. Each uses four MO's (a_g,b_{3g},a_u,b_{2u}) to describe the d-holes and four MO's (a_g,b_{1g},b_{2u},b_{3u}) to describe the one-electron bonds. In the first MCSCF, we use all symmetry-allowed configurations of eight electrons in these eight orbitals. In the second MCSCF, we include only the configurations having four electrons in the four MO's describing the one-electron bonds and two electrons in each pair of MO's describing the d-

holes across a diagonal. In the third MCSCF, we further restrict the four electrons in the one-electron bonds to be coupled singlet.

Table 10. Three SCF Energies (+155 h_0) @ 2.5 Å			
State	No Restrictions	Occupation Rest.	Occ + Spin Rest.
$^1B_{1g}$	-.960800	-.960595	-.959800
$^3B_{1g}$	-.961017	-.960809	-.959916
$^3B_{3u}$	-.961226	-.961018	-.960027
$^5B_{1g}$	-.961450	-.961249	-.960165
^1A_g	-.962803	-.962597	-.960063
$^3B_{2u}$	-.962809	-.962603	-.960074

Note that these six states are all lower than the lowest state having *d*-holes which span the same irreducible representations as the *s* orbitals. The occupation restrictions above can be seen to cost very little energy and to leave the relative energies of the states unchanged. These occupation restrictions permit a rigorous evaluation of the spin coupling among the *d* electrons as well as the spin polarization of the *s* electrons. Restricting the *s* electrons to be coupled singlet can be seen to change completely the relative energies of the states.

We can fit the energies of these states with effective Heisenberg coupling constants. The two lowest states are sufficient to find the coupling between *d*'s across the longer diagonal:

$$J_l = \tfrac{1}{2}[E(^1A_g) - E(^3B_{2u})]$$

The second and fourth lowest states are sufficient to determine the coupling between *d*'s across the shorter diagonal:

$$J_s = \tfrac{1}{2}[E(^1A_g) - E(^3B_{3u})]$$

The four lowest states are sufficient to determine all the couplings between the d's. The couplings between d's across each of the four edges are the same:

$$J_s = \tfrac{1}{2}[E(^3B_{2u}) - E(^1A_g) - E(^5B_{1g}) + E(^3B_{3u})]$$

The fifth state permits a check on the validity of J_s:

$$J_s' = \tfrac{1}{4}[E(^3B_{1g}) - E(^5B_{1g})]$$

The sixth state permits a second check on J_s:

$$J_s'' = \tfrac{1}{2}[E(^1B_{1g}) - E(^3B_{1g})]$$

Table 11. Heisenberg Coupling Constants (cm^{-1}) @ 2.5 Å			
Type	No Restrictions	Occupation Rest.	Occ + Spin Rest.
J_l	0.7	0.7	1.2
J_s	-173.1	-173.3	-4.0
J_s	23.9	24.7	13.9
J_s'	23.8	24.1	13.7
J_s''	23.8	23.5	12.7

We can see how these Heisenberg coupling constants vary with distance by using our preliminary SCF energies:

Table 12. Heisenberg Constants (cm^{-1}) from Preliminary SCF's				
Type	2.0 Å	2.5 Å	3.0 Å	3.5 Å
J_l	7.4	0.5	0.0	0.0
J_s	-145.6	-93.3	-129.7	-169.0
J_s	-67.7	23.8	18.0	14.8
J_s'	-76.5	23.6	17.9	14.8
J_s''	-94.5	22.3	17.9	15.4

The above coupling constants at 3.5 Å are for delocalized one-electron bonds. However, at this distance, the lowest states have localized s orbitals. To obtain the actual Heisenberg constants at 3.5 Å, we can use our s-orbital CI energies. Assuming the s orbitals are coupled $^1B_{1g}$ in each of the six lowest-lying states, we obtain the following equations for effective $d-d$ coupling constants:

$$J_l = \tfrac{1}{2}[E(^1B_{1g})-E(^3B_{3u})]$$

$$J_s = \tfrac{1}{2}[E(^1B_{1g})-E(^3B_{2u})]$$

$$J_e = \tfrac{1}{2}[E(^3B_{3u})-E(^1B_{1g})-E(^5A_g)+E(^3B_{2u})]$$

$$J_e' = \tfrac{1}{2}[E(^3A_g)-E(^5A_g)]$$

$$J_e'' = \tfrac{1}{2}[E(^1A_g)-E(^3A_g)]$$

Table 13. Heisenberg Constants (cm^{-1}) from s-Orbital CI's

Type	3.5 Å
J_l	178.1
J_s	80.5
J_e	9.4
J_e'	-94.6
J_e''	-80.4

It is clear that the singlet ground state at 3.5 Å is the result of an antiferromagnetic J_e. However, the discrepancies between our checks for J_e force us to question our assumption that the s's are coupled $^1B_{1g}$. We know that at very large distances, the s's will be extensively spin-polarized, because the lowest states will consist of triplet nickel atoms coupled in various ways. A significant component of this coupling is com-

plicating our simplistic analysis at 3.5 Å.

Let us assume for the moment that the lowest states at 3.5 Å are dominantly triplet nickel atoms coupled in various ways. The lowest three states (^1A_g, ^3A_g, and ^5A_g) form an antiferromagnetic Heisenberg spectrum:

$$E = a - JS(S+1)$$

The lowest two states yield $J = -80.4\ cm^{-1}$. Note that this value was previously obtained as

$$J_e'' = \tfrac{1}{2}[E(^1A_g) - E(^3A_g)]$$

The second and third lowest states yield $J = -94.6\ cm^{-1}$. Note that this value was previously obtained as

$$J_e' = \tfrac{1}{4}[E(^3A_g) - E(^5A_g)]$$

The only way to obtain ^3A_g is to couple the triplet atoms into quintets across each diagonal, and then to couple the two quintets into an overall triplet. Given the Heisenberg spectrum of these states, the spin coupling must be similar for all three states. The ^1A_g ground state must be dominantly coupled into quintets across each diagonal, singlet overall. Although triplet atoms coupled into singlets across each diagonal would have the same symmetry, this coupling must be negligible. The ^5A_g excited state must be dominantly coupled into quintets across each diagonal, quintet overall. Although two other couplings with singlet coupling across one diagonal and quintet coupling across the other would have the same symmetry, these couplings must make only minor contributions.

What exactly is our Heisenberg coupling constant J? The three lowest states have two sets of four high-spin electrons coupled into overall singlet, triplet, and quintet. The constant J which gives the

relative energies of these states

$$E = a - JS(S+1)$$

is simply the average of all sixteen exchange constants between the two sets of four high-spin electrons. Each set of electrons contains the s and unpaired d on each of the two atoms across one diagonal. The sixteen exchange constants between the two sets include four $d-d$ interactions, four $s-s$ interactions, and eight $s-d$ interactions. All of these interactions are along the edges of the cluster, so our constant J is really J_e. Note that this interpretation of J maps into the interpretation of J_e as an effective Heisenberg coupling between d's with the s's coupled dominantly $^1B_{1g}$. At long distances, the spins of the d's cannot move independently from the spins of the s's. For all low-lying states, each unpaired d must remain parallel to the s on the same atom. Thus, a formal Heisenberg coupling between d's is really an effective Heisenberg coupling between triplet s^1d^9 units.

Let us now view the exchange force responsible for the ferromagnetic nature of our cluster at small distances and the antiferromagnetic nature at large distances:

Table 14. Exchange Coupling (cm^{-1}) vs. Atomic Separation

Type	2.0 Å	2.5 Å	3.0 Å	3.5 Å	∞
J_e	-68	24	18	-80	0

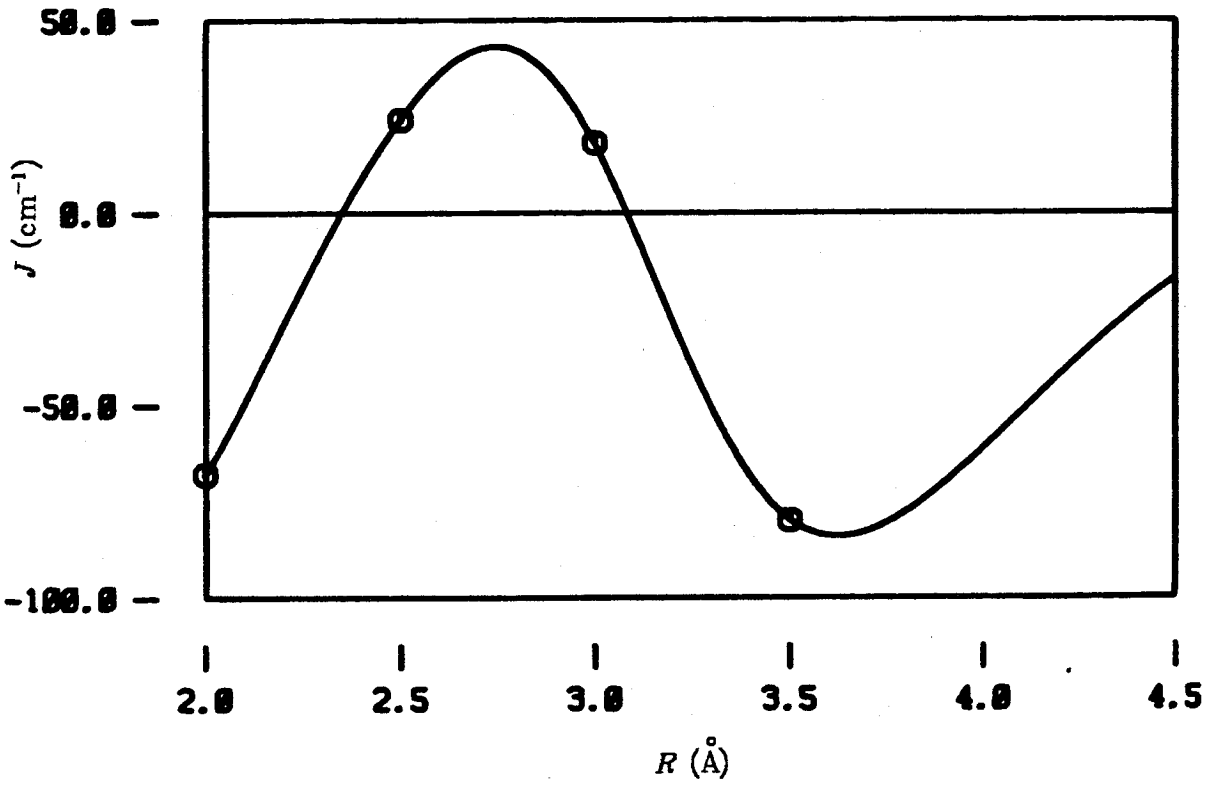

Figure 2. J (exchange coupling) versus R (atomic separation).

B. Spin Coupling

Ideal Heisenberg couplings are given below for each of the six low-lying states of our cluster.

Table 15. Ideal Heisenberg Couplings

State	U_e	U_s	U_t
$^1B_{1g}$	+½	-1	-1
$^3B_{1g}$	0	-1	-1
$^3B_{3u}$	−½	-1	+1
$^5B_{1g}$	-1	-1	-1
^1A_g	−½	+1	+1
$^3B_{2u}$	−½	+1	-1

The actual couplings are very close to ideal:

Table 16. Actual $d-d$ Couplings

State	U_e	U_s	U_t
$^1B_{1g}$	+.493	-.986	-1.000
$^3B_{1g}$	-.005	-.981	-.999
$^3B_{3u}$	-.500	-.977	+.999
$^5B_{1g}$	-.993	-.974	-1.000
^1A_g	-.500	+.951	+.999
$^3B_{2u}$	-.497	+.952	-1.000

The discrepancies arise because of spin-polarization of the s-space:

Table 17. Spin-Polarization of s-Space

State	$\langle\hat{S}^2\rangle_{tot}$	$\langle\hat{S}^2\rangle_d$	$\langle\hat{S}^2\rangle_s$
$^1B_{1g}$	0	.014	.014
$^3B_{1g}$	2	1.999	.019
$^3B_{3u}$	2	1.978	.023
$^5B_{1g}$	6	5.947	.027
^1A_g	0	.049	.049
$^3B_{2u}$	2	2.037	.049

Note that the spin moments of the d and s spaces can be parallel, antiparallel, or orthogonal. We shall investigate the origin of each case shortly.

The spin-polarization of the s-space occurs by mixing in configurations having triplet coupling in the s-space. If the density of configurations having singlet coupling is ρ_1 and the density of configurations having triplet coupling is ρ_2, then

$$\langle\hat{S}^2\rangle_s = 0\rho_1 + 2\rho_2$$

We take the total wavefunction to be an eigenfunction of spin.

$$\langle\hat{S}^2\rangle_{tot} = S(S+1)$$

If the triplet excitation in the s-space leaves the spin of the d's unchanged,

$$\begin{aligned}\langle\hat{S}^2\rangle_d &= S(S+1)\rho_1 + S(S+1)\rho_2 \\ &= S(S+1)\end{aligned}$$

then the spin moment of the s-space neither adds to nor subtracts from the spin moment of the d-space. We say that the moments are orthogonal, although we do not mean that the spin vectors are at a right angle.

This would lead to

$$\langle \hat{S}^2 \rangle_{tot} = \langle \hat{S}^2 \rangle_d + \langle \hat{S}^2 \rangle_s$$

If the triplet excitation in the s-space is accompanied by a simultaneous increase in the spin of the d's,

$$\begin{aligned} \langle \hat{S}^2 \rangle_d &= S(S+1)\rho_1 + (S+1)(S+2)\rho_2 \\ &= S(S+1) + 2(S+1)\rho_2 \end{aligned}$$

then the s and d moments are antiparallel. If the triplet excitation in the s-space is accompanied by a simultaneous decrease in the spin of the d's,

$$\begin{aligned} \langle \hat{S}^2 \rangle_d &= S(S+1)\rho_1 + (S-1)S\rho_2 \\ &= S(S+1) - 2S\rho_2 \end{aligned}$$

then the s and d moments are parallel. In all cases except the ground state, the mechanism of spin-polarization is cleanly one of the three mechanisms.

Table 18. Spin-Polarization of s-Space

State	$\langle \hat{S}^2 \rangle_{tot}$	$\langle \hat{S}^2 \rangle_d$	$\langle \hat{S}^2 \rangle_s$
$^1B_{1g}$	0	$0+2\rho_2$	$2\rho_2$
$^3B_{1g}$	2	$2+0\rho_2$	$2\rho_2$
$^3B_{3u}$	2	$2-2\rho_2$	$2\rho_2$
$^5B_{1g}$	6	$6-4\rho_2$	$2\rho_2$
^1A_g	0	$0+2\rho_2$	$2\rho_2$
$^3B_{2u}$	2	$2+?\,\rho_2$	$2\rho_2$

Moreover, each observed d-d coupling for a given state is simply ρ_1 times the ideal coupling for that state symmetry plus ρ_2 times the ideal coupling for a second symmetry:

Table 19. Actual d–d Couplings

State	U_e	U_s	U_t
$^1B_{1g}$	$+\frac{1}{2}\rho_1-\frac{1}{2}\rho_2$	$-1\rho_1+1\rho_2$	-1
$^3B_{1g}$	$0\rho_1-\frac{1}{2}\rho_2$	$-1\rho_1+1\rho_2$	-1
$^3B_{3u}$	$-\frac{1}{2}$	$-1\rho_1+1\rho_2$	+1
$^5B_{1g}$	$-1\rho_1-\frac{1}{2}\rho_2$	$-1\rho_1+1\rho_2$	-1
^1A_g	$-\frac{1}{2}$	$+1\rho_1-1\rho_2$	+1
$^3B_{2u}$	$-\frac{1}{2}\rho_1+?\,\rho_2$	$+1\rho_1-1\rho_2$	-1

The second symmetry is related to the first simply by a change in the sign of U_s. We shall see that this is the result of a simultaneous triplet excitation of a singlet pair of one-electron bonding orbitals coupled parallel to the shorter diagonal. The spatial symmetry of the second state is related to the first by a change in the parity of reflection in the plane perpendicular to the shorter diagonal. The value of U_t remains unchanged. For all states except the ground state, the change in sign of U_s uniquely defines the spin symmetry of the second state.

For the ground state, the change in sign of U_s yields three possible spins for the d's: 0, 1, and 2, with U_s = +½, 0, and -1, respectively. Each of these states contributes a fraction to the density ρ_2:

$$\rho_2 = f_0+f_1+f_2$$

We have two other relationships for these fractions:

$$\langle\hat{S}^2\rangle_d = 2-2f_0+0f_1+4f_2$$

and

$$U_s = -\tfrac{1}{2}\rho_1+\tfrac{1}{2}f_0+0f_1-1f_2$$

Unfortunately, these two relationships are linearly dependent. Thus,

each fraction cannot be uniquely determined from these data.

V. Discussion

A. Exchange Coupling Constants

In this system, we have one unpaired *d* electron on each of four centers. These *d* electrons are well localized, and the interatomic overlaps between them are very small. This situation is ideal for describing all low-lying states with a model Heisenberg Hamiltonian:

$$\hat{H}_{eff} = -2\sum_{i>j} J_{ij}\hat{s}_i\cdot\hat{s}_j$$

If we include all six J_{ij}'s between the four unpaired *d* electrons, then we should be able to describe the energetics of all low-lying states: two singlets, three triplets, and one quintet. Because of symmetry, we have only three different J_{ij}'s. The exchange coupling along each edge, J_e, is the same. The exchange across the shorter diagonal, J_s, and the exchange across the longer diagonal, J_l, are different.

We have calculated all six low-lying states, and we find that their energies are fit precisely with the following couplings: J_e=24 cm^{-1} (ferromagnetic), J_s=−173 cm^{-1} (strongly antiferromagnetic), and J_l=0.7 cm^{-1} (negligible). These couplings are significant because they give an indication of why nickel is ferromagnetic and why nickel has only about half a magnetic electron per center. We wish to learn what causes each of these couplings.

An explanation of how these constants were fit is in order. The expectation value for transposing the spatial coordinates of two electrons shall be denoted as U_{ij}. Using the relation

$$U_{ij} = -\tfrac{1}{2}-2\langle\hat{s}_i\cdot\hat{s}_j\rangle$$

we can write the expectation value of the Heisenberg Hamiltonian

(shifted by a constant energy) as

$$E_{eff} = \sum_{i>j} J_{ij} U_{ij}$$

By symmetry, the U_{ij}'s for each of our six low-lying states are fixed. The spatial wavefunction must be either symmetric or antisymmetric to reflection in each of the three planes of symmetry. Reflection in the plane of the electrons leaves the wavefunction unchanged. One reflection transposes two electrons across the shorter diagonal, so $U_s=\pm 1$. Another reflection transposes two electrons across the longer diagonal, so $U_l=\pm 1$. Given that two electrons, 1 and 2, are triplet coupled ($U_{12}=-1$), then for any third electron, $U_{13}=U_{23}$. Given that two electrons, 1 and 2, are singlet coupled ($U_{12}=+1$), then for any third electron, $U_{13}=U_{23}=-\frac{1}{2}$. For a given state, the coupling across each diagonal is either singlet or triplet, so the couplings along each edge U_e must be equal. When one of the diagonal couplings is singlet, $U_e=-\frac{1}{2}$. When both diagonal couplings are triplet, $U_e=-1,0,+\frac{1}{2}$ for total spin quintet, triplet, and singlet, respectively.

We find that three constants J_e, J_s, and J_l make a good fit to the relative energies of our six states (a fit of five values with three parameters). These constants are not simply parameters to fit energies. These couplings really do represent to a good approximation the actual forces encountered when changing the relative orientations of these four spins. However, these couplings need not be the result of direct exchange forces between the d's. The s's do not remain perfectly singlet and totally symmetric. They spin polarize slightly in response to the various orientations of the four d spins. The s space remains over 97% singlet in each of the six low-lying states, so the magnitude of spin polarization is quite small. However, the magnitude of this effect on our observed coupling constants remains to be determined. The actual U_{ij}'s between the d's deviate only

slightly (at most 5%) from our predictions based on a totally symmetric singlet *s* space. Thus, our model Heisenberg wavefunctions are fairly accurate representations of the spin coupling among the *d*'s in these states, and our coupling constants based on this model are fairly accurate representations of the actual forces encountered when changing the relative orientations of the *d* spins.

We wish to determine how much of our observed coupling constants is the result of direct exchange forces between the *d*'s and how much is the result of indirect exchange through spin polarization of the *s*-space. We can eliminate the possibility of indirect exchange by restricting the *s*-space to be rigorously singlet coupled (see Appendix E). We have calculated SCF wavefunctions with perfectly singlet *s* electrons for all six low-lying states. The energies of these restricted wavefunctions are accurately given by the following couplings: $J_a = 14\ cm^{-1}$ (ferromagnetic), $J_s = -4\ cm^{-1}$ (negligible), and $J_l = 1.2\ cm^{-1}$ (negligible). These couplings are the direct exchange interactions between the *d*'s. The only significant value is the ferromagnetic exchange along each edge.

The differential energies of our *un*restricted wavefunctions are the result of direct exchange forces between the *d*'s plus indirect exchange forces which arise through the spin polarization of the *s*'s. We can describe the combined effect of direct and indirect exchange with three coupling constants. The differential energies of our restricted wavefunctions with singlet *s*'s are the result of direct exchange only. The three coupling constants that describe these energies are the direct exchange interactions between the *d*'s. We can obtain the indirect exchange interactions between the *d*'s as the total exchange minus the direct exchange. The indirect exchange couplings are: $J_a = 10\ cm^{-1}$ (fer-

romagnetic), J_s=−169 cm^{-1} (strongly antiferromagnetic), and J_l=−0.5 cm^{-1} (negligible). Thus, indirect exchange accounts for all the strongly antiferromagnetic force across the shorter diagonal. Indirect exchange also accounts for about half the ferromagnetic force along each edge of the cluster.

Table 20. Measured Exchange (Total = Direct + Indirect)

Type	Total	Direct	Indirect
J_e(cm^{-1})	24	14	10
J_s(cm^{-1})	-173	-4	-169
J_l(cm^{-1})	0.7	1.2	-0.5

We observe two types of indirect exchange in this cluster. A very strong antiferromagnetic indirect exchange occurs across the shorter diagonal, and a much weaker ferromagnetic indirect exchange occurs along each edge. We wish to understand the mechanism that gives rise to each type of indirect exchange. Qualitatively, we can describe the mechanism for each of these effects with simple vector diagrams.

Consider first the indirect ferromagnetic coupling. Two *d* electrons which favor parallel spins with the same *s* electron indirectly favor parallel spins with each other:

$$d(\uparrow)\text{----}s(\uparrow)\text{----}d(\uparrow)$$

In our wavefunctions, the *d* electrons do favor parallel spins with neighboring *s* electrons. However, note that indirect ferromagnetic coupling would still result if the *d* electrons were to favor antiparallel spins with neighboring *s* electrons.

$$d(\uparrow)\text{----}s(\downarrow)\text{----}d(\uparrow)$$

Thus, two d's which interact with the same s electron will indirectly favor ferromagnetic coupling.

Consider now the indirect antiferromagnetic coupling. Two d electrons which favor parallel spins with s electrons favoring antiparallel spins indirectly favor antiparallel spins with each other:

$$d(\uparrow)----s(\uparrow)----s(\downarrow)----d(\downarrow)$$

As before, the same antiferromagnetic coupling would result even if the d electons favored antiparallel spins with neighboring s's.

$$d(\uparrow)----s(\downarrow)----s(\uparrow)----d(\downarrow)$$

Thus, two d's which interact through an antiferromagnetic pair of s electrons will indirectly favor antiferromagnetic coupling.

In order to understand the indirect exchange in our cluster, we must first know the location of the bonding s electrons and how they are coupled. In this cluster, the four s electrons are delocalized from the nuclei and make one-electron bonds across the four edges. These one-electron orbitals are coupled into singlet pairs parallel to the shorter diagonal. The indirect J_s is ferromagnetic, because the two d's defining each edge interact with the one-electron bond between them. The indirect J_s is antiferromagnetic, because the two d's defining the shorter diagonal interact through the two singlet pairs of one-electron orbitals parallel to the shorter diagonal.

Now let us consider these indirect mechanisms in a more precise way. We wish to understand why the indirect antiferromagnetic exchange in our cluster is an order of magnitude stronger than the indirect ferromagnetic exchange. We need to know the relative magnitudes of indirect exchange to be expected from different mechanisms in order to

predict which effects will dominate in other systems.

Consider first the indirect antiferromagnetic coupling. We shall see what indirect exchange results when two d's interact through an antiferromagnetic pair of s electrons:

$$d_1 - - (J_{sd}) - - s_1 - - (J_{ss}) - - s_2 - - (J_{sd}) - - d_2$$

The energy difference between singlet and triplet states will be twice the indirect exchange. To solve for the optimal singlet, we choose the following basis:

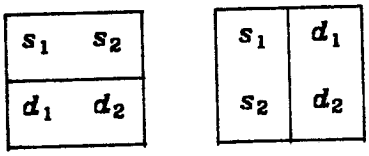

In this basis, the Hamiltonian matrix is

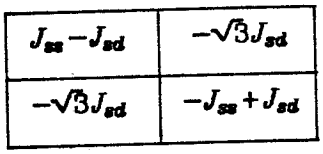

The energy of the optimal singlet is

$$E(S=0) = -\sqrt{(\bar{J}_{ss}-\bar{J}_{sd})^2+3(\bar{J}_{sd})^2}$$

To solve for the optimal triplet, we choose the following orthogonal basis:

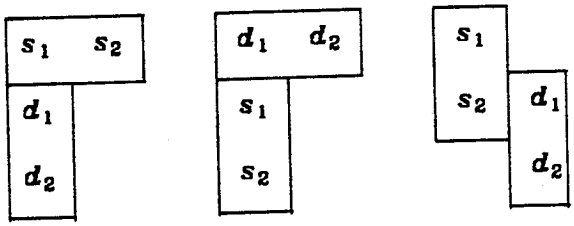

Note that

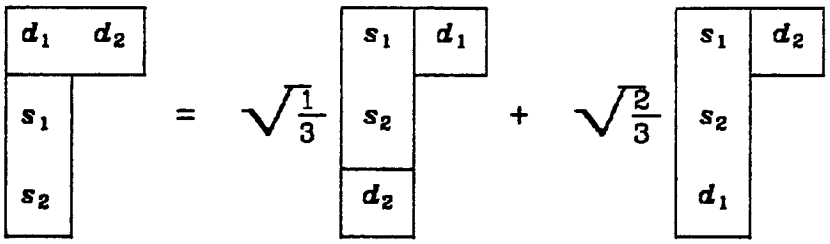

and that

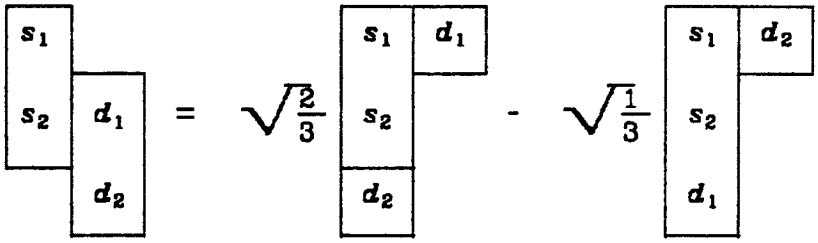

We have chosen this basis because it simplifies the Hamiltonian matrix:

$J_{ss}-J_{sd}$	$-J_{sd}$	0
$-J_{sd}$	$-J_{ss}-J_{sd}$	0
0	0	$-J_{ss}$

The energy of the optimal triplet is

$$E(S=1) = -J_{sd}-\sqrt{(J_{ss})^2+(J_{sd})^2}$$

To calculate the indirect exchange J_{dd} between d_1 and d_2, we take

$$J_{dd} = \tfrac{1}{2}[E(S=0)-E(S=1)]$$

However, rather than using the precise energy expressions, let us use our knowledge of the relative magnitudes of these exchanges to obtain simpler energy expressions. The s electrons are assumed to be strongly antiferromagnetic, so they want to be singlet coupled. Thus, the first function in our chosen basis set should dominate for both singlet and triplet. Note that when the s's are perfectly singlet coupled, the singlet and triplet states are degenerate. (Observe that the first matrix element in each Hamiltonian is $J_{ss}-J_{sd}$.) Both singlet and triplet states obtain lower

energy by spin-polarizing the s's. This involves mixing in an excited state with the s's triplet coupled. This excitation energy is roughly twice the magnitude of J_{ss}, and we assume it to be very large compared with the magnitude of of J_{sd}. For both singlet and triplet, we shall approximate the energy lowering as the square of the off-diagonal Hamiltonian matrix element connecting the two states divided by the excitation energy. The approximate energy of the singlet is

$$E(S=0) \approx J_{ss} - J_{sd} - \frac{3(J_{sd})^2}{-2J_{ss}+2J_{sd}}$$

The approximate energy of the triplet is

$$E(S=1) \approx J_{ss} - J_{sd} - \frac{(J_{sd})^2}{-2J_{ss}}$$

Thus, the approximate indirect exchange is

$$J_{dd} \approx -\frac{(J_{sd})^2}{-2J_{ss}}$$

Note that we have about the same antiferromagnetic J_{dd} whether $J_{sd}<0$ or $J_{sd}>0$. (However, our results show that changing the sign of J_{sd} does not give exactly the same J_{dd}. For negative J_{sd}, the indirect coupling should be stronger.)

We should remark that our approximate results equate to second-order perturbation theory. The indirect exchange calculated by Ruderman and Kittel is similarly based on second-order perturbation theory, but only excitations of the conduction electrons were considered by them.[13] Note that in our model, both s and d electrons are excited.

Consider now the indirect ferromagnetic coupling. We shall calculate what indirect exchange results when two d's interact with the same s electron. We recognize that this s is a member of an antiferromagnetic

pair of s electrons:

$$s_1\text{--}(J_{ss})\text{--}s_2$$

However, only one of the s's interacts with the two d's:

$$d_1\text{--}(J_{sd})\text{--}s_2\text{--}(J_{sd})\text{--}d_2$$

Again, the energy difference between singlet and triplet states will be twice the indirect exchange. To solve for the optimal singlet, we use the following basis:

s_1	s_2
d_1	d_2

s_1	d_1
s_2	d_2

In this basis, the Hamiltonian matrix is

$J_{ss}-J_{sd}$	0
0	$-J_{ss}+J_{sd}$

Thus, the energy of the optimal singlet is simply

$$E(S=0) = J_{ss}-J_{sd}$$

There is no spin-polarization of the s's. To solve for the optimal triplet, we use the following basis:

s_1	s_2
d_1	
d_2	

s_1	
s_2	d_1
	d_2

d_1	d_2
s_1	
s_2	

The second and third functions have been previously defined. Their order has been reversed here to factor the Hamiltonian matrix:

$J_{ss}-J_{sd}$	$\sqrt{2}J_{sd}$	0
$\sqrt{2}J_{sd}$	$-J_{ss}$	0
0	0	$-J_{ss}-J_{sd}$

The energy of the optimal triplet is

$$E(S=1) = -\tfrac{1}{2}J_{sd} - \sqrt{(J_{ss}-\tfrac{1}{2}J_{sd})^2 + 2(J_{sd})^2}$$

As before, the indirect exchange J_{dd} between d_1 and d_2 is

$$J_{dd} = \tfrac{1}{2}[E(S=0)-E(S=1)]$$

The s's do not spin-polarize in the singlet state, so the energy remains

$$E(S=0) = J_{ss}-J_{sd}$$

The triplet state does obtain energy lowering by mixing in an excited configuration in which the s's are triplet coupled. We can approximate the energy lowering as the square of the off-diagonal Hamiltonian matrix element connecting the two configurations divided by the exitation energy. The approximate energy of the triplet is

$$E(S=1) \approx J_{ss}-J_{sd}-\frac{2(J_{sd})^2}{-2J_{ss}+J_{sd}}$$

Thus, the approximate indirect exchange is

$$J_{dd} \approx +\frac{(J_{sd})^2}{-2J_{ss}}$$

Note that here too we have nearly the same ferromagnetic J_{dd} whether $J_{sd}<0$ or $J_{sd}>0$. (As before, our results show that changing the sign of J_{sd} results in slightly different J_{dd}. A negative J_{sd} should yield slightly stronger indirect coupling.)

At this point, we must recognize that our model gives the same magnitude of indirect exchange for both ferromagnetic and

antiferromagnetic mechanisms. However, in our cluster, we observe indirect antiferromagnetic exchange an order of magnitude stronger than the indirect ferromagnetic exchange. Why is there a discrepancy?

In our cluster, the indirect ferromagnetic exchange is complicated by the fact that not just one of the antiferromagnetic pair of s electrons interacts with the two d's. One of the d's interacts with just one s electron:

$$s_1\text{--}(J_{ss})\text{--}s_2\text{--}(J_{sd})\text{--}d_1$$

However, the other d interacts symmetrically with both s's:

$$s_1\text{--}(J_{sd}')\text{--}d_2\text{--}(J_{sd}')\text{--}s_2$$

We shall distinguish between the different J_{sd} interactions, because we shall find that J_{sd} will be responsible for the same second-order energy lowering in both singlet and triplet, whereas J_{sd}' will have no effect through second-order. Moreover, in our cluster, J_{sd} and J_{sd}' are not required to have exactly the same values. We solve for the optimal singlet with the following basis:

s_1	s_2
d_1	d_2

s_1	d_1
s_2	d_2

In this basis, the Hamiltonian matrix is

$J_{ss}-\frac{1}{2}J_{sd}-J_{sd}'$	$\frac{\sqrt{3}}{2}J_{sd}$
$\frac{\sqrt{3}}{2}J_{sd}$	$-J_{ss}+\frac{1}{2}J_{sd}+J_{sd}'$

To solve for the optimal triplet, we use the standard basis:

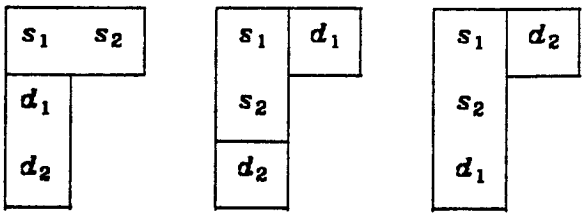

In this basis, only one excited configuration interacts directly with the first. The Hamiltonian matrix is

$J_{ss}-\frac{1}{2}J_{sd}-J_{sd}'$	$\frac{\sqrt{3}}{2}J_{sd}$	0
$\frac{\sqrt{3}}{2}J_{sd}$	$-J_{ss}+\frac{1}{2}J_{sd}-\frac{5}{3}J_{sd}'$	$-\frac{2\sqrt{2}}{3}J_{sd}'$
0	$-\frac{2\sqrt{2}}{3}J_{sd}'$	$-J_{ss}-J_{sd}+\frac{2}{3}J_{sd}'$

Looking at the singlet Hamiltonian matrix, we see that the second-order energy is

$$E(S=0) \approx J_{ss}-\tfrac{1}{2}J_{sd}-J_{sd}'-\frac{\tfrac{3}{4}(J_{sd})^2}{-2J_{ss}+J_{sd}+2J_{sd}'}$$

Looking at the triplet Hamiltonian matrix, we see that the second-order energy is

$$E(S=1) \approx J_{ss}-\tfrac{1}{2}J_{sd}-J_{sd}'-\frac{\tfrac{3}{4}(J_{sd})^2}{-2J_{ss}+J_{sd}-\frac{2}{3}J_{sd}'}$$

To the order of this analysis, $J_{dd}=0$. If $J_{sd}'>0$, as it is in our wavefunctions, then we see that the triplet state is slightly more stable than the singlet. The triplet state also has additional energy stabilization from the third configuration, which does not contribute to second-order. Thus, we expect a weak indirect ferromagnetic J_{dd}.

To understand why the ferromagnetic indirect exchange is so weak, we should consider the fact that only J_{sd} is responsible for the second-order energy lowering of both singlet and triplet. Through

second-order, J_{sd}' has no effect on the energy lowering. Our results show that when a d interacts symmetrically with two antiferromagnetic s's, the spin-polarization of those s's cannot make the sum of those interactions more favorable through second-order. Thus, the J_{sd}' interactions in our model are largely impotent. In fact, if we entirely eliminate the J_{sd}' interactions, we find that the singlet and triplet Hamiltonian matrices become identical (the triplet matrix rigorously factoring into a 2x2 and 1x1). Since d_2 no longer interacts with the other three electrons, the singlet matrix and triplet matrix each reduce to the same three-electron doublet matrix. In our model, we see that the two J_{sd}' interactions actually cancel. Consider first all the interactions:

$$s_1\text{--}(J_{ss})\text{--}s_2\text{--}(J_{sd})\text{--}d_1$$

and

$$s_1\text{--}(J_{sd}')\text{--}d_2\text{--}(J_{sd}')\text{--}s_2$$

If we eliminate the J_{sd}' interaction between d_2 and s_2, we are left with

$$d_2\text{--}(J_{sd}')\text{--}s_1\text{--}(J_{ss})\text{--}s_2\text{--}(J_{sd})\text{--}d_1$$

which yields a second-order antiferromagnetic J_{dd}. If we eliminate the J_{sd}' interaction between d_2 and s_1, we have

$$s_1\text{--}(J_{ss})\text{--}s_2$$

and

$$d_2\text{--}(J_{sd}')\text{--}s_2\text{--}(J_{sd})\text{--}d_1$$

which yields a second-order ferromagnetic J_{dd}. The interaction between d_2 and s_1 yields an indirect antiferromagnetic J_{dd}, and the interaction between d_2 and s_2 yields an indirect ferromagnetic J_{dd}. To second order in energy, these interactions cancel. (To higher order, J_{dd} is

ferromagnetic.) Thus, the spin-polarization of two antiferromagnetic *s*'s cannot yield a strong indirect exchange interaction between two *d*'s if one of the *d*'s has the same interaction with both *s*'s.

B. Exchange Coupling vs. Distance

In 1930, Slater[1] proposed that the exchange coupling responsible for ferromagnetism is zero at infinite internuclear distance, reaches a maximum as internuclear distance is decreased, then goes to zero and changes sign. In 1951, Zener[14] proposed that this change in sign results because direct exchange dominates at small distance while indirect exchange dominates at large distance. Zener thought that indirect coupling via the conduction electrons was always positive. However, we find that at large distance, the indirect coupling is negative. Thus, as internuclear distance is increased, the exchange coupling goes from negative to positve to negative, approaching zero as $R \rightarrow \infty$.

Ruderman and Kittel have shown that indirect exchange can be positive or negative. The RKKY interaction is oscillatory, being positive at small distance, oscillating between negative and positive at larger distances, approaching zero as $R \rightarrow \infty$. However, the the change in sign we see at large distance is not due to this effect. In our cluster, the indirect exchange changes in sign only once. This sign change arises from a localizing of the bonding orbitals onto each atom as the internuclear distance is increased. This bonding transition in our cluster corresponds to the Mott transition between conductor and insulator.

We have seen that the ground state of our model cluster is $S=1$, even though ferromagnetic coupling of all four d^9 centers would result in $S=2$. We have seen how the dominant resonance bonding structure gives the observed spin coupling of the d's via an indirect mechanism. For the solid (fcc) structure, we propose that dominant resonance bonding structures would also give less than maximal spin coupling of the d's. Of course, the resonant combination of all bonding structures would give a

symmetric coupling of all centers, such that all centers would be equivalent, each having partial magnetic and partial nonmagnetic character.

The magnetism of the iron transition series has been thought inconsistent with localized spins, since the number of Bohr magnetons per atom is usually far from integer. This thinking is the result of the limited conceptual model afforded by Hartree-Fock theory. The unfilled *d*-shells do not have to be coupled to maximal spin (ferromagnetic) or to minimal spin (antiferromagnetic). The ground state could be coupled to less than maximal spin and still be ferromagnetic.

The relative orientation of the magnetic moments of the *s* and *d* spaces is a matter of some theoretical controversy. Zener[14] predicted that the coupling between conduction electrons and inner-shell *d* electrons is ferromagnetic. This is based on the positive exchange integral between atomic *s* and *d* orbitals. However, the R.K.K.Y. effect[15] predicts the interaction to be antiferromagnetic. Viewing the conduction band as having 'up' and 'down' spin electrons, and the *d*-states as having excess 'up' electrons, the 'down' spin *s*-electrons are more stabilized by virtual excitations into the empty *d*-states. Hence, the *s* and *d* spaces are predicted to favor antiparallel spins.

For the iron group metals, the magnetic moment of the conduction band is parallel to that of the *d* electrons. For the rare earth metals, the conduction-band moment is antiparallel to that of the *f* electrons. Hence, neither of the above theories is totally correct. Our calculations show that both parallel and antiparallel moments can result. We have analyzed our calculations to determine what conditions give each case.

In our wavefunctions, the *s* and *d* spaces can be taken orthogonal

with very little energy loss and without changing the relative energies of the low-lying states. In these restricted calculations, the *s* and *d* character is allowed to mix via hybridization, but the orbitals of one space are orthogonal to the orbitals of the other, and the electrons of one space are not allowed to excite into the other space. Thus, the local interaction between *s* and *d* spaces must be ferromagnetic. However, the total magnetic moments of the two spaces are not necessarily parallel. We find that the orientation of the two moments depends on the character of *s*–*d* correlations responsible for spin polarizing the *s* space. An excitation which increases the spin of the *s* space but leaves the spin of the *d* space unchanged will yield orthogonal *s* and *d* moments. An excitation which increases the spin of the *s* space but decreases the spin of the *d* space will yield parallel moments. An excitation which simultaneously increases the spin of the *s* and *d* spaces will yield antiparallel moments. Note that antiparallel moments can occur only when the *d* space is coupled to less than maximal spin.

Consider now extrapolating our results for this cluster to other clusters, and finally to infinite latices. Using the elementary mechanisms of indirect exchange we found in our cluster, we can predict the magnetic properties of other systems. The biggest problem we will have is deciding which resonanting valence bond structures of the *s*-space will dominate.

General statements can be made regarding the magnetic properties of any cluster. At large internuclear separation, the *s* electrons localize on each center. The largest interaction is the ferromagnetic *s*–*d* exchange on each atom. The next largest interaction is the antiferromagnetic *s*–*s* exchange between atoms. Since the *s* and *d* spins on each atom stongly favor parallel orientation, the antiferromagnetic exchange

between *s* electrons on different atoms yields an antiferromagnetic cluster. As the internuclear distance is decreased, the *s* electrons delocalize to give the possibility of indirect ferromagnetic interactions between *d*'s. In general, the centers will not be totally ferromagnetic. Only centers related by spatial symmetry must have the same percent magnetic and nonmagnetic character. To predict the dominant character of each center, one can look at the dominant bonding configuration(s) and apply the indirect exchange mechanisms we learned from Ni_4.

Consider an infinite chain of nickel atoms. At long internuclear distance, the *s* electrons will localize on each atom, and the chain will be nonferromagnetic. At smaller internuclear distance, the *s* electrons will delocalize and form one-electron bonds between the atoms. If the internuclear distance is not too small, indirect exchange will dominate. We can assess the magnetic properties of this chain by looking at the dominant interactions. Our view of indirect exchanges in this system is radical in two respects. First, we view nearest neighbor interactions alone as inadequate to model ferromagnetism. Second, we find that next-nearest neighbor interactions are ***stronger*** than nearest neighbor interactions. In fact, we find that antiferromagnetic next-nearest neighbor exchanges are an order of magnitude stronger than ferromagnetic nearest neighbor exchanges. Assuming the nearest neighbor exchange to be a perturbation on the next-nearest neighbor exchange, we predict the *d*-cores to be spin-coupled into two singlet next-nearest neighbor chains. Thus, a chain of nickel atoms will be singlet.

This view of a chain of nickel atoms is supported by model Heisenberg Hamiltonian calculations. We have considered rings of spin 1/2 *d*-cores bound together by one-electron bonds. The one-electron bonds

have nearest-neighbor antiferromagnetic exchanges, J_{ss}, so they prefer to be coupled singlet. Each spin 1/2 d-core has a small ferromagnetic exchange, J_{sd}, with each of its two neighboring one-electron bonds. We have chosen $J_{sd} = -0.1J_{ss}$, so the results should be consistent with our indirect exchange mechanisms derived for the perturbative spin polarization of a singlet s-space. For a four-atom ring, we obtain a singlet ground state.† From the excited triplet and quintet states, we can calculate the effective exchange integrals between the d-cores. We find the antiferromagnetic next-nearest neighbor exchange to be 50 times as large as the ferromagnetic nearest neighbor exchange. For a six-atom ring, we also obtain a singlet ground state, with an antiferromagnetic spectrum of excited states.

We could modify the relative values of J_{ss} and J_{sd} in our model to change these results. Obviously, if J_{sd} were to dominate, the ground state would be high spin. However, we believe our antiferromagnetic results to properly model actual rings of nickel atoms. There are two important lessons to be learned from this result. First, next-nearest neighbor interactions can be larger than nearest neighbor interactions. Second, an indirect interaction between two d's is effectively canceled if the two antiferromagnetic s's being spin polarized have the same $s-d$ exchange with one of the d's. This is why indirect nearest neighbor exchanges are so small for rings and chains of nickel atoms.

Our model D_{2h} cluster has led us to think about indirect coupling as the result of very small spin polarization of a singlet s-space. This leads to a strong antiferromagnetic mechanism, but only a very weak

† Preliminary calculations (biased for high-spin) on a square D_{4h} cluster of nickel atoms yield a septet ground state. Resolving the issue of the ground state for a *square* nickel cluster deserves further study.

ferromagnetic mechanism. In fact, this model does not give a satisfactory explanation of strong ferromagnetic interactions. For larger clusters, the one-electron bond orbitals should be very easily excited to higher spin states. Substantial spin-polarization of this space should yield strong indirect ferromagnetic interactions between d cores in exactly the manner postulated by Zener. The problem with Zener's analysis is that it predicts indirect coupling to be always ferromagnetic. We find that when the valence electrons are located on each atom, as in an insulator, the indirect coupling is antiferromagnetic. Only when the valence electrons are located between the atoms, as in a conductor, do we find ferromagnetic indirect coupling.

In our model, we obtained very little spin-polarization in the s-space, so we examined the elementary indirect exchange mechanisms in that limit. Recall that we obtained the same magnitude effect for both the ferromagnetic and antiferromagnetic mechanisms. Consider now these mechanisms in the limit of large spin-polarization in the s-space. To do so, we can simply take $J_{ss} = 0$ in our exact energy expressions. For the antiferromagnetic mechanism, we see that the singlet and triplet states are degenerate with $E = -2J_{sd}$. Thus, the antiferromagnetic mechanism becomes very weak for large spin-polarization. For the ferromagnetic mechanism, we see that the energy of the singlet is $E = -J_{sd}$, while the energy of the triplet is $E = -2J_{sd}$. Thus, the ferromagnetic mechanism becomes very strong for large spin-polarization. Hence, the indirect ferromagnetic forces we see in our cluster can become dominant for larger clusters with bonding orbitals farther separated.

Consider the magnetism of *bcc* iron. A Heisenberg Hamiltonian with nearest neighbor antiferromagnetic exchange and next-nearest

neighbor ferromagnetic exchange would yield an antiferromagnetic ground state. Now consider a Heisenberg Hamiltonian with nearest neighbor ferromagnetic exchange and next-nearest neighbor antiferromagnetic exchange. Furthermore, consider the possibility that the next-nearest neighbor antiferromagnetic exchange may be *larger* than the nearest neighbor ferromagnetic exchange. To our knowledge, such Heisenberg Hamiltonians have never been considered. We expect that for dominant nearest neighbor exchange, the ground state will be high spin. For dominant next-nearest neighbor exchange, the ground state will consist of two interpenetrating simple-cubic singlet lattices. For comparable magnitudes of nearest neighbor and next-nearest neighbor exchange, we hope for a ground state of intermediate spin.

Our results lead to interesting deviations from the Ruderman-Kittel interaction. First, let us get a physical understanding of why conduction electrons respond to a local spin perturbation by spin polarizing with oscillations having a characteristic wavelength equal to half the de Broglie wavelength of the highest-energy conduction electrons. To become acclimated to thinking about this problem, first consider a one-dimensional electron gas with one electron per unit length. If the electrons were in the *high-spin state*, the highest-energy occupied orbital would have a wavelength of two units.

$$+ \quad - \quad + \quad - \quad +$$

One can combine this band of high-spin orbitals (unitary transformation) to yield localized orthogonal orbitals separated by one unit.

$$\alpha \quad \alpha \quad \alpha \quad \alpha \quad \alpha$$

Consider now the *singlet state* described with a UHF wavefunction. The

highest-energy occupied orbital of each spin has a wavelength of four units.

$$+ \cdot - \cdot + \qquad (1)$$

Linear combinations of orbitals with like spin can yield localized orbitals of like spin separated by two units. Electrostatic repulsion between the electrons of different spin leads to an interleaving of these two chains of localized orbitals such that orbitals of different spin are separated by one unit.

$$\alpha \ \beta \ \alpha \ \beta \ \alpha \qquad (2)$$

The orbitals of different spin can have spatial overlap, leading to net bonding. Viewing the conduction electrons in this localized representation, we can easily see how they should respond to a local spin perturbation. Recall from (1) that the de Broglie wavelength of the highest-energy conduction electrons is four units. Assume that a local spin perturbation attracts an α-spin conduction electron. Then the conduction electrons will be spin-polarized with β-spin electrons dominating at one unit from the perturbation and α-spin electrons dominating at two units, as suggested by (2). Thus, the oscillation of spin polarization has a wavelength of two units, half the de Broglie wavelength of the highest-energy conduction electrons.

In a real system, the conduction electrons do not have uniform density at each point in space. Consider a string of atoms, each contributing one conduction electron. When the lattice spacing is small, the conduction electrons will have maximum density between the atoms. When the lattice spacing is large, the valence electrons will localize on the atoms, and the system will become an insulator. If each atom has an

unfilled inner shell, then the valence electrons will receive a local spin perturbation at each atom. When we considered an electron gas, we assumed that a local spin perturbation attracting an α-spin electron would result in an α-spin electron sitting *on the site* of perturbation. However, when the perturbation is located on the atoms and the conduction electrons are located *between the atoms*, this cannot occur.

First we consider the case in which the valence electrons are located on the atoms. For our string of atoms, this would occur at sufficiently large lattice spacing that the system is an insulator. Thus we assume that the valence electrons are localized on the atoms, and we assume that the valence electrons are described with a UHF wavefunction. The highest-energy occupied orbital of each spin has a wavelength of four lattice spacings (1). Taking linear combinations of orbitals with like spin, we can obtain localized orbitals of like spin separated by two lattice spacings. Electrostatic repulsion between the electrons of different spin leads to an interleaving of these two chains of localized orbitals such that orbitals of different spin are separated by one lattice spacing.

$$\alpha \quad \beta \quad \alpha \quad \beta \quad \alpha$$

Thus, the *indirect coupling between nearest neighbor inner shells is antiferromagnetic*, and the *coupling between next- nearest neighbors is ferromagnetic*. The indirect coupling oscillates with a wavelength of two lattice spacings.

Consider now our string of atoms at sufficiently small lattice spacing that the system is a conductor with the *conduction electrons located between the atoms*. The localized representation of a UHF description of the conduction electrons in our string of atoms has orbitals localized

between the atoms.

$$\alpha \cdot \beta \cdot \alpha \cdot \beta \cdot \alpha \cdot \beta$$

We find that the nearest neighbor interaction between inner shells (located at atoms) should be very weak, due to the cancellation of strong indirect ferromagnetic and antiferromagnetic forces. However, the next-nearest neighbor interaction should be strongly antiferromagnetic. Our results are opposite to the predictions of Ruderman and Kittel, who predict that the nearest neighbor interaction should be the strongest and antiferromagnetic. (We find this interaction to be very weakly ferromagnetic.) Ruderman and Kittel predict the coupling between next-nearest neighbors to be ferromagnetic. (We find this next-nearest neighbor interaction to be strong and antiferromagnetic.) In fact, we obtain the opposite interaction from Ruderman and Kittel for all larger spacings.

VI. Conclusion

Our calculations show that the exchange forces responsible for ferromagnetism are not direct $d-d$ interactions but rather *indirect* through the conduction band.

We find that nearest-neighbor interactions are ferromagnetic, while next-nearest-neighbor interactions are *anti*ferromagnetic, being *opposite* to the prediction of RKKY theory. Indeed, these antiferromagnetic next-nearest-neighbor interactions can be *larger* than the ferromagnetic nearest-neighbor interactions!

In our Ni_4 model cluster, four $S=1/2$ d^9 centers couple to a total spin of $S=1$. This calculation is consistent with all atoms in bulk Ni being d^9 while the observed moment/atom is only $\mu_m = 0.6\,\mu_B$ at 0°K.

We find ferromagnetism for only a short range of atomic separation. At short R, direct antiferromagnetism arises from $d-d$ interactions. At large R, indirect antiferromagnetism arises from the Mott transition.

References

(1) J.C. Slater, *Phys. Rev.* **1930,** *36*, 57.

(2) C.J. Ballhausen, *Introduction to Ligand Field Theory* (McGraw-Hill, New York, 1962), p. 74.

(3) M.H. McAdon and W.A. Goddard III, *J. Phys. Chem.* to be submitted.

(4) T.H. Upton and W.A. Goddard III, *J. Am. Chem. Soc.* **1978,** *100*, 5659.

(5) A.K. Rappe and W.A. Goddard III, *J. Am. Chem. Soc.* **1977,** *99*, 3966.

(6) T.H. Upton, Ph.D. Thesis, California Institute of Technology, 1980.

(7) H. Basch, M.D. Newton, and J.W. Moskowitz, *J. Chem. Phys.* **1980,** *73*, 4492.

(8) C.F. Melius, B.D. Olafson, and W.A. Goddard III, *Chem. Phys. Letters* **1974,** *28*, 457.

(9) M. Sollenberger, M.S. Thesis, California Institute of Technology, 1977.

(10) A.K. Rappe, T.A. Smedley, and W.A. Goddard III, *J. Phys. Chem.* **1981,** *85*, 2607.

(11) C.E. Moore, *Atomic Energy Levels* (National Bureau of Standards, Washington, D.C., 1949).

(12) C. Froese-Fischer, *Comput. Phys. Commun.* **1972**, *4*, 107.

(13) D.C. Mattis, *The Theory of Magnetism* (Harper & Row, New York, 1965), p. 196.

(14) C. Zener, *Phys. Rev.* **1951**, *81*, 440.

(15) J.M. Ziman, *Principles of the Theory of Solids* (Cambridge University Press, Cambridge, 1972), p. 344.

CHAPTER 3

Multiple Bonding in Transition-Metal Dimers

I. Introduction

When we began our study of metal-metal multiple bonding, the goal was to study the quadruple bond attributed to such complexes as $[Mo_2Cl_8]^{4-}$ and $[Cr_2(CH_3)_8]^{4-}$. To our dismay, calculations on model complexes expected to have Cr-Cr quadruple bonds e.g., $H_2Cr-CrH_2$, had no bond strength! Our wavefunctions at that time were inadequate to allow the optimal spin coupling of the eight bonding electrons, so a major programming effort was undertaken to increase the flexibility of our wavefunctions. However, after achieving this goal, we found that $H_2Cr-CrH_2$ still had no bond strength. Of course, most experimentally observed systems with quadruple bonds are ionic species, so that we could not make direct comparisons. The only neutral species are the structures with bridging carboxylate ligands, which do not permit an evaluation of the direct metal-metal bonding interactions. Thus, there is no observed quadruple-bond species to provide an unambiguous metal-metal bond strength. Our theoretical quadruple-bond models were dimers of CrH_2 and $CrCl_2$ in both D_{2h} and D_{2d} geometries. These models should have yielded Cr-Cr quadruple bond strengths; however, no significant bonding was found even after allowing optimal spin coupling. We then questioned the validity of our models for describing the experimentally observed systems.

At this point, we were led to consider eliminating the ligands and describing the bonding interactions in the dimer. Despite the apparent simplicity of this system, it is theoretically more challenging than the

quadruple-bond, for it can have a formal sextuple bond. This requires the optimal spin coupling of twelve bonding electrons. Another major programming effort was required to remove from our codes certain dependencies that increase geometrically with the number of optimally coupled electrons. Once this goal was accomplished, we were able to examine Cr_2. This species is the most challenging theoretically of the transition-metal dimers, for it contains the maximal number of valence electrons requiring optimal spin coupling in the ground state.

II. Discussion

When we began this investigation, the experimental data for Cr_2 were very uncertain. The dimer was thought to have been observed in three environments. The first was was in matrix isolation studies of Cr atoms in Ar matrices.[1] This yielded an absorption band from the ground state. Resonance Raman spectra using this band yielded a vibrational frequency which we now know to be incorrect. The second was in equilibrium with the monomer over the metal heated in a Knudsen cell.[2] This yielded a bond energy for the dimer, but only with assumed molecular parameters. The estimates of vibrational frequency and bond distance were quite rough, and excited electronic states were assumed to have no thermal population. These estimates were of course inaccurate; hence, so was the bond energy. The third experiment involved photodissociation of the hexacarbonyl.[3] This yielded a bond distance if the observed species was assumed to be Cr_2. The experimentalists could not determine whether the observed species was CrO_2, CrC_2, or Cr_2! However, recent experiments show that this bond distance is in fact accurate. Thus, the one experimental value which proved to be accurate was mainly disregarded by many researchers.

Consider now the theoretical difficulties of describing Cr_2 (Figure 1). The HF description makes a severe correlation error, forcing far too much ionic character in each bond. The HF wavefunction for Cr_2 is over 20 eV *above* the energy of the HF atoms! The wavefunction cannot dissociate properly, resulting in even worse energies at larger distances. The UHF wavefunction for Cr_2 does allow for proper dissociation; however, it cannot properly describe bonding. The UHF wavefunction describes high-spin coupling on each atom, but with a molecular coupling that is a

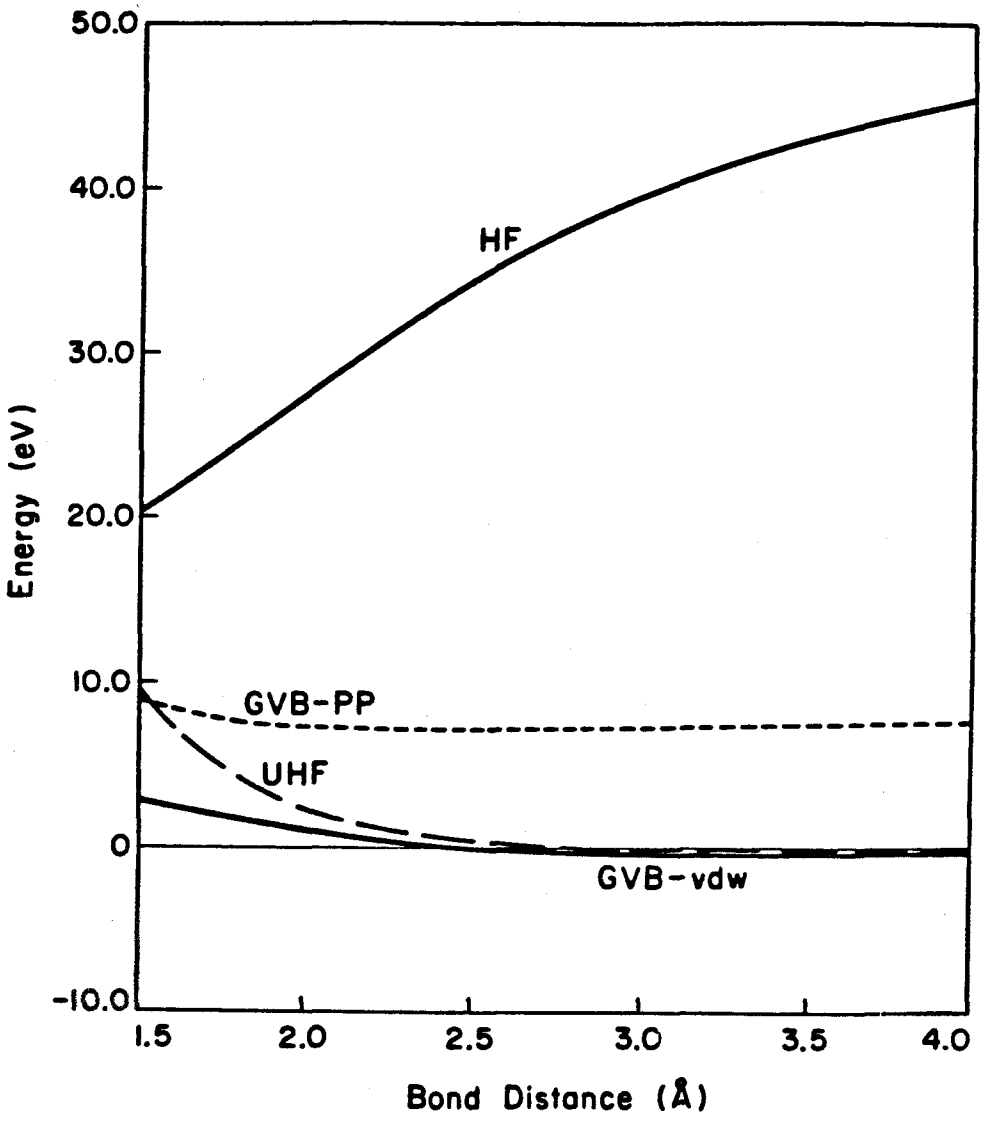

Figure 1. Comparison of potential curves for Cr_2.

mixture of spin states from S=0 to S=6! Moreover, the UHF wavefunction is incapable of describing strong bonding interactions without giving up the favorable spin coupling on each atom and building in too much ionic character, in short, without collapsing into the HF wavefunction. The GVB-PP wavefunction describes strong bonding interactions with optimal ionic character in each bond. This wavefunction has strong-bond character at all distances. The GVB-PP wavefunction dissociates to neutral atoms but with the unpaired electrons having spins oriented randomly on each atom. Thus, the SCF wavefunction which dissociates properly cannot describe strong bonding, and the SCF wavefunction which can describe strong bonding does not dissociate properly.

Using orbitals from GVB-PP and UHF wavefunctions, we examined CI wavefunctions allowing for the optimal spin coupling of all twelve valence electrons and dissociating to high-spin HF atoms. To our surprise, the dimer was unbound at small distances where $d-d$ bonding was expected, and only weakly bound at large distances where only $s-s$ bonding was expected. We then decided that the orbitals might undergo significant shape readjustments if optimized self-consistently with the optimal spin coupling of our CI wavefunctions. At this time, we had a general MCSCF program into which one could give hand-generated energy expressions. A significant programming effort was undertaken to write a program which generates the symbolic energy expression for a CI wavefunction. Only small CI's (less than approx. 250 configurations) could be handled by this approach. Unfortunately, this allowed us to solve for only the higher-spin excited states of the dimer. The ground state was too large. A more efficient procedure allowing for large CI's was conceived. The implementation of this approach required another significant

programming effort to write a program which generates the one- and two-electron density matrices for a CI wavefunction. Having completed this task, we could perform MCSCF calculations with thousands of configurations. We tried a 6000-configuration MCSCF for Cr_2 which allows proper dissociation to high-spin HF atoms, optimal spin coupling of all twelve valence electrons, interpair correlations among the six bonds, and all intrapair correlations in the $s-s$ bond leading to van der Waals interactions at long distances. The same result was obtained: unbound where $d-d$ bonding was expected and only weakly bound where $s-s$ bonding was expected (GVB-vdw in Figure 1).

At this point, we made many attempts to find either a basis set deficiency or missing correlation. The $3s,3p,3d$-space was given $3-\zeta$ freedom, a diffuse d function was included, f functions were optimized, and even bond functions were tried. A full-CI in the twelve valence orbitals yielded very little improvement. Various excitations into the virtual orbitals were explored. At each step, we ran into the limits of our program capabilities. The problem was simply too large to permit the inclusion of additional classes of correlation without exceeding program limitations. The energy lowering from subsets of these excitations could not be assumed additive. We were faced with the fundamental problem of the variational method: we had no way to determine how close our bond energy was to the accurate value. One thing was certain: we had optimized a wavefunction sufficiently general to permit strong $d-d$ bonding, and the system chose to make only a single $s-s$ bond. Having found the basis set to be adequate and having tested for additional correlation within our program limitations, we decided that the $d-d$ bonding was apparently too weak to overcome repulsive interactions at short dis-

tance.[4]

We decided to test our approach with Mo_2. For Mo atom, the valence *d* orbitals are more diffuse relative to the size of the valence *s* orbital and core *p* orbitals than for Cr atom. This is because the *d* orbitals of Cr atom have no radial node. Thus, we expect that $d-d$ bonding in Mo_2 should be more important than in Cr_2. At first, the picture looked very much the same for Mo_2 as for Cr_2. However, when we optimized a set of *f* functions, Mo_2 became bound at short distance. A potential surface revealed two minima: one at short distance ($d-d$ bonding) and another at long distance ($s-s$ bonding) (GVB-vdw in Figure 2a). Thus, it was clear that our method was capable of describing $d-d$ bonding and did so for Mo_2.[5] It was also clear that $d-d$ bonding should be less important in Cr_2 and might not even produce a bound minimum at short distance.

The double well of Mo_2 required an explanation, and the first thought was an avoided crossing between two states. This idea was quickly dismissed with an excited-state calculation. In fact, avoided crossings have been observed to produce double wells in potential curves of *excited* electronic states for many systems, but not for the *ground* state. The ground state of a dimer always gets the maximal bonding at each internuclear distance. Even though the character of the ground state may change radically with distance, the ground-state potential curve seems always to be able to drop monotonically as the optimal bond distance is approached. Thus, the double well we found in the ground state of Mo_2 was unique and required new understanding for an explanation. We knew that the bonding was changing with distance, but we had no way to determine just what changes were occurring. The wavefunction for the ground state was not easily interpreted, because hundreds of

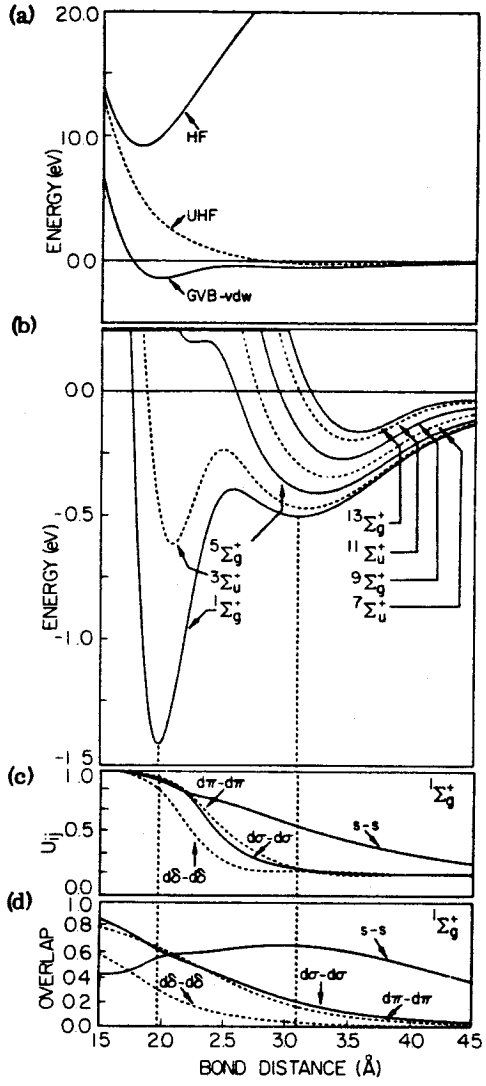

Figure 2. (a) Comparison of potential curves for Mo_2 from our ground-state wavefunction (GVB-vdw) and the corresponding HF and UHF wavefunctions. (b) The potential curves (GVB-vdw) for Mo_2. (c) The spin coupling (U_{ij}) for each bond of Mo_2. (d) The overlap between bonding orbitals of Mo_2.

configurations made significant contributions, and no one configuration made a large contribution. We decided that an analysis of the spin coupling was required to understand the character of the wavefunction. This required writing a new program to analyze the coupling between electrons in a CI wavefunction. Such analysis of Mo_2 revealed that only $s-s$ bonding was occurring at the outer minimum, but $d-d$ bonding was occurring at the inner minimum. The bond couplings are shown in Figure 2c. The puzzling question was why the two wells were separated by a hump. Analysis of bond overlaps provided an answer. We found that the $s-s$ overlap reached a maximum at the outer well of the potential curve. The bond overlaps are shown in Figure 2d. Thus, as the bond distance is decreased from the outer well, the $s-s$ bond is being pushed up its inner repulsive wall before $d-d$ bonds have sufficient overlap to compensate for this repulsion and cause an inner well.

Our result for Cr_2 with a long, weak $s-s$ bond and *no* $d-d$ bonds is logically consistent with our result for Mo_2 with a long, weak $s-s$ bond but *short, strong* $d-d$ bonds. At long distance, the $s-s$ bond is only 1/6 as strong as a simple $s-s$ bond, because the s electron on each center is one of six high-spin electrons on that center. A strong $s-s$ bonding interaction requires sacrificing $s-d$ exchange interactions on both centers. Thus, we expect a weak $s-s$ bond. The $d-d$ bonds can occur only at short distance where there is strong electrostatic repulsion between the two positive d-cores. Thus, the $d-d$ bonds must be strong to overcome this repulsion, and we have good reason to expect only weak $d-d$ bonds for Cr_2. As the bond distance is decreased and $d-d$ bonds first begin to form, each $d-d$ bond is less than 1/5 as strong as a simple $d-d$ bond, because even if the $s-s$ bond is strong, each d electron is one of

five high-spin electrons on a center. A strong $d-d$ bonding interaction requires sacrificing large intraatomic $d-d$ exchange interactions. For Cr atom, these $d-d$ exchange interactions are larger than for Mo atom. More importantly, the difference in radial extent between the diffuse valence s orbital and the tight valence d's is greater for Cr atom than for Mo atom. Comparing Cr_2 with Mo_2, we expect Cr_2 to have more unshielded electrostatic repulsion between the d-cores and weaker $d-d$ bonds to try to overcome that repulsion. Hence, even though we find the ground state of Mo_2 to have a short bond distance with $d-d$ bonds, it is perfectly reasonable to expect the dimer of smaller isoelectronic Cr atoms to have a longer bond distance with only a single $s-s$ bond.

When we presented our Cr_2 results,[4] they were consistent with all the firm experimental data at that time. We corrected the experimental dissociation energy with our molecular partition function, and obtained 1.0±0.3 eV. Our computed bond energy was 0.3_5 eV, so we had a discrepancy. However, since effusion flow was not maintained in the experiments, we doubted the accuracy of the experimental dissociation energy.[2] Our bond distance of 3.0_6 Å was completely different from the experimental distance of 1.7 Å obtained from photodissociation of $Cr(CO)_6$.[3] However, this experimental band could have been CrO_2 or CrC_2. We and other researchers considered it unlikely that this band was due to Cr_2. The most reliable experimental data on Cr_2 came from matrix isolation studies of Cr atoms in Ar matrices.[1] An absorption band was convincingly assigned to the ground state of Cr_2. Our lowest dipole-allowed transition, $^1\Sigma_u^+ \leftarrow {}^1\Sigma_g^+$ (Figure 3), corresponded very closely with this observed transition, and was even consistent with expected matrix shift for that transition. Our calculations were consistent with all known

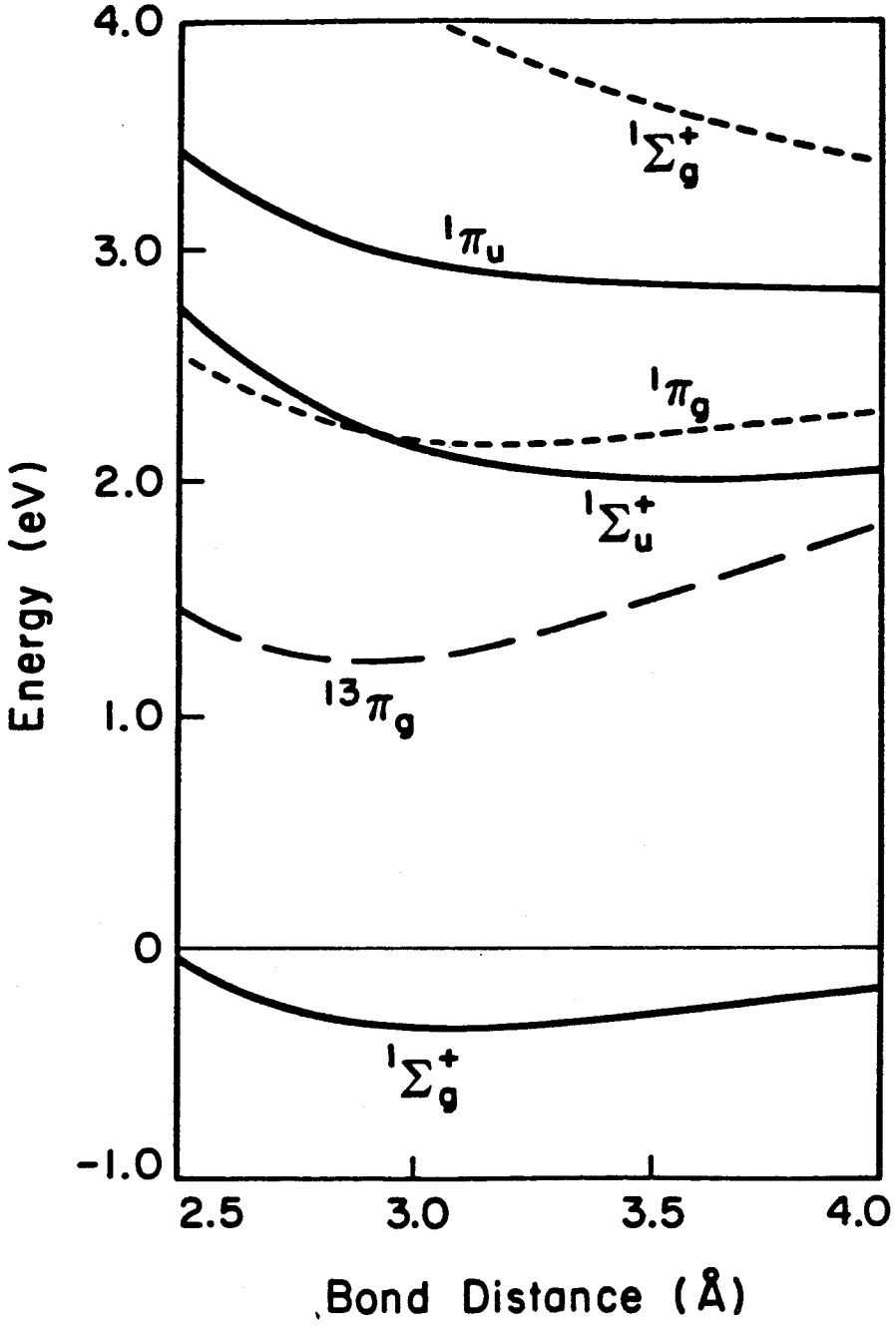

Figure 3. Excited-state curves for Cr_2.

experimental data, given the stated experimental uncertainties.

Soon after we published our result for Cr_2, a new experimental technique, resonant two-photon ionization spectroscopy, was used to show conclusively that the bond distance is short, about 1.7 Å.[6] We first considered the possibility that a long-lived excited state with strong $d-d$ bonding was being observed. An excited state consistent with this hypothesis would have at least one of the atoms excited to the d^6 configuration, thereby eliminating the electrostatic repulsion between two positive d^5 cores. Our potential curves for these excited states did not yield very attractive wells at short distance, however. Thus, we were faced with the fact that our computed $d-d$ bonds were simply not strong enough to explain the experimental spectrum. We then examined the experiment more closely and determined that the lower state in the observed transition must be either Σ_g^+ or Σ_u^-. It was likely that any spin multiplicity could be observed with the spectral resolution, so both states were assumed singlet. Given that the vibrational and rotational degrees of freedom are cold, it is likely that the lower state in this electronic transition is indeed the ground state. All of our computed states have $d-d$ bonds which are too weak, and increased $d-d$ bonding should lower all our states by roughly the same amount. Thus, we can confidently say that the lowest state we compute for Cr_2, $^1\Sigma_g^+$, is indeed the ground state. We consider this to be the most likely lower state in the observed transition.

After the bond length was proved short by resonant two-photon ionization spectroscopy, Kok and Hall[7] published CI calculations which yield a short bond length for Cr_2. These calculations are inconsistent. The first inconsistency is that the basis set includes bond functions at the

midpoint of the bond. This method effectively increases the size of the basis over the atom-centered functions when the interatomic distance is small and thus artificially biases the calculation toward small bond distance. The second inconsistency is that the wavefunction does not properly dissociate to ground state atoms. The orbitals were optimized by a method almost equivalent to GVB-PP, and the CI included all single and double excitations from the 64 PP-configurations into the twelve valence orbitals, a total of 3520 configurations. This CI does not dissociate to high-spin HF atoms. Based on our calculations, we know that this calculation must in fact have higher energy than HF atoms. Thus, the bond length obtained from this calculation is simply an artifact of improper dissociation.

For a consistent calculation, the wavefunction must properly dissociate to ground state atoms. Including only the configurations necessary to permit dissociation to HF atoms, we obtain a long, weak bond. To improve this result, we shall try to include as many as possible additional configurations consistent with HF atoms. Note that the biggest CI consistent with HF atoms would be a full GVB-CI in the twelve valence orbitals times singles into the virtuals plus an RCI in the twelve valence orbitals times intrapair doubles into the virtuals. This prescription insures that a double excitation into the virtuals results from a single on one atom times a single on the other. We tried localizing orbitals to permit more types of correlation consistent with HF atoms; however, tests with the high-spin state, for which localization was unambiguous, revealed significant contamination of intraatomic correlation. Thus, the GVB-CI times singles plus RCI times intrapair doubles is the largest reliable CI. Unfortunately, with current program limitations, we can include only a

small fraction of these configurations.

We now face the problem of trying to include sufficient correlation to describe $d-d$ bonding accurately. At the experimental bond distance (we used 3.2 a_0), the 6000-configuration MCSCF we published is unbound by 1.46 eV. This includes core relaxation (worth 6.7 mh), f-polarization functions (worth 18.5 mh), and van der Waals correlations (worth 15.0 mh). The best calculation we have to date is unbound by 0.74 eV. This number was obtained by freezing the twelve GVB natural orbitals from a 1516-configuration MCSCF, optimizing four virtual δ-orbitals in a 11364-configuration MCSCF including vertical singles and intrapair doubles only in the δ-space, optimizing four virtual π-orbitals in a 11364-configuration MCSCF including vertical singles and intrapair doubles only in the π-space, optimizing four virtual σ-orbitals (two s and two d) in a 11364-configuration MCSCF including vertical singles and intrapair doubles only in the σ-space, and finally performing the 31060-configuration CI which includes vertical singles and intrapair doubles from the GVB wavefunction into optimized virtuals. This wavefunction treats all pairs equivalently and includes all types of correlation consistent with HF atoms.

What are the important configurations we are excluding? From a full GVB-CI on Mo_2, we know that only about 5 mh lowering can be expected from a GVB-CI over an RCI. Since our virtual orbitals are optimized, we can assume that no other singles would be important. However, there are many intrapair doubles which we have excluded from our calculation. One such omission is the angular correlation of the $s-s$ bond. We would have to include intrapair doubles from the $s-s$ bond into four virtual p_π-orbitals in order to make our largest calculation include all 6000 configurations of our published wavefunction as a subset. These addi-

tional correlations were not included because of the current limitation of 32767 configurations in our CI program. This limitation could be removed; however, assuming we had included these p_π configurations and also the GVB-CI configurations, Cr_2 at this distance would still have been unbound. There are an enormous number of intrapair doubles from the $d-d$ bonds which we have omitted. These include excitations into virtual p and f orbitals. We have tried to identify virtuals of dominant importance, but it seems that small amounts of energy lowering come from many sources. The simultaneous inclusion of all these effects is currently beyond *ab initio* state-of-the-art technology.

We expect that in the not-so-distant future, a direct-CI approach could yield an accurate *ab initio* description of Cr_2. To be useful, this method would have to be efficient for restricted excitations from a multiconfigurational reference. Such programs are certain to be developed. However, before such methods become available, and even after, we shall want an approach which will not require an enormous amount of computing to obtain a reliable description of metal-metal bonding.

An approximate technique might give us reliable results if we are careful to mimic the missing electron correlation and not simply introduce a parameter to fit the experimental bond energy. What can we learn about the missing correlation? Let us look at our largest calculation: vertical singles and intrapair doubles from the GVB wavefunction. We have separate energy contributions from each orbital symmetry. Including the vertical excitations in just the δ-orbitals results in 21.0 mh energy lowering from GVB. Excitations in just the π-space yield 14.1 mh lowering. The σ-space gives only 9.4 mh. These effects are not quite additive.

The sum of these energy lowerings is 44.5 mh, whereas the actual energy lowering obtained in our large CI over GVB is only 41.4 mh. Note that the energy lowering is largest in the δ-space. It is interesting that the weakest bonds should have the largest correlation corrections. What are the important correlations beyond GVB? Examining the excitations into the virtual δ-orbitals, we find that vertical singles into the virtuals are actually more important than vertical intrapair doubles. This is remarkable, since single excitations from optimized MCSCF orbitals should not be important. We find the most important type of virtual excitation to be a vertical single from a bond pair whose electrons in this configuration are coupled ungerade singlet. This type of excitation aids a bond pair which is instantaneously in an ionic configuration. Thus, we have identified the dominant correlation error with ionic configurations in the bond pairs. Since ionic configurations contribute much less in weaker bonds, why do we obtain the largest energy lowering in the δ-bonds? Consider the energy lowerings we obtain at 0.2 a_0 longer distance. The δ-lowering decreases from 21.0 to 19.8 mh, the π-lowering *increases* from 14.1 to 15.4 mh, and the σ-lowering also increases from 9.4 to 9.9 mh. These data show conclusively that the δ-bonds are not different because of symmetry. When the internuclear distance is increased, the ionic character in each bond pair decreases to zero, but the energy lowering resulting from correlating these ionic configurations increases to a maximum before decreasing to zero. The interpretation of this is not unambiguous, because at small distance, ionic and covalent configurations overlap. Note that the virtual excitations we have tried result in about the same total energy lowering at 3.2 and 3.4 a_0, so these excitations yield roughly a constant energy correction near the experimental minimum. This

behavior cannot be typical for the excitations we are excluding. Since the GVB wavefunction is repulsive at the experimental bond distance, the maximal energy lowering from the sum of all excitations beyond GVB must occur at smaller distance than experimental.

We have developed an approximate method to mimic the excitations beyond GVB. This method recognizes that the dominant correlation error arises from ionic configurations in the bond pairs. The energy correction for ionic configurations is uniquely determined by atomic correlation error. We have applied this atomic correlation correction (ACC) to the $d-d$ bonds of our 6000-configuration MCSCF for Cr_2. The $s-s$ bond is assumed to be adequately correlated with eight natural orbitals. This ACC method yields precisely the same long-distance minimum as our *ab initio* calculation, but it also gives a short-distance minimum corresponding to experiment (Figure 4). Thus, we obtain a *double minimum* for Cr_2!

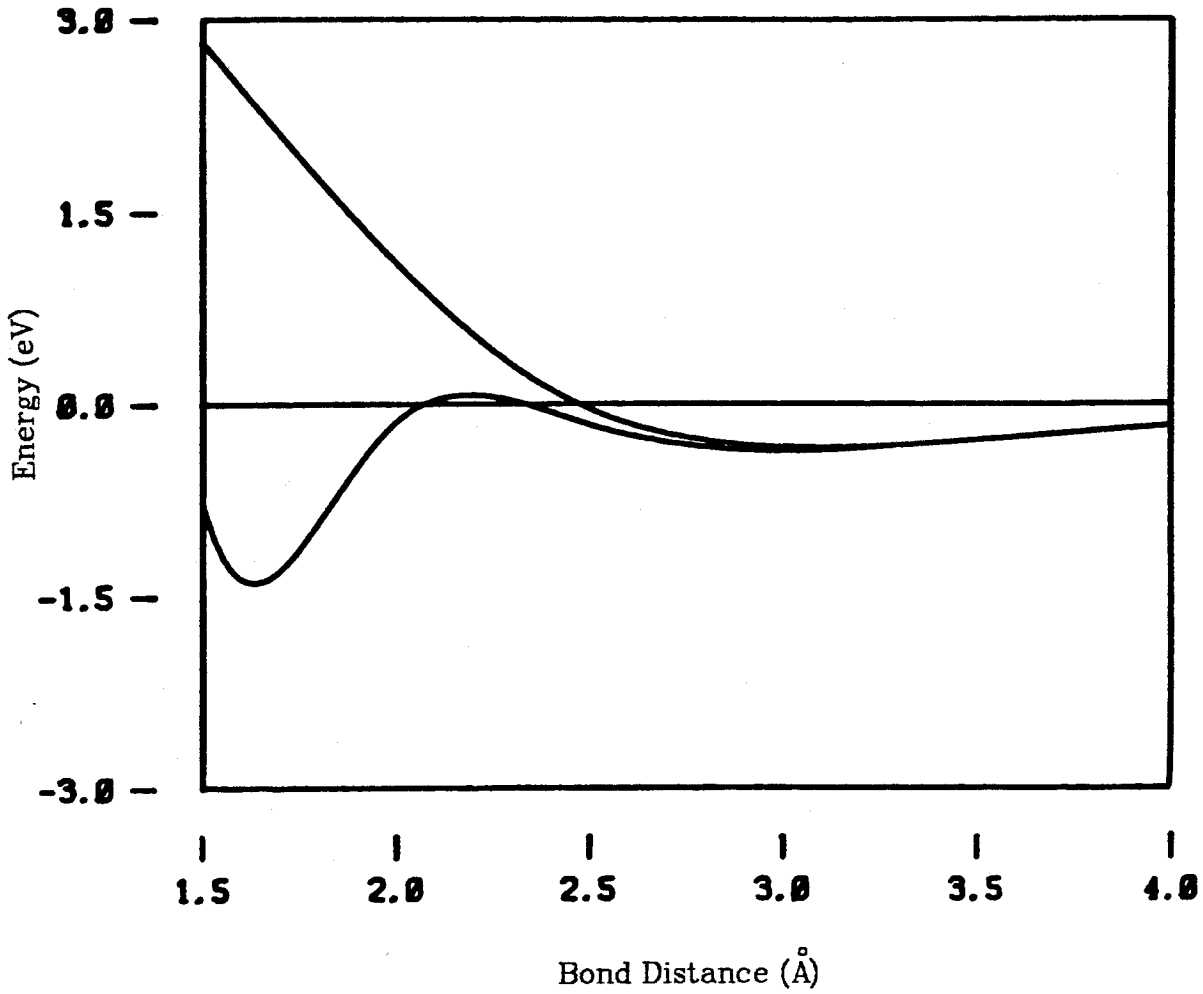

Figure 4. Comparison between *ab initio* (upper) and ACC (lower) potential curves for Cr_2.

III. Approximate Method

We have found that very extensive *ab initio* calculations fail to account for the short bond distance of Cr_2. We have found further that the dominant correlation error beyond GVB is associated with ionic configurations in the bond pairs. We desire an approximate method to correct for this correlation error.

A. Development with H_2

We shall outline the steps we have taken in developing such an approximate method. For simplicity, let us consider H_2. At infinite distance, the exact wavefunction is covalent

$$\Psi_{cov} = [\varphi_l \varphi_r + \varphi_r \varphi_l](\alpha\beta - \beta\alpha)$$

where φ_l and φ_r are singly-occupied orbitals on the left and right centers. At small distances, we find that this valence-bond covalent wavefunction wants to mix with an ionic wavefunction

$$\Psi_{ion} = [\varphi_l \varphi_l + \varphi_r \varphi_r](\alpha\beta - \beta\alpha)$$

Because φ_l overlaps φ_r, the covalent and ionic wavefunctions overlap.

The MO wavefunction has two electrons in a bonding orbital

$$\varphi_g = \varphi_l + \varphi_r$$

This MO wavefunction is restricted to have equal amounts of ionic and covalent character (ignoring normalization):

$$\Psi_{MO} = \varphi_g \varphi_g (\alpha\beta - \beta\alpha) = \Psi_{cov} + \Psi_{ion}$$

Consider now the optimal mixture of ionic and covalent character:

$$\Psi_{CI} = C_c \Psi_{cov} + C_i \Psi_{ion}$$

The easiest way to solve for this CI wavefunction is with two orthogonal

configurations: two electrons in a bonding orbital

$$\varphi_g = \varphi_l + \varphi_r$$

and two electrons in an antibonding orbital.

$$\varphi_u = \varphi_l - \varphi_r$$

The GVB wavefunction optimizes the shape of the orbitals for this two-configuration CI. A particular linear combination of the natural orbitals yields one-electron orbitals

$$\varphi'_l = \varphi_g + \lambda\varphi_u$$
$$\varphi'_r = \varphi_g - \lambda\varphi_u$$

With these orbitals, the GVB wavefunction can be written in covalent form:

$$\Psi_{GVB} = [\varphi'_l\varphi'_r + \varphi'_r\varphi'_l](\alpha\beta - \beta\alpha)$$

However, the GVB wavefunction is really a mixture of covalent and ionic character:

$$\Psi_{GVB} = C_c\Psi_{cov} + C_i\Psi_{ion}$$

As the bond is broken ($R\rightarrow\infty$), the GVB wavefunction goes to the covalent wavefunction ($C_i\rightarrow 0$). At large R, the GVB description is exact, but at finite R there are additional electron correlation effects not explicitly treated in the GVB wavefunction. Important additional effects can be seen to arise in the ionic part of the GVB wavefunction, since doubly-occupied atomic orbitals typically have about 1 eV of correlation energy. This leads to less than optimal mixing of the ionic terms into the GVB wavefunction.

We wish to build into the GVB wavefunction a correction for the atomic correlation error in the ionic part of the wavefunction. First, we

must define the covalent and ionic character. Unfortunately, localized atomic orbitals are not uniquely defined by this wavefunction. Consider λ as an arbitrary parameter for generating localized orbitals to interpret the wavefunction. The value of λ determines how much ionic character we interpret the wavefunction to have. The λ which yields GVB orbitals is too small, since the GVB one-electron orbitals are more delocalized and have higher overlap than atomic orbitals. This value always gives zero ionic character. We shall take $\lambda = 1$, since this will yield *orthogonal* localized orbitals. This value might be considered too large, since localized atomic orbitals would have nonzero overlap at finite distances. As a result, the value $\lambda = 1$ could yield an overestimate of ionic character. However, we shall be certain to formulate this method so as not to overestimate ionic character (see Appendix VII). The value $\lambda = 1$ is unique in providing orthogonal localized orbitals. This makes energy corrections for ionic and covalent configurations unambiguous, since ionic and covalent configurations are orthogonal. Most important, the two ionic configurations are orthogonal to each other, and we avoid the possibility of any double counting of ionic energy corrections. We shall see that orthogonal localized orbitals do in fact give us precisely the estimate of ionic character necessary for a nearly quantitative ionic energy correction.

How shall we apply an energy correction to this wavefunction? Consider H_2 at infinite separation. The covalent wavefunction is exact, and no correlation error exists. However, the ionic wavefunction has a correlation error equal to that of H^-. We wish to correct the energy of the ionic wavefunction relative to the covalent wavefunction. This correction involves both the IP (ionization potential) and EA (electron affinity) of H

atom. The excitation energy from the covalent to the ionic wavefunction is IP-EA. The experimental excitation energy (hartrees) is

$$0.472249 = 0.5 - 0.027751$$

while the numerical Hartree-Fock excitation energy is

$$0.512073 = 0.5 - (-0.012073)$$

Thus, the correlation error is 0.039824 hartrees in the ionic wavefunction.

In our molecular calculation, we use a finite basis of atom-centered functions. The ionic wavefunction has a more severe basis deficiency than the covalent wavefunction. Consider again H_2 at infinite separation. Given our Huzinaga 6-gaussian basis contracted 3-ζ, the Hartree-Fock excitation energy is

$$0.523304 = 0.499940 - (-0.023364)$$

Thus, the basis error is 0.011231 hartrees greater in the ionic wavefunction than in the covalent wavefunction. We could lower the energy of our ionic configurations by 0.051055 hartrees and thereby correct for both correlation and basis error.

How shall we actually make this energy correction? We shall perform a two-configuration MCSCF on H_2 using inversion symmetry. All quantities are evaluated strictly *ab initio* except that a constant of energy is added to ionic configurations in the CI. The orbitals respond only indirectly to this energy correction, as there will be more ionic character in the CI wavefunction. If the CI does not permit a mixing of covalent and ionic character (as in $^1\Sigma_u^+$ HF), then the orbitals do not respond at all to this correction. In terms of our localized orthogonal orbitals φ_l and φ_r, ionic configurations have two-electron energy J_{ll} or J_{rr}. The covalent configurations use other two-electron integrals. Thus, if we

add our constant energy of correction to J_{ll} and J_{rr}, we will properly stabilize ionic configurations relative to covalent configurations. Since we are using symmetry, we must determine the correction to be added to each two-electron integral over natural orbitals. By expanding each integral over natural orbitals into integrals over localized orthogonal orbitals, we find that to add a constant energy to J_{ll} and J_{rr}, we must add half that constant to each of the integrals J_{gg}, J_{uu}, J_{gu}, and K_{gu}. These constants are added only to the integrals used in setting up the CI matrix. Thus, the orbital optimization is not directly affected. Indeed, the energy correction to be applied is independent of orbital shapes, although orbital shapes may change in response to an increase in ionic character of the CI.

Our results for the ground state of H_2 are extremely encouraging! We used our 3–ζ s basis plus a p gaussian of exponent 1.1 for a wide range of distances. The correlation correction was -0.039824 h, and the correlation plus basis correction was -0.051055 h.

Table 1. Results for H_2

Wavefunction	$R_{min}(a_0)$	$E_{min}(h)$	$k_{min}(a.u.)$
GVB	1.43	-0.151	0.34
GVB(corr.)	1.42	-0.167	0.35
GVB(corr.+basis)	1.42	-0.172	0.36
EXACT	1.40	-0.174	0.37

The curves were plotted out to 6 a_0, and they show excellent behavior. The correlation-corrected curve lies between GVB and EXACT, but much closer to EXACT (Figure 5). The curve with both correlation and basis correction lies almost on top of EXACT (Figure 6). The fine quality of this

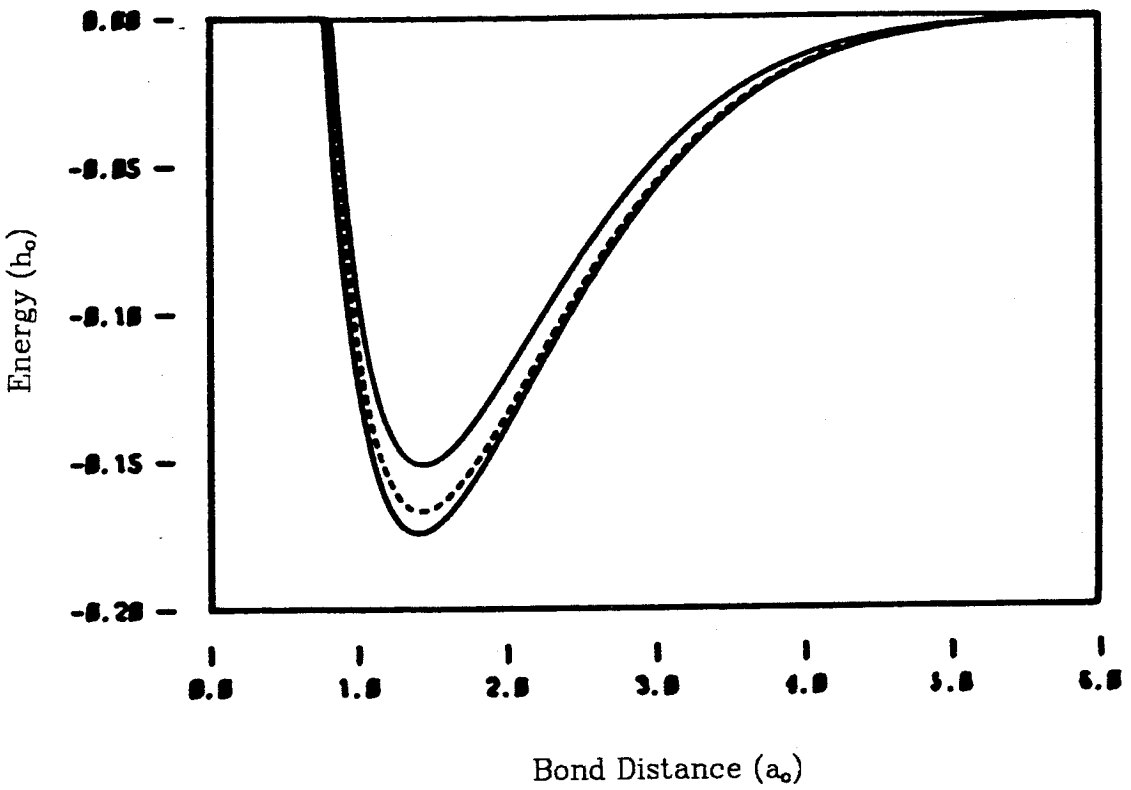

Figure 5. H_2 $^1\Sigma_g^+$ ACC(-.039824 h) (dashed) compared with GVB (upper solid) and EXACT (lower solid).

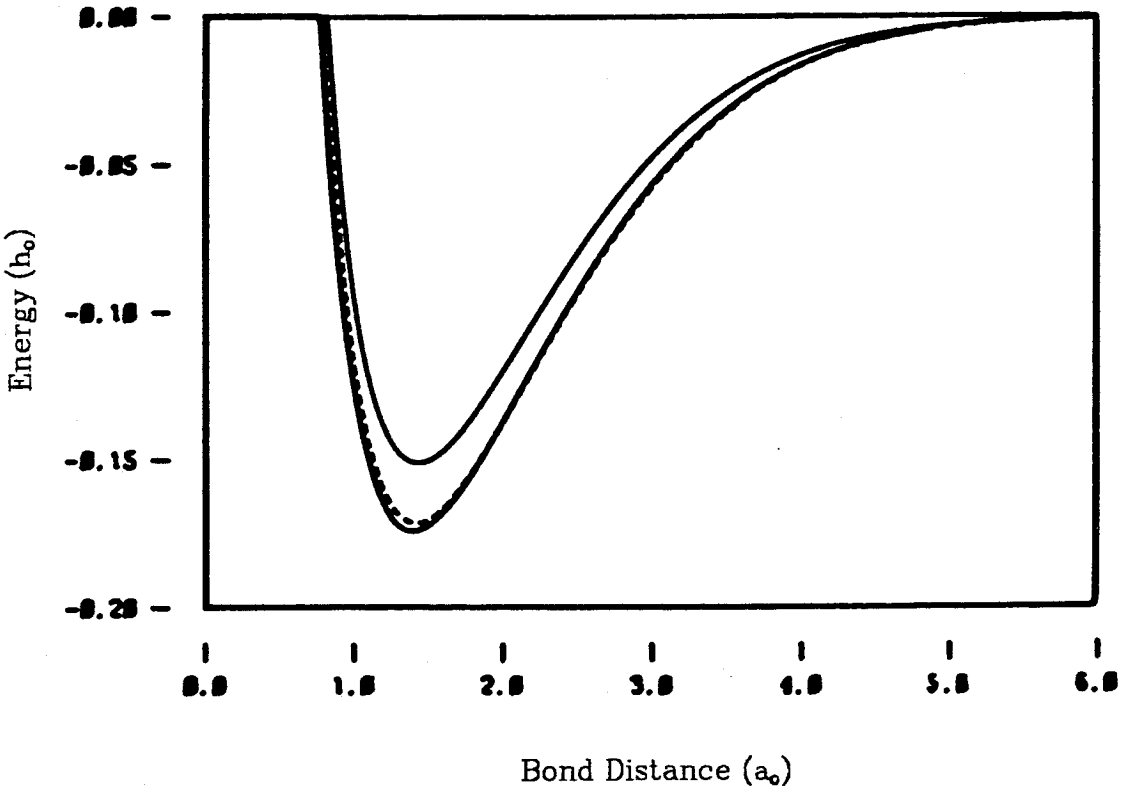

Figure 6. $H_2\ ^1\Sigma_g^+$ ACC(-.051055 h) (dashed) compared with GVB (upper solid) and EXACT (lower solid).

simple correction is astonishing.

At this time, we should point out that this method does have a flaw. When the amount of ionic character in the wavefunction becomes very large, the orbitals respond by effectively reducing the actual ionic character. This may be accomplished by the bonding and antibonding orbitals developing different radial extent. The HF wavefunction for the $^1\Sigma_u^+$ excited state of H_2 is a good example. At long distances, the singly-occupied bonding orbital becomes diffuse to maximize bonding and the singly-occupied antibonding orbital becomes tight to minimize antibonding. However, at short distances, the singly-occupied bonding orbital becomes tight to approach a He 1*s* orbital and the singly-occupied antibonding orbital becomes diffuse to approach a He 2*p* orbital. The HF curve for this state has a single minimum but does reveal this transition in orbital shapes with an inflection point on either side of the transition. The exact potential curve for this excited state does not contain these inflections. Thus, they are an artifact of the HF wavefunction. We should desire our approximate technique to correct this artifact of HF. However, our method allows for only a constant correction to this curve. Thus, the shape of the potential must remain the same. Since our method assumes the bonding and antibonding orbitals to have the same radial extent, we apply the full ionic correction at all internuclear distances. We expect and observe that we overcorrect this curve at all distances except where the orbital transition occurs (using correlation plus basis correction of -0.051055 h) (Figure 7).

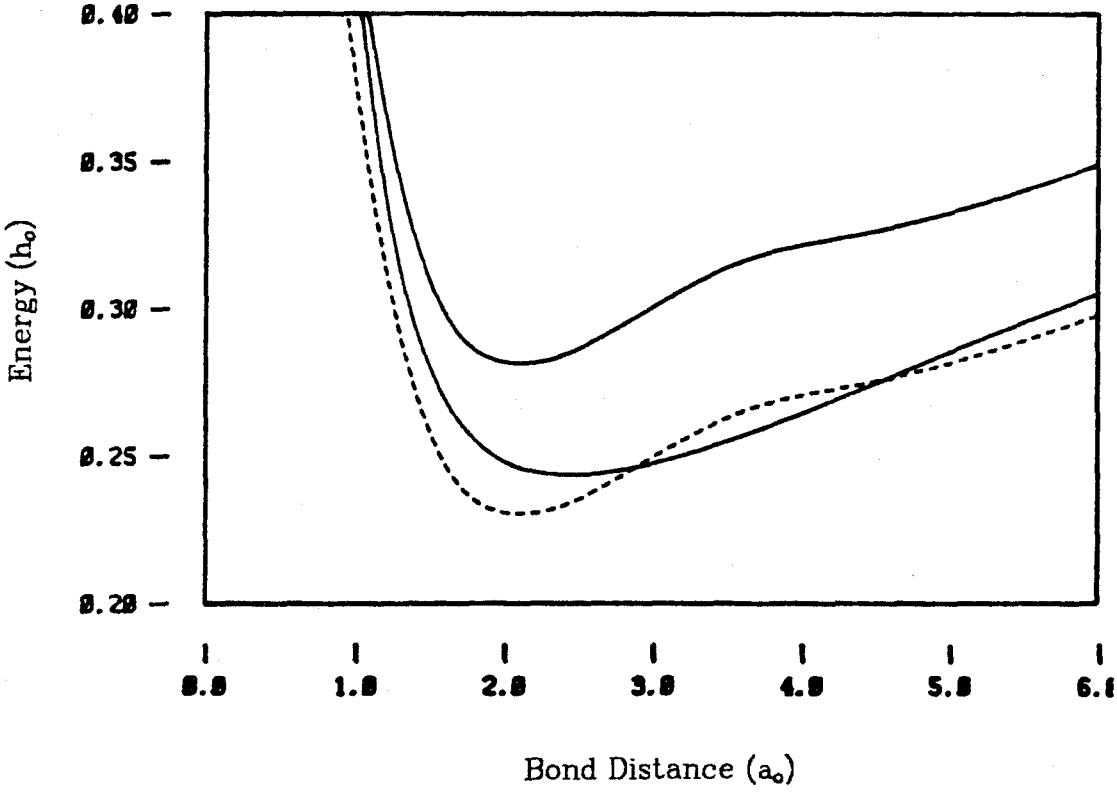

Figure 7. H_2 $^1\Sigma_u^+$ ACC(-.051055 h) (dashed) compared with HF (upper solid) and EXACT (lower solid).

Table 2. Results for H_2 $^1\Sigma_u^+$			
Wavefunction	$R_{min}(a_0)$	$E_{min}(h)$	$k_{min}(a.u.)$
HF	2.10	+0.281	0.077
HF(corr.+basis)	2.10	+0.230	0.077
EXACT	2.43	+0.243	0.033

We see that our approximate method yields excellent results for the ground state of H_2. However, we also see that the $^1\Sigma_u^+$ ionic excited state has some difficulties. For this excited state, our method retains the artifacts of Hartree-Fock: a bond distance too short and a force constant too strong. The problem with this excited state is seen to be that our energy correction is independent of orbital shapes. Our method of assigning ionic character with orthogonal localized orbitals seems consistent. We overcorrect only when the bonding and antibonding orbitals develop different atomic character in order to reduce the ionic nature of the bond. The open-shell singlet Hartree-Fock wavefunction is fully ionic when the atomic character of bonding and antibonding orbitals is the same. However, if the atomic character is orthogonal, say $1s$ and $2s$, then the Hartree-Fock wavefunction is half ionic and half covalent (ignoring normalization). Moreover, the covalent half has one excited atom $2s^1$, and the ionic half has one excited ion $1s^12s^1$. Thus, by developing different bonding and antibonding character, the open-shell singlet wavefunction can reduce its ionic character to half, and the remaining ionic character has less correlation error than the ground-state ion.

Let us consider a way to eliminate the flaw in our approximate method. We want to add our energy correction to ionic configurations only when the orbital shapes are consistent with closed-shell ionic char-

acter. Rather than add a constant correction independent of orbital shapes, we shall use a projection operator such that the ionic correction is applied to only the desired configurations. Consider the following two-electron projection operator:

$$C_l\,|\varphi_l\varphi_l><\varphi_l\varphi_l| + C_r\,|\varphi_r\varphi_r><\varphi_r\varphi_r|$$

This operator could be used to modify AO two-electron integrals prior to MCSCF. Thus, this projected ionic correction would directly affect both the CI wavefunction and the orbital shapes.

Consider applying this projection approach to H_2. If we choose φ to be the HF orbital of H^-, then the energy correction is precisely the same as we previously derived. If we choose φ to be the HF orbital of H, then the ionic energy correction must be determined iteratively, for the HF orbital of H^- will change with a change in the energy constant being projected. In order to avoid any double counting of the ionic correction at small distances, we should take φ_l and φ_r to be symmetrically orthogonal. To test this approach, we should transform our AO integrals into integrals over orthonormal MO's. Using symmetry, we take the first two MO's to be

$$\varphi_g = \varphi_l + \varphi_r$$

and

$$\varphi_u = \varphi_l - \varphi_r$$

The other MO's are Schmidt orthogonalized to these two. We add half our ionic energy correction to each of the four two-electron integrals J_{gg}, J_{uu}, J_{gu}, and K_{gu}. No other two-electron integrals are affected by the projection operator. These modified integrals over MO's can now be used straightforwardly in any MCSCF calculation. The bonding and antibonding

orbitals can mix in any character they wish. However, the full ionic energy correction will be applied only when both bonding and antibonding orbitals are linear combinations of φ_l and φ_r.

For the excited state of H_2, we have obtained dramatically improved results with projection. Projecting the correlation plus basis correction of -0.051055 h through H^- HF orbitals, we find that the minimum is no longer overcorrected. Projection produces remarkable agreement with the exact curve at small distances (Figure 8). Note that the projected results must be higher in energy than the unprojected results at all distances. Thus, the projected curve must depart from the exact curve where the unprojected curve is above exact. The projected and unprojected curves almost meet where the HF wavefunction is almost purely ionic. This occurs where the HF wavefunction experiences an orbital transition as the internuclear distance is changed. The artifactual shape of the HF curve continues to plague us, but projection has produced a curve whose shape is much closer to exact.

Table 3. Results for H_2 $^1\Sigma_u^+$

Wavefunction	$R_{min}(a_0)$	$E_{min}(h)$	$k_{min}(a.u.)$
HF	2.10	+0.281	0.077
HF(corr.+basis)	2.10	+0.230	0.077
HF(project H^-)	2.27	+0.246	0.063
EXACT	2.43	+0.243	0.033

How might we further improve these results? The short bond distance and strong force constant cannot be further improved without making the curve more stable where the HF orbital transition occurs. At this transition, the HF wavefunction becomes almost purely ionic. The HF

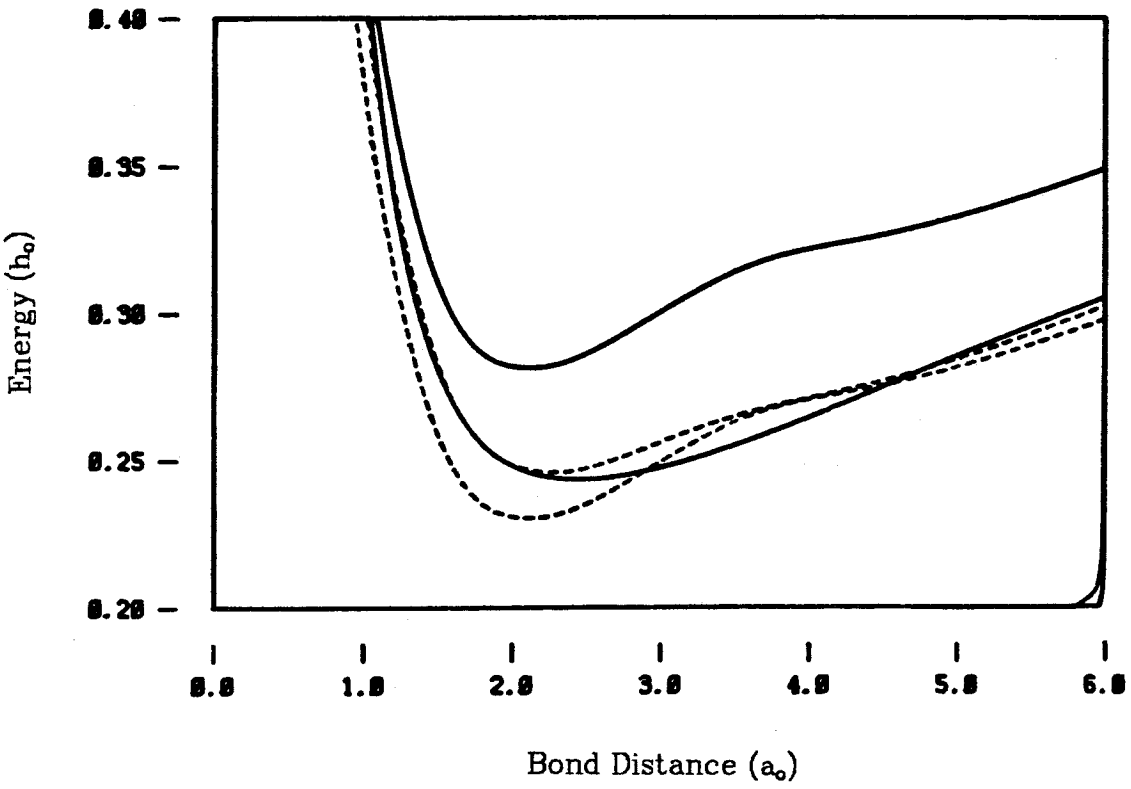

Figure 8. H_2 $^1\Sigma_u^+$ ACC(-.051055 h, H^- projected) (upper dashed) compared with ACC(-.051055 h) (lower dashed), HF (upper solid), and EXACT (lower solid).

wavefunction is too restrictive to allow the optimal mixing of ionic and covalent character. The exact wavefunction has maximal ionic character at this distance, but the exact wavefunction has more covalent character than HF. Thus, to improve our results, we must do more than stabilize the almost purely ionic character of the HF wavefunction at this distance. We must also try to correct for the restriction that the HF wavefunction cannot optimally mix in covalent character. We cannot obtain an energy lower than the unprojected -0.051055 h result without applying a stronger energy correction. If we choose any orbital other than the H^- HF orbital for our projection operator, the energy correction will be stronger than -0.051055 h. The energy correction will have to be solved iteratively to obtain the desired energy for H^-. In our basis, we desire an energy of -0.527631 h for H^- in order to match the experimental IP-EA:

$$0.472249 = 0.499940 - (-0.499940 + 0.527631)$$

If we select the HF orbital of H atom for our projection, then we find iteratively that an energy correction of -0.060972 h yields the proper excitation energy.

Projecting an ionic correction of -0.060972 h through H atom orbitals, we find that the problem at the HF orbital transition appears partly corrected (Figure 9). However, the spectroscopic constants are only slightly improved.

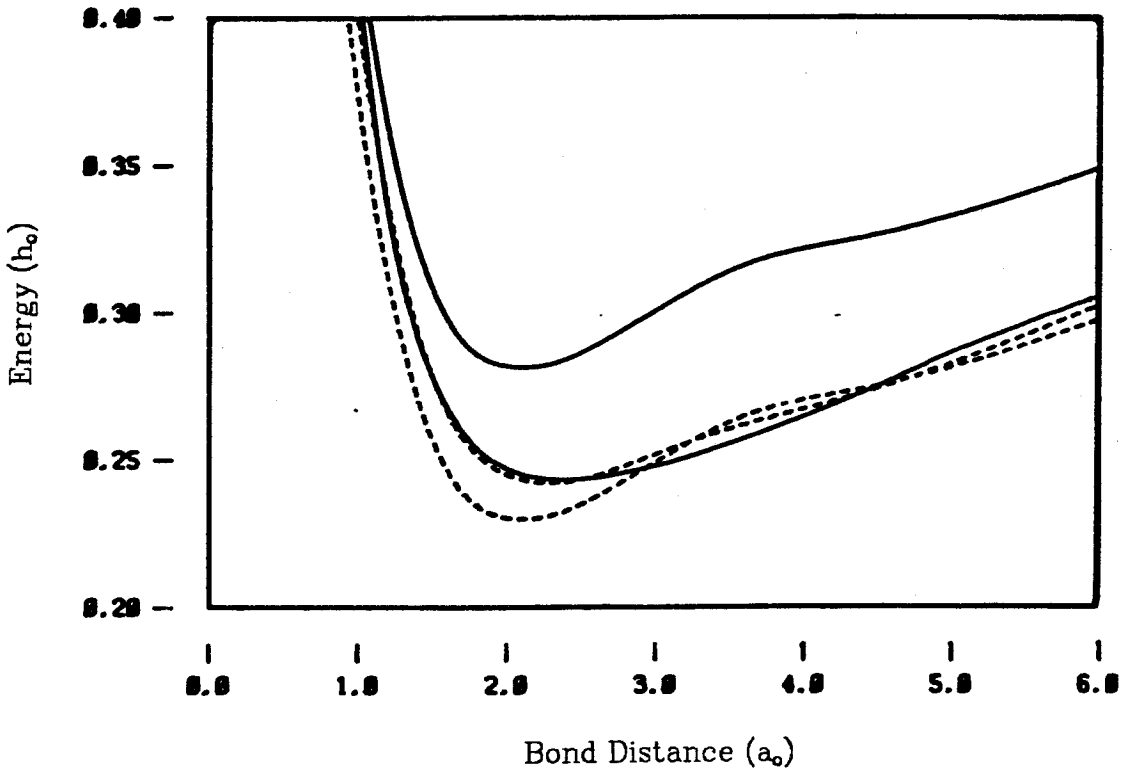

Figure 9. H_2 $^1\Sigma_u^+$ ACC(-.060972 h, H projected) (upper dashed) compared with ACC(-.051055 h) (lower dashed), HF (upper solid), and EXACT (lower solid).

Table 4. Results for H_2 $^1\Sigma_u^+$			
Wavefunction	$R_{min}(a_0)$	$E_{min}(h)$	$k_{min}(a.u.)$
HF	2.10	+0.281	0.077
HF(corr.+basis)	2.10	+0.230	0.077
HF(project H^-)	2.27	+0.246	0.063
HF(project $H\cdot$)	2.29	+0.242	0.063
EXACT	2.43	+0.243	0.033

The insensitivity of these results to the orbital being projected is encouraging. The safest approach would be to project through the orbital yielding the weakest (noniterative) energy correction. However, improved results might be obtained with another orbital having a stronger (iterative) energy correction. Consider the ground state of H_2 using these two projections (Figures 10 and 11).

Table 5. Results for H_2			
Wavefunction	$R_{min}(a_0)$	$E_{min}(h)$	$k_{min}(a.u.)$
GVB	1.43	-0.151	0.34
GVB(corr.)	1.42	-0.167	0.35
GVB(corr.+basis)	1.42	-0.172	0.36
GVB(project H^-)	1.43	-0.165	0.34
GVB(project $H\cdot$)	1.42	-0.175	0.36
EXACT	1.40	-0.174	0.37

We may find that projecting through ground-state singly-occupied orbitals will yield the best overall agreement with exact potential curves.

In the examples to follow, we shall use projection to assess how much we may be overcorrecting for the ionic character in our unpro-

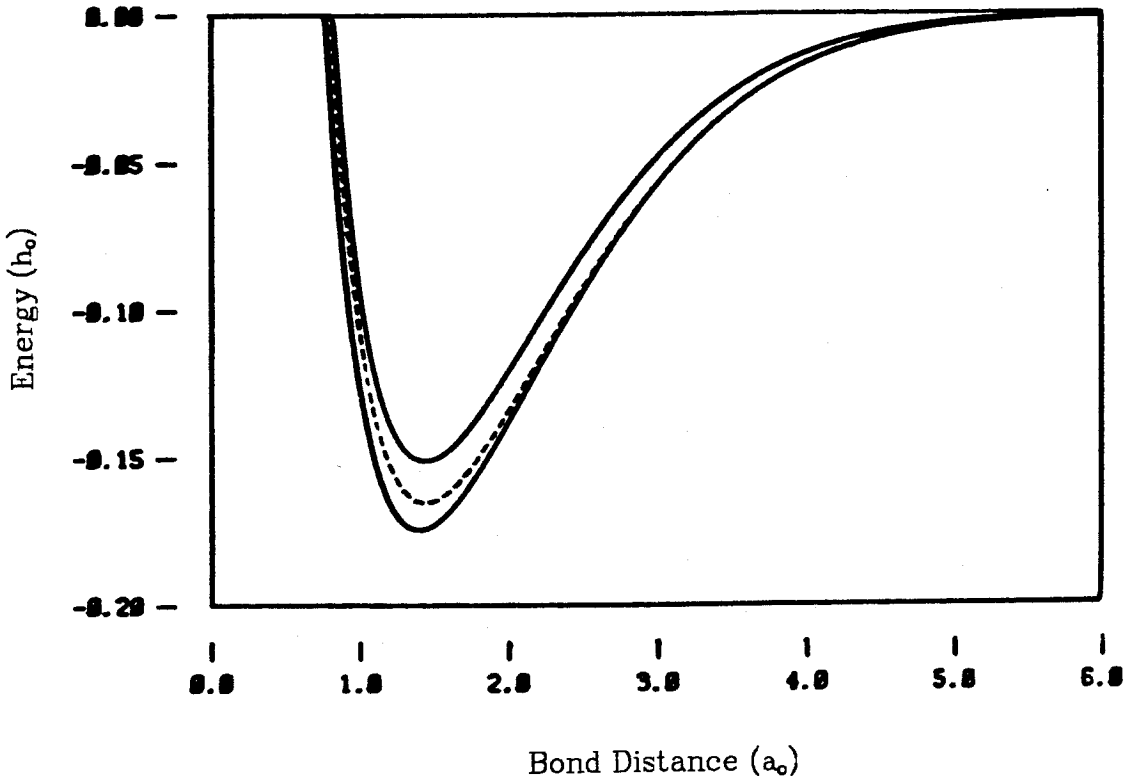

Figure 10. H_2 $^1\Sigma_g^+$ ACC(-.051055 h, H^- projected) (dashed) compared with GVB (upper solid) and EXACT (lower solid).

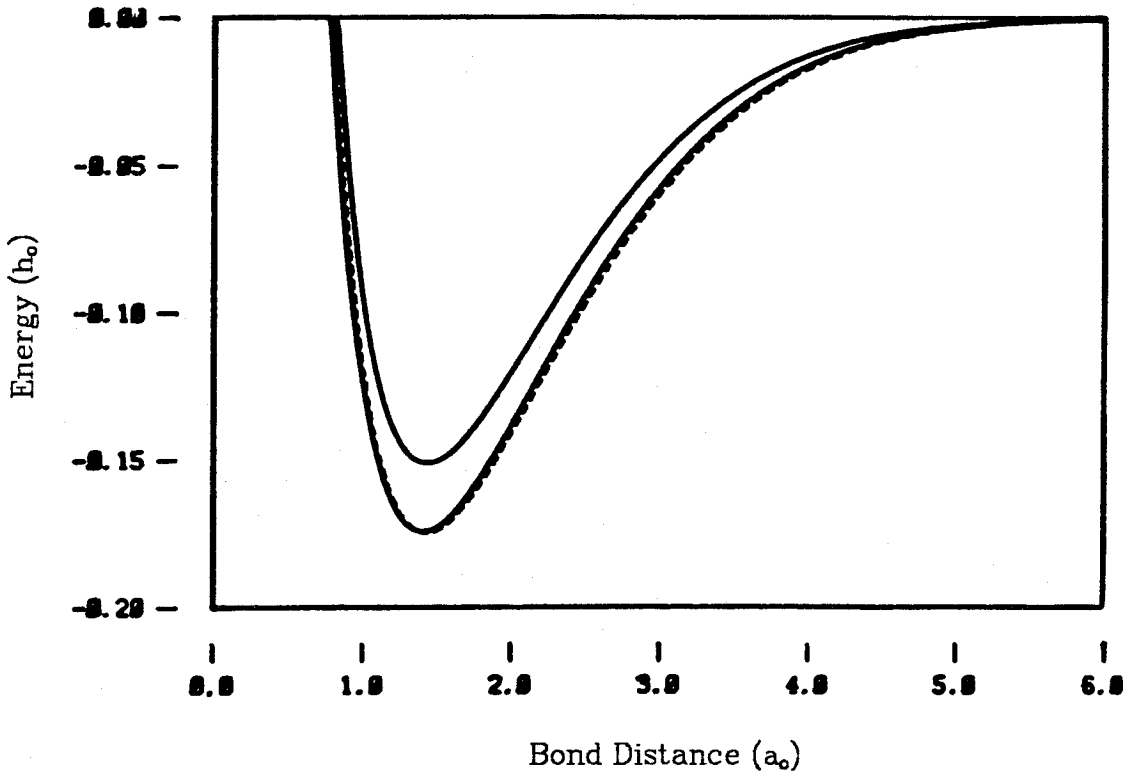

Figure 11. H_2 $^1\Sigma_g^+$ ACC(-.060972 h, H projected) (dashed) compared with GVB (upper solid) and EXACT (lower solid).

jected method. Thus, we shall consider projection as a test of the accuracy of our unprojected results. As a test, we shall take the same ionic energy correction used in the unprojected calculations and project that correction through the orbitals which give the lowest energy. The overcorrection for ionic character cannot be larger than the difference between projected and unprojected energies. Thus, we want projection orbitals which yield the lowest projected energy. For the excited ionic state of H_2, projecting through H^- orbitals would be expected to yield the lowest energy. However, for the ground state of H_2, projecting through H^- orbitals would be expected to yield the lowest energy. Consider the ground state of H_2 with the correlation plus basis correction of -0.051055 h (Figure 6). Our projection test (Figure 12) proves that overcorrection for ionic terms in the ground state, unlike the excited state, is an insignificant problem.

Table 6. Results for H_2

Wavefunction	$R_{min}(a_0)$	$E_{min}(h)$	$k_{min}(a.u.)$
GVB	1.43	-0.151	0.34
GVB(project H^-)	1.42	-0.171	0.35
GVB(corr.+basis)	1.42	-0.172	0.36
EXACT	1.40	-0.174	0.37

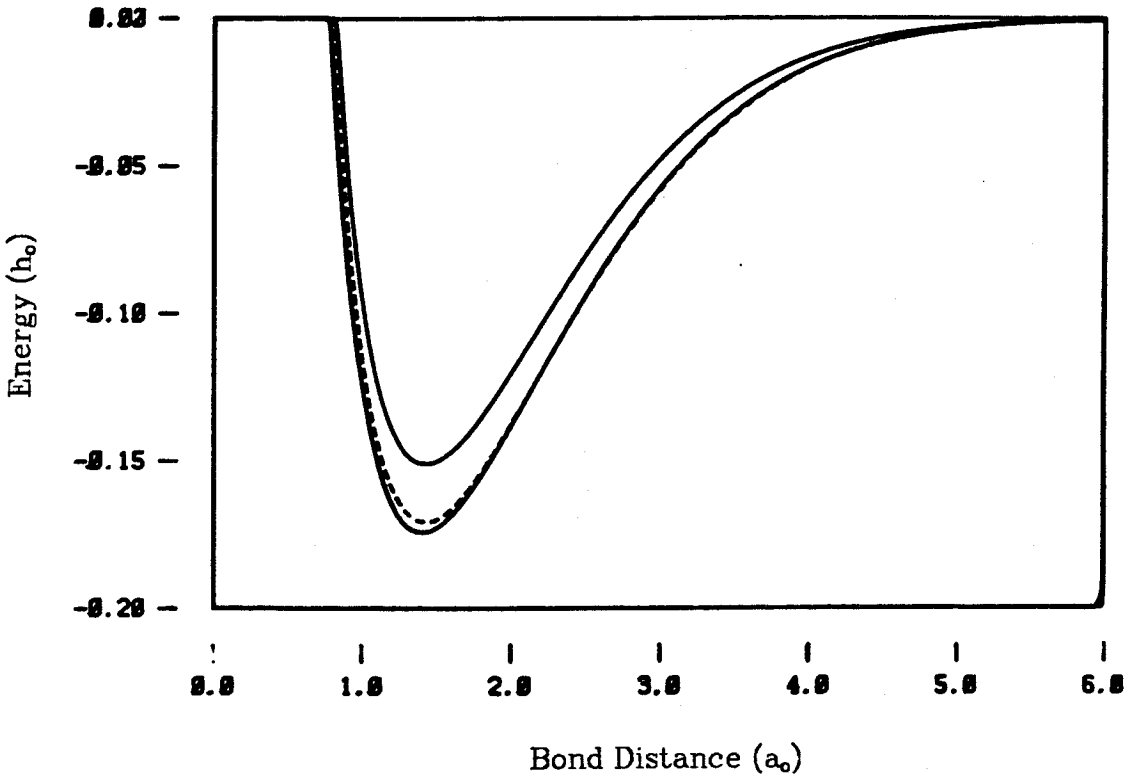

Figure 12. H_2 $^1\Sigma_g^+$ ACC(-.051055 h, H projected) (dashed) compared with GVB (upper solid) and EXACT (lower solid).

B. Multiple- Bond Test with N_2

We have demonstrated that our approximate method is excellent for H_2. However, we must show that the method also yields accurate results for multiple bonds. N_2 has been selected for this test. We need to obtain ionic corrections for each of the $p-p$ bonds. These corrections shall be obtained from atomic calculations and thus apply rigorously only to infinite separation. However, we find that excellent results are obtained by applying this atomic correction over the full potential surface. The covalent wavefunction of N_2 has two ground-state atoms:

$$(p^3)_l - (p^3)_r$$

An ionic configuration in one of the $p-p$ bonds yields a cation and an anion:

$$(p^2)_l - (p^4)_r$$

The anion is not thought to be stable relative to the ground-state atom. The experimental estimate for the excitation energy from the covalent to ionic configuration, IP-EA (eV), is

$$14.63 = 14.56 - (-0.07)$$

HF calculations in our basis yield

$$16.02 = 14.00 - (-2.02)$$

Thus, the energy correction to ionic configurations in the $p-p$ bonds should be 1.39 eV. This correction is for both correlation and basis set errors, which are larger for the ionic configurations than for the covalent wavefunction. Our basis is the $(9s\,5p/3s\,2p)$ Dunning[8] contraction of the Huzinaga basis for N atom plus a set of diffuse s and p gaussians (ζ_s=0.066, ζ_p=0.045) and a set of d polarization functions (ζ_d=0.76).

Consider the correlation errors we are correcting. The error in our HF IP is simply the correlation error between the electron being ionized and all other electrons in the atom. The error in our HF EA is the correlation error between the electron being added and all other electrons in the anion. The part of this correlation error that is between the added electron and electrons in other orbitals is nearly the same as the correlation error in the HF IP. The correlation error in an ionic configuration is larger than the correlation error in the covalent wavefunction because of the correlation error between the two electrons in the doubly-occupied p orbital of the anion. Thus, our correlation correction is simply an intrapair correction. The basis correction is mostly an intrapair correction, because a doubly-occupied p orbital wants to be more diffuse than a singly-occupied p orbital. We shall apply an ionic correlation plus basis correction of 1.39 eV to each p–p bond. Since this ionic correction is an intrapair correction, the correction applied to one bond pair is independent of the correction applied to another pair.

We have chosen to treat N_2 with symmetry. Each bond is described with a bonding and an antibonding orbital. The wavefunction includes all symmetry-allowed configurations with two electrons in each of the three bonds and the rest of the electrons in HF core. We consider this MCSCF to be the proper *ab initio* wavefunction upon which to base an approximate correction for the correlation error associated with ionic configurations. We may refer to this MCSCF as a GVB wavefunction; however, this MCSCF includes interpair correlations not included in GVB, which are found to be important for N_2. Because of interpair correlations, an ionic configuration in one bond may be correlated with ionic

configurations in the other bonds to partially neutralize the charge transfer. To the extent that our ionic correction of 1.39 eV is strictly an intrapair correction, we wish to correct the energy of a CI configuration by the full 1.39 eV for *each* ionic $p-p$ bond.

For our unprojected method, we modify the MCSCF procedure by correcting the integrals used to set up the CI matrix. Each of the three $p-p$ bonds is described with a bonding and an antibonding orbital. We add -(1.39/2) eV to each of the integrals J_{gg}, J_{uu}, J_{gu}, and K_{gu} for each of the three $p-p$ bonds. Thus, we modify twelve of the two-electron integrals used to construct the CI matrix. This method applies the full ionic correction regardless of orbital shapes. Possible overcorrection of ionic terms can be tested with projection.

Our projection test involves projecting the same correction of 1.39 eV through atomic p orbitals. For each of the $p-p$ bonds, we apply the projection operator

$$C_p\,|p_l p_l><p_l p_l\,| + C_p\,|p_r p_r><p_r p_r\,|$$

This projection is actually accomplished with symmetry orbitals. We take symmetry combinations of atomic p orbitals and orthogonalize these MO's to the core functions from our unprojected method. Thus, the p orbitals in our projection operator are atomic p orbitals which are orthogonalized to the molecular core and symmetrically orthogonalized to each other. We freeze the core to prevent any artifactual energy lowering resulting from HF core orbitals rotating with bonding orbitals. However, a test of this effect at R_e results in negligible energy lowering upon relaxing the core.

Our calculations were peformed at five distances: the experimental R_e and two points at 0.05 Å increments on either side of R_e. A spline

fit was used to obtain equilibrium parameters.

Table 7. Results for N_2

Wavefunction	R_e(Å)	D_e(eV)	$\omega_e(cm^{-1})$
GVB-PP	1.112	6.72	2379
GVB-AI	1.122	8.36	2334
GVB-CC	1.118	10.09	2373
GVB-PC	1.119	10.01	2366
EXACT	1.0977	9.901	2358

These results are extremely encouraging. We find that possible over-correction of ionic terms is not a significant problem. All our computed spectroscopic parameters are brought close to the experimental values. Comparing our results with those of Dunning,[9] we expect a more flexible basis to contract our bond distance by 0.019 Å, increase our dissociation energy by 0.22 eV, and increase our vibrational frequency by 11 cm^{-1}. The *ab initio* calculation, GVB-AI, should have a longer bond distance, smaller dissociation energy, and smaller vibrational frequency than experimental. The GVB calculation with constant correction for ionic terms, GVB-CC, yields a slightly shorter bond distance and slightly larger vibrational frequency than GVB-AI. The bond energy is corrected by 1.7 eV to be within a few tenths eV of the experimental bond energy. The GVB calculation with projected correction for ionic terms, GVB-PC, yields almost the same parameters as GVB-CC. Thus, the overcorrecting of ionic terms is not a significant problem here.

Dunning[9] has plotted the experimental RKR curve for N_2 with the equivalent of our GVB-AI curve. The experimental curve was extrapolated beyond the highest observed vibrational level. This extrapolation yields a

larger energy difference between GVB-AI and RKR at larger internuclear distances than where the extrapolation first begins. We would expect that our method would apply a smaller energy correction as the internuclear distance is increased, suggesting that our corrected curve will also deviate from the extrapolated region of the RKR curve. It will be interesting to carry out calculations in this region to determine whether the problem is with the calculation or with the RKR extrapolation.

C. Results for Cr_2 and Mo_2

We have tried our approximate method (without projection operators) on Cr_2, and we obtain extremely encouraging results. How shall we obtain ionic corrections for this system? Just as for H_2, we shall consider Cr_2 at infinite separation. In this way, we shall obtain the atomic correction for correlation error which we shall apply over the full potential surface. The covalent wavefunction has two ground-state atoms:

$$(s^1d^5)_l - (s^1d^5)_r$$

Ionic configurations in the $s-s$ bond have one ground-state Cr^+ and one ground-state Cr^-:

$$(s^0d^5)_l - (s^2d^5)_r$$

To determine the ionic correction in the $s-s$ bond, we simply find the error in our excitation energy from the covalent to the ionic wavefunction:

$$E(s^0d^5) + E(s^2d^5) - 2E(s^1d^5) = IP_{Cr} - EA_{Cr}$$

The experimental excitation energy, IP-EA (eV), is

$$6.11 = 6.77 - 0.66$$

while HF calculations in our basis yield

$$6.77 = 5.95 - (-0.82)$$

Thus, the energy correction to ionic configurations in our $s-s$ bond should be 0.66 eV. This corrects for the greater correlation and basis error in the ionic wavefunction than in the covalent wavefunction. (Note that numerical Hartree-Fock results were not readily available for Cr^-. Thus, we were unable to separate correlation error from basis error.)

How shall we obtain the ionic correction for a $d-d$ bond? An ionic configuration in one $d-d$ bond has an excited-state Cr^+ and an excited-state Cr^-:

$$(s^1d^4)_l - (s^1d^6)_r$$

To determine the ionic correction in a $d-d$ bond, we simply find the error in our excitation energy from the covalent to the ionic wavefunction:

$$E(s^1d^4) + E(s^1d^6) - 2E(s^1d^5) = IP^*_{d_r} - EA^*_{d_r}$$

The $IP^*_{d_r}$ is simply the ionization potential of a d electron from the ground state. The $EA^*_{d_r}$ is the electron affinity of the ground state for adding a d electron. This electron affinity is negative both theoretically and experimentally. When we add a d electron to the ground s^1d^5 configuration to give s^1d^6, the valence s electron ionizes to yield s^0d^6. Thus, $-EA^*_{d_r}$ is the excitation energy from s^1d^5 to s^0d^6. Experimentally, the excitation energy from the covalent to the ionic wavefunction (with a continuum s electron from Cr^-), $IP^*_{d_r} - EA^*_{d_r}$ (eV), is

$$12.69 = 8.29 - (-4.40)$$

Numerical Hartree-Fock calculations yield

$$14.09 = 7.06 - (-7.03)$$

Thus, the correlation error is 1.40 eV greater in the ionic wavefunction than in the covalent wavefunction. In our basis, the Hartree-Fock excitation energy is

$$14.43 = 7.42 - (-7.01)$$

To correct for both basis and correlation error, we can apply 1.74 eV energy correction to ionic configurations in $d-d$ bonds.

Before we had arrived at this very logical procedure for obtaining ionic corrections, we had obtained an almost identical result from an alternative approach. To find the intrapair correlation error in a doubly-occupied d orbital, we examined the error numerical Hartree-Fock calculations make in ionizing an electron from a doubly-occupied d versus the error in ionizing a singly-occupied d. Numerical Hartree-Fock predicts that ionizing an electron from the doubly-occupied d orbital of Cr d^6 to give Cr d^5 results in 1.12 eV energy lowering. Experimentally, however, this process is 2.36 eV endothermic. Thus, there is a total of 3.48 eV correlation error in describing this ionization. Numerical Hartree-Fock predicts that ionizing an electron from a singly-occupied d orbital of V d^5 to give V d^4 costs 2.54 eV. Experimentally, this process costs 4.26 eV. Thus, there is only 1.72 eV correlation error in describing this ionization. The difference in correlation errors between these two ionizations, 1.76 eV, is the correlation error between the two electrons in the doubly-occupied d orbital. This is the value we used for the energy correction of ionic terms in $d-d$ bonds of Cr_2. The new value of 1.74 eV we obtain from just Cr states (not V) is so close that the Cr_2 results should be virtually identical.

How did we apply this ionic correction to Cr_2? First, we decided to treat the $s-s$ bond fully *ab initio* and thus to test only the $d-d$ effect. The $s-s$ bond was described with eight orbitals including all correlations leading to van der Waals interactions at large distances. It would be interesting to test the $s-s$ effect, as our correction would not properly mimic the covalent van der Waals interactions but would properly mimic the correlations of ionic terms. An ionic correction of 1.76 eV was applied to each $d-d$ bond. The ionic correction we have chosen is strictly an

intrapair correction. The ionic correction applied to one pair is independent of the correction applied to another pair. Thus, the energy of a given CI configuration must be corrected by 1.76 eV for *each* ionic $d-d$ bond. The simplest way to apply this correction to ionic configurations in the CI is to modify the integrals used to set up the CI matrix. Each $d-d$ bond is described with a bonding and an antibonding orbital. We add -0.88 eV (-1.76/2) to each of the integrals J_{gg}, J_{uu}, J_{gu}, and K_{gu} for each of the five $d-d$ bonds. Thus, we add the same constant energy correction to twenty of the two-electron integrals used to set up the CI matrix.

Our preliminary results for the ground state of Cr_2 are quite promising. We applied an *un*projected ionic correction of 1.76 eV to each $d-d$ bond. (An almost identical value of 1.74 eV corresponds to our most rigorous derivation of a correlation plus basis correction.)

Table 8. Results for Cr_2

Wavefunction	R_{min}(Å)	$E_{min}(eV)$	$\omega_e(cm^{-1})$
GVB-vdw	3.06	-0.35	110
GVB-vdw(corr.+basis)	1.63	-1.39	690
EXPERIMENT	1.68	-1.56	470

Our approximate correction yields the same long-distance minimum as was obtained in a fully *ab initio* calculation. However, this method also yields a short-distance minimum which corresponds to the experimentally observed well (Figure 13). A substantial hump is found between these two wells. This is very strong evidence that the ground state of Cr_2 has a *double well*.

Note that our bond distance is a little too short and our vibrational frequency is too large. We have already seen in H_2 that this is to be

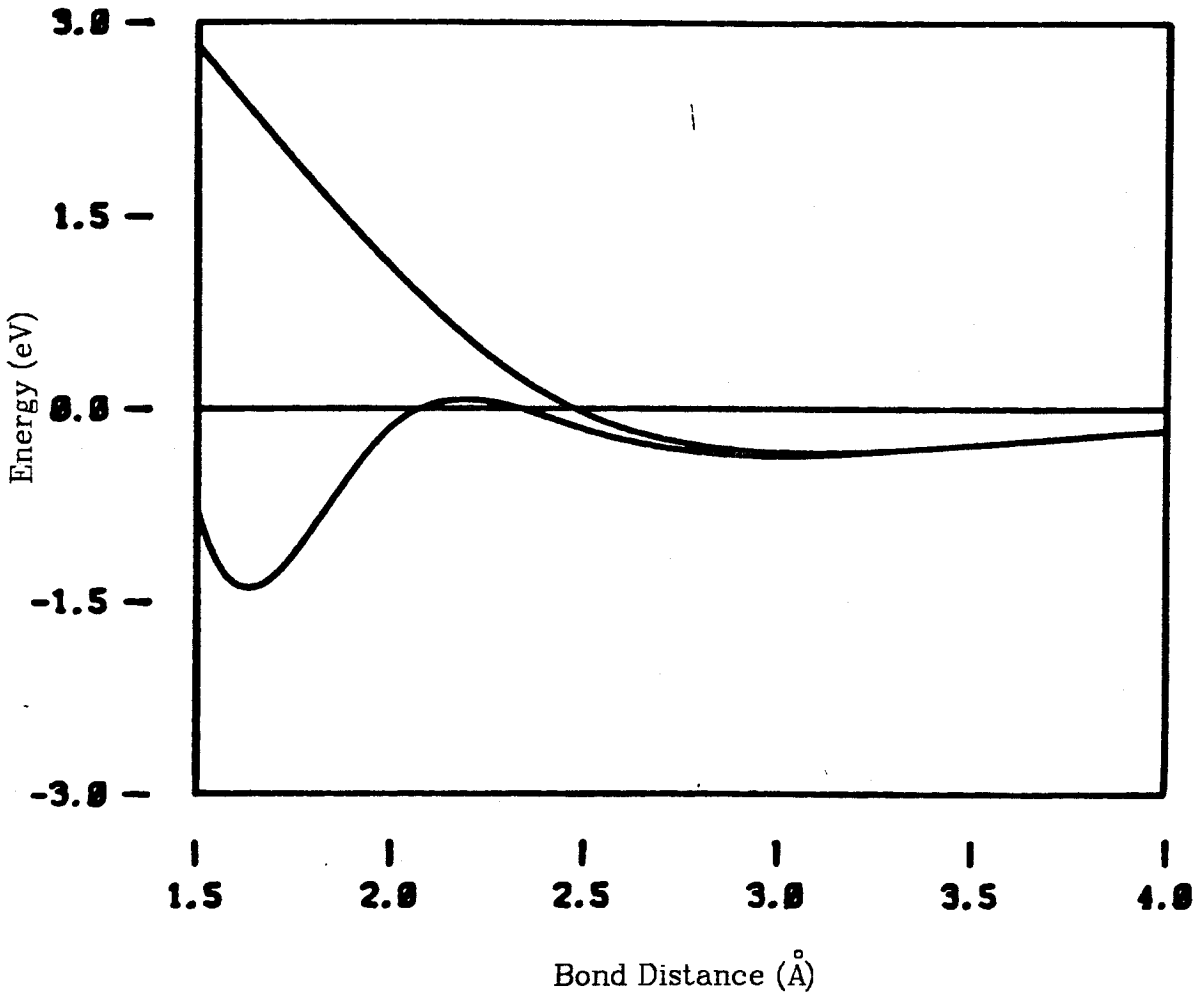

Figure 13. Comparison between ***ab initio*** (upper) and ACC (lower) potential curves for Cr_2.

expected when an unprojected ionic correction is being applied and the orbitals readjust to reduce the actual ionic character. Unlike H_2, the ground state of Cr_2 can have substantial open-shell singlet character in the bond pairs. This ionic character is responsible for interpair correlations in the ground state of Cr_2. Thus, the artifacts we observed in the excited state of H_2 may be evident in the ground state of Cr_2. However, the double well is *not* an artifact. If we were to apply a *projected* ionic correction, we would necessarily obtain a potential curve that is less stable at all distances than our *un*projected results. Since the outer minimum of Cr_2 is obtained without any ionic correction, the hump would remain, and Cr_2 would still have a double well. Thus, we would expect projected ionic corrections to give us virtually the same results but with improved spectroscopic constants for the inner well.

We attempted to apply unprojected ionic corrections to the excited $^1\Sigma_u^+$ state of Cr_2. Unfortunately, the problems we encountered in the excited state of H_2 seem quite evident here as well. We first tried the 3408-configuration MCSCF we used to obtain the dipole-allowed transitions from our 6064-configuration MCSCF of the ground state at the outer minimum. For the $^1\Sigma_u^+$ excited state, this wavefunction restricts the $4s$ and $4p_\sigma$ electrons to be orthogonal. At long distance, this orthogonality restriction is not very important. However, at short distance, it becomes necessary to include CI configurations in which these two electrons are allowed to overlap in the $4s$-space. With our unprojected ionic correction for the $d-d$ bonds, we observe that the $^1\Sigma_u^+$ state develops dominant $\delta \rightarrow \delta^*$ character. The experimental transition is 21750 cm^{-1}, whereas our calculations lead to an excitation of 16000 cm^{-1}. It appears that our unprojected ionic correction for the $d-d$ bonds is overcorrecting for the

excited $^1\Sigma_u^+$ state of Cr_2 in the same way that it overcorrects for the excited $^1\Sigma_u^+$ state of H_2.

We decided to test the effect of projection on our Cr_2 potential. For direct comparison, we used the same ionic correction of 1.76 eV for each $d-d$ bond. We selected the d orbitals from the ground s^1d^5 state for projection. The test was made at 3.2 a_0, the experimental minimum. The effect of projection on the ground state was only 1.0 mh. The effect on the excited $^1\Sigma_u^+$ state was only about 1.3 mh. (The unprojected result had not been fully converged. Otherwise, we should have obtained an effect of 1.5 mh, as explained shortly.) Thus, Cr_2 does not suffer the large projection errors we encountered for the excited $^1\Sigma_u^+$ state of H_2. The ground-state curve is virtually identical, except that the inner well should have slightly improved spectroscopic constants. The ground-state curve definitely has a double well. The excited state is also virtually unchanged with projection. This state retains dominant $\delta \rightarrow \delta^*$ character with projection. At 3.2 a_0, we make 2.07 ionic $d-d$ corrections for the ground state and 3.08 ionic $d-d$ corrections for the excited state. Clearly, the excited state has an additional ionic $d-d$ bond. This is why we expected for the excited state to have 3/2 the effect of projection as the ground state. The excitation energy to the excited state is still too small with projection. However, we expect this to dramatically improve with refinements of our approximate method. Further refinements are expected to yield smaller ionic energy corrections than we have obtained in this test. Since the excited state has one more ionic $d-d$ correction than the ground state, we expect these refinements to increase the state splitting. The correction constant should be weaker (-1.74 eV), and the d orbital used for projection should be more diffuse. The latter change is expected

to yield significantly improved results.

We shall now consider some improvements in our approximate method as applied to Cr_2. Let us consider making ionic corrections in the $s-s$ bond as well as in the $d-d$ bonds. We then have a projection operator for ionic terms in the $s-s$ bond

$$C_s\,|s_l s_l><s_l s_l\,| + C_s\,|s_r s_r><s_r s_r\,|$$

and each of the $d-d$ bonds

$$C_d\,|d_l d_l><d_l d_l\,| + C_d\,|d_r d_r><d_r d_r\,|$$

If we choose the s orbital being projected to have the shape of the valence s orbital in s^2d^5, then C_s = -0.66 eV. If we choose the d orbital being projected to have the shape of the doubly-occupied d orbital in s^0d^6, then C_d = -1.74 eV. Another alternative is to choose the valence orbitals of s^1d^5, but this choice requires an iterative determination of C_s and C_d. Perhaps the best s orbital to use is from an SCF which is the average of s^0d^5 and s^2d^5. This corresponds to the actual ionic limit in our symmetry-restricted calculation. The value of C_s could be determined *non*iteratively, once the energy of this SCF is known. Perhaps the best d orbital to use is from an SCF which is the average of s^1d^4 and s^1d^6. The valence s orbital should be stable in this SCF. This should correspond to an actual ionic limit in our symmetry-restricted calculation. The value of C_d could be determined *non*iteratively, if the experimental energy for s^1d^6 were known. Unfortunately, a resonance corresponding to this unbound state is not known. The answer may be to use an SCF which is the average of s^1d^4 and s^0d^6.

The approximate method of projecting ionic energy corrections through symmetrically orthogonalized valence orbitals can be extended

to general multicenter heteroatom bonding. The possibilities for obtaining accurate bonding interactions in complicated transition-metal systems are very exciting. The main difficulty will be to obtain the necessary experimental IP's and EA's for ionic corrections. These quantities can be so difficult to determine accurately even for an atom that we do not wish to depend on theoretical estimates of the exact IP's and EA's. For Cr_2, we were able to obtain the necessary ionic correction energy even though the desired experimental EA was not known. Undoubtedly, similar creative applications of the known experimental data will be useful for other systems as well.

We were so encouraged by the approximate results for Cr_2 that we decided to see how much bonding would be obtained for Mo_2. The calculation was performed exactly like that for Cr_2. We applied an ionic correction to each $d-d$ bond. Our ionic correction was obtained in precisely the same way that the correction of 1.76 eV was obtained for Cr. We obtained the intrapair correlation error in a doubly-occupied d orbital by examining the error numerical Hartree-Fock calculations make in ionizing an electron from a doubly-occupied d versus the error in ionizing an electron from a singly-occupied d. Ionizing an electron from the doubly-occupied d orbital of Mo d^6 to give Mo d^5 costs 3.92 eV experimentally, but only 1.95 eV with numerical Hartree-Fock. Thus, there is 1.97 eV correlation error in describing this ionization. Ionizing an electron from the singly-occupied d orbital of Nb d^5 to give Nb d^4 costs 5.46 eV experimentally, but only 4.49 eV with numerical Hartree-Fock. Thus, there is 0.97 eV correlation error in describing this ionization. The difference in correlation errors between these two ionizations, 1.00 eV, is the correlation error between the two electrons in the doubly-occupied d orbital. We

used this value, 1.00 eV, for the energy correction of ionic terms in $d-d$ bonds of Mo_2.

We calculated four geometries for Mo_2: experimental R_e, points 0.1 Å on either side of R_e, and 2.2 Å. We compare the parameters from the spline-fit of the same four points of the *ab initio* calculation.

Table 9. Results for Mo_2

Wavefunction	R_{min}(Å)	$E_{min}(eV)$	$\omega_e(cm^{-1})$
GVB-vdw	1.97	-1.41	459
GVB-vdw(1eV CC)	1.94	-3.27	532
EXPERIMENT	1.93	-4.20	477

These results are quite encouraging. Even with this crude estimate for an ionic correlation correction, we have obtained good results.

IV. Conclusion

Now that we have used the atomic correlation correction (ACC) to look at Cr_2 and Mo_2, we should compare with other approximate methods. The most sophisticated approximate method applied to Cr_2 or Mo_2 is the local-spin-density (LSD) approach. For these molecules, LSD yields excellent bond distances and reasonable bond energies.[10] However, the shapes of the curves are questionable. This method does *not* describe the changes in spin coupling that occur with internuclear distance. We know that at large distances, the $d-d$ bond couplings lead to less than 1/5 maximal bonding. However, the LSD method does not account for this factor. Since the parameters in LSD lead to a nearly proper bond energy (about 20% high) at R_e, where the $d-d$ bond coupling is near unity, the LSD method must overestimate $d-d$ bonding at longer R. The curve for Cr_2 looks especially suspicious. As the molecule dissociates from R_e, the energy appears to increase *linearly*. It is even possible that the curve has a discontinuous slope near the minimum. Such a discontinuity is expected at the point where UHF degenerates to HF (at which point the system changes from a net spin density to no spin density).

Looking critically at our own results, we see that both Cr_2 and Mo_2 have bonds that appear to be a bit too weak. The experimental bond energy for Cr_2 is quoted as 36±7 kcal = 1.56±.3 eV.[2] However, using the latest parameters (g_2=1, ω_e=470 cm^{-1}, r_e=1.68 Å),[11] this third law value should be corrected to 45±7 kcal = 1.95±.3 eV. Thus, our bond energies of 1.39 eV and 3.27 eV for Cr_2 and Mo_2 are about 0.6 eV and 0.9 eV too small, respectively. Coupled with the fact that our vibrational frequencies are too large for these molecules, we must ask what effect is missing. One simple answer is that we are not applying full correlation correction to

the $s-s$ bond. This could significantly improve our results. Another answer is that we still have errors in atomic state splittings. Should the ground state wish to mix in some atomic d^6 character, our correction scheme does not fully account for the correlation error in this state relative to the ground s^1d^5 state. Experimentally, this excitation is 4.40 eV, while HF in our basis gives 7.03 eV. With the intrapair correction of 1.76 eV used for Cr_2, we would calculate an excitation energy of 5.27 eV, still 0.87 eV high.

The ACC calculation could also be improved by including both d and s projected ionic corrections. Fortunately, our error in the s-IP (0.82 eV) is very close to our error in the d-IP (0.87 eV). Thus, we can project IP-EA corrections into s and d orbitals independent from where the electrons are ionized. We can then allow electronic excitations *between* the two σ-bonds. This calculation should yield full correlation in the $s-s$ bond and allow the correlation-corrected d^6 state to optimally contribute to the bonding.

We expect improved calculations such as those described above will yield potential curves for Cr_2 and Mo_2 in much better agreement with the experimental bond energies and vibrational frequencies. The double well of ground-state Mo_2 will likely be washed out by the correlation correction. However, the double well will surely remain in the triplet or quintet state. It appears that the double well of ground-state Cr_2 will survive any further improvements in the calculations.

References

(1) E.P. Kundig, M. Moskovits, and G.A. Ozin, *Nature (London)* **1975,** *254*, 503.

(2) A. Kant and B. Strauss, *J. Chem. Phys.* **1966,** *45*, 3161.

(3) Yu.M. Efremov, A.N. Samoilova, and L.V. Gurvich, *Opt. Spektrosk.* **1974,** *36*, 654.

(4) M.M. Goodgame and W.A. Goddard III, *J. Phys. Chem.* **1981,** *85*, 215.

(5) M.M. Goodgame and W.A. Goddard III, *Phys. Rev. Lett.* **1982,** *48*, 135.

(6) D.L. Michalopoulos, M.E. Geusic, S.G. Hansen, D.E. Powers, and R.E. Smalley, *J. Phys. Chem.* **1982,** *86*, 3914.

(7) R.A. Kok and M.B. Hall, *J. Phys. Chem.* **1983,** *87*, 715.

(8) T.J. Dunning, Jr., *J. Chem. Phys.* **1970,** *53*, 2823.

(9) T.H. Dunning, Jr., D.C. Cartwright, W.J. Hunt, P.J. Hay, and F.W. Bobrowicz, *J. Chem. Phys.* **1976,** *64*, 4755.

(10) B. Delley, A.J. Freeman, and D.E. Ellis, *Phys. Rev. Lett.* **1983,** *50*, 488.

(11) V.E. Bondybey and J.H. English, *Chem. Phys. Letters* **1983,** *94*, 443.

Conclusion to Thesis

We now understand what has made metal-metal multiple bonds so difficult to treat. There are two major difficulties. One has to do with the problem of properly describing the high-spin coupling optimal within an atom while simultaneously accounting for the couplings of spins on different centers (which favor low-spin coupling). We have been able to generate programs and procedures for handling this problem, albeit with wavefunctions rapidly becoming too costly for even moderate sized systems (e.g. four transition-metal atoms). The second difficulty is the large correlation error associated with the charge transfer into a localized *d*-orbital that is an intrinsic part of covalent *d*-bonds. When electronegative ligands such as O or N species are bonded to a transition metal, there is significant charge transfer from the metal to the ligand, but not vice versa. The very same correlation error which hurts charge transfer into a *d*-orbital actually enhances charge transfer out of a *d*-orbital. Thus, we can calculate *d*-bonds to electronegative ligands with reasonable accuracy. For more covalent *d*-bonds to H or C species, the error starts to become quite significant. For purely covalent metal-metal $d-d$ bonds, the correlation error in bonding is far larger than we have ever before encountered. In order to provide estimates of these effects, we have developed the atomic correlation correction (ACC) procedure for correcting *ab initio* GVB wavefunctions. This procedure seems to provide good estimates of the remaining effects.

APPENDICES

Appendix A. CI with Arbitrary No. Open-Shell Electrons

I modified CIGEN, the configuration generator for CI calculations written by Barry D. Olafson, to allow more than six open-shell electrons. The default maximum number of open shells is set to six so that new default calculations will be consistent with calculations prior to the change. The user may override the default maximum number of open shells to any desired value. The program will construct a table giving the number of spineigenfunctions and the number of determinants for each possible number of open shells with the current spin state. This table is used to count the total number of spineigenfunctions and the total number of determinants in the final configuration list, data which are passed to the CI program. The CIGEN program was modified to determine the maximum number of open shells in the final configuration list. This number may be smaller than the override value provided by the user. The minimal value is passed to the CI program so that it can quickly assess whether sufficient energy expression data are available for this computation and so that only the minimal amount of energy expression information need be stored.

I wrote a new program HAMILTON to generate the energy expression information needed by the CI program. These data had previously been generated manually for up to six open-shell electrons and stored in the CI program. For more than six open shells, the energy expression data rapidly become too complex to generate manually and soon become too lengthy even to store in the CI program. The energy expression information generated by HAMILTON is stored in a binary data file which can be read by the new CI program, a program with no restrictions on the number of open shells. The new CI program reads only the information

pertaining to the current spin state and maximum number of open shells, leaving maximal space for storage of integrals, etc. The HAMILTON program will generate a data file containing just the information for the maximal number of open shells specified for each spin. The program should be run once at each new installation to produce a permanent data file containing sufficent information for general use. The program can also be run to produce a very large temporary data file for a specific case which exceeds the limitations of the permanent file.

The program HAMILTON actually constructs Young Tableaux. These tableaux are used to set up small pointer arrays needed by the CI program and also to generate U matrices for the elementary transpositions. The U matrices for non-elementary transpositions are generated by matrix multiplication. The U matrix for each transposition is symmetric, so only the unique half of the matrix is generated and stored. The U matrices are conveniently generated with the pair of spineigenfunctions as the most rapidly varying index. However, a CI matrix element between a pair of spineigenfunctions is most efficiently calculated from U matrices in which the transposition is the most rapidly varying index. The U matrices are transformed into the desired form as they are written to the data file. These matrices grow rapidly in size with the number of open-shell electrons. They are stored as a two-byte integer array of indices pointing to an eight-byte real array containing only the unique elements of the U matrices. Unique elements for smaller numbers of open shells with the same spin are generated first, so the CI program needs to read only the first part of this array, and the file does not contain duplicate information for smaller numbers of open shells.

The program HAMILTON constructs spineigenfunctions as a linear

combination of determinants. These spineigenfunctions are generated in a standard order which results from a branching diagram. The determinants are also generated in a specific order so that the $\alpha-\beta$ symmetry of the singlet determinants can be utilized in the CI program. The determinants are generated with α's and β's stored as "on" and "off" bits in four-byte integers. The current algorithm for generating these determinants in desired order uses a loop structure which must be extended to increase the number of β-spins in a determinant. This loop structure can be easily extended for more β-spins. Besides this section of code, HAMILTON can be made to handle larger cases by simply increasing array dimensions.

The phases of the spineigenfunctions generated by raising and lowering operators are made consistent with the U matrices by multiplying each spineigenfunction by the parity of the permutation which takes this tableau into the GF tableau. The spineigenfunctions were generated as an expansion of determinants each containing the product of spatial orbitals in standard order times a different spin function. We desire the spineigenfunctions as an expansion of determinants each having the same spin function, the product of all α's times the product of all β's, with the product of α spatial orbitals and the product of β spatial orbitals each in standard order. The parity of the permutation which takes each determinant into the desired form is multiplied by the expansion coefficient for this determinant in each spineigenfunction. A list of determinants as an ordered product of α orbitals times an ordered product of β orbitals and the corresponding expansion coefficients for the spineigenfunctions are written to the data file. A single array contains the list of determinants for a given spin, with the determinants for smaller numbers of

open shells first. A single array contains the expansion coefficients for the determinants of a given spin, again with the smaller numbers of open shells appearing first. Thus, the CI program needs to read and store only the first part of each of these arrays.

I modified CITWO, the CI program written by Frank W. Bobrowicz, to handle any spin state with any number of open shells. The program had been restricted to a maximum of six open shells, with the energy expression information for all spin states with up to six open shells stored in the program. All arrays which could change with a different spin state and number of open shells were changed from fixed to variable length, and the information to fill these arrays was no longer stored in the program but read from a data file. Thus, the new CI program has absolutely no restrictions regarding the spin state or number of open-shell electrons.

Appendix B. MCSCF with Energy Expressions

I wrote a new program ENERGEN to generate the energy expression for a general CI wavefunction. This program is patterned after the new CI program, so it has no restrictions regarding the spin state or number of open-shell electrons. The CI wavefunction is defined by a configuration list generated by the program CIGEN. Energy expression information is read from the data file generated by the program HAMILTON, the same data file read by the new CI program. The energy expression for the CI wavefunction is generated in symbolic form, valid for any set of orthonormal orbitals and for any normalized CI vector. The starting guess for the CI vector is obtained from an output file generated by the CI program. Both the symbolic energy expression and the starting guess for the CI vector are written to a data file to be read by GVB3.

GVB3 is a generalized MCSCF program written by Larry G. Yaffe. Major modifications have been made by Ray Bair. Since I was the first person to use this program for really complicated wavefunctions, I encountered several errors and had to make corrections myself. The first step in wavefunction optimization is to rotate the orbitals based on the current CI vector, so a reasonable starting guess for the CI vector must be given to GVB3. The second step is to optimize the CI vector based on the current set of orbitals. These two steps are repeated until the energy of the wavefunction converges.

GVB3 calculates the energy terms arising from the core orbitals and GVB pairs. When I wrote ENERGEN, GVB3 could not properly calculate these terms if the CI included single excitations. I decided the effort to include single-excitation matrix elements in ENERGEN was not justified. I have since modified GVB3 to properly calculate these terms

with the core orbitals and GVB pairs when the CI includes single excitations. Single-excitation matrix elements were not then included in ENERGEN, because a new procedure utilizing density matrices rather than symbolic energy expressions was found to be more efficient for large wavefunctions. MCSCF wavefunctions with single excitations can be optimized with this new density-matrix procedure.

Appendix C. MCSCF with Density Matrices

This appendix describes the second generation of programs I have developed to optimize wavefunctions having optimal spin coupling for any number of electrons. In practice, the first-generation programs quickly run out of space to store the massive quantity of energy expression information needed for larger numbers of open-shell electrons. The U matrices are the first data to become too large. This occurs when the number of unique elements exceeds $2^{15}-1 = 32767$, the largest integer which can be stored in the two-byte index array. Since U matrices are not essential to calculating CI matrix elements, but rather are used to calculate CI matrix elements more efficiently, I decided to include U matrices only for a smaller number of open shells than the maximum for which the essential information must be calculated. Of this essential information, the largest data are the expansion coefficients for the determinants which yield the spineigenfunctions. These coefficients are generated as integers by spin raising and lowering operators, so I decided to store the coefficients as two-byte integers rather than eight-byte reals. This results in a significant reduction in the length of the energy expression information.

I modified HAMILTON to generate a data file containing all essential information for the maximal number of open shells specified for each spin but containing U matrices for a possibly smaller maximal number of open shells which can be specified for each spin. The determinant-spineigenfunction transformation coefficients are stored as integers, along with a normalization factor for each spineigenfunction. The permanent data file I have set up for general use contains all the information to calculate twelve open shells for any spin but contains U matrices only

for a maximum of eight open shells. A data file to exceed these limitations for a specific case can easily be generated.

I modified the new CI program to calculate CI matrix elements with U matrices when possible but to use determinant expansions when the U matrices are not available. For this, I had to write a new section of the subroutine SEFDET to calculate diagonal matrix elements. Other changes were required because the expansion coefficients are stored as integers. Because of the changes in the data file generated by HAMILTON, the first-generation programs HAMILTON, CI, and ENERGEN are incompatible with the second-generation programs.

I wrote a new program DENSITY to generate the one- and two-electron density matrices for a general CI wavefunction. This program is patterned after the second-generation CI program. The CI wavefunction is defined by a configuration list generated by the program CIGEN. Energy expression information is read from a second-generation HAMILTON file. A CI vector is read from an output file generated by the CI program. The one- and two-electron density matrices that are generated for this CI vector are valid for any set of orthonormal orbitals. These density matrices are written to a data file to be read by GVB3.

The first step in optimizing an MCSCF wavefunction with density matrices is to optimize a CI vector for the current set of orbitals. The second step is to generate the density matrices for this CI vector. The third step is to optimize the orbitals for this CI vector. These three steps are repeated until the energy of the wavefunction converges. Currently, these steps are performed with separate programs. The last step of orbital optimization is performed with GVB3. This program has no knowledge of the CI expansion. It optimizes the orbitals with density matrices. The

density matrices for a CI vector are typically very small compared with the corresponding symbolic energy expression. My experience has been that symbolic energy expressions too large to store can correspond to density matrices containing only a few hundred elements. Without this density-matrix approach, I could not have performed the calculations in this thesis.

Appendix D. Spin Coupling Analysis

In order to calculate accurate wavefunctions for molecules, it is necessary to use a wavefunction written in terms of orthogonal configurations comprised of orthogonal one-electron orbitals. This greatly obscures interpretation of the wavefunction. For many wavefunctions, this difficulty is obviated by using GVB-PP orbitals which can be used to interpret the GVB-RCI wavefunction in terms of VB orbital ideas. However, this approach does *not* provide spin coupling information required to describe magnetic couplings and bonding in transition metal systems. To solve this problem, I wrote a new program SPINANAL based on the second-generation program DENSITY to perform spin analyses on CI wavefunctions.

Because of the Pauli principle, the spin coupling in the wavefunction is directly related to the permutational symmetry for the spatial coordinates of the wavefunction. By Pauli's principle, the expectation value for a permutation of spin coordinates equals the expectation value for the permutation of spatial coordinates times the parity of the permutation. Since each spatial configuration of the CI wavefunction differs in the occupation of at least one orbital and since these orbitals are orthogonal, no permutation of the spatial coordinates can connect *different* spatial configurations. Thus, this program need calculate only the contributions to the one- and two-electron density matrices involving different spin eigenfunctions of the same spatial configuration.

The program SPINANAL allows the user to partition the wavefunction into subsets of orbitals for each of which several properties are evaluated:

(1) The first property is the number of electrons in the subset. This is just the sum of diagonal one-electron densities, $\langle N \rangle = \sum_i D_i^i$.

(2) The second property is the expectation value for the number of two-body interactions. This is the sum of Coulomb densities, $\langle N(N-1)/2 \rangle = \sum_{i>j} D_{ij}^{ij}$.

(3) The third property is the expectation value for the sum of all spatial transpositions. This is the sum of exchange densities, $\langle \sum_{i>j} \hat{\tau}_{ij} \rangle = \sum_{i>j} D_{ji}^{ij}$.

(4) The fourth property is the expectation value for $\hat{S}^2$ (within the subset), $\langle \hat{S}^2 \rangle$, which is related to the first three properties as follows:

$$\begin{aligned}
\langle \Phi | \sum_{i>j} \hat{\tau}_{ij} | \Phi \rangle &= \langle \chi | \sum_{i>j} -\hat{\tau}_{ij} | \chi \rangle \\
&= \langle \chi | \sum_{i>j} (-\tfrac{1}{2} - 2\hat{s}_i \cdot \hat{s}_j) | \chi \rangle \\
&= \langle \chi | \sum_{i>j} (-\tfrac{1}{2}) + \sum_i (\hat{s}_i^2) - \hat{S}^2 | \chi \rangle \\
&= -\tfrac{1}{2} \langle N(N-1)/2 \rangle + \tfrac{3}{4} \langle N \rangle - \langle \hat{S}^2 \rangle
\end{aligned}$$

Thus, the expectation value for $\hat{S}^2$ is 3/4 the sum of diagonal one-electron densities -1/2 the sum of Coulomb densities minus the sum of exchange densities.

Note that the exchange density matrix element D_{ji}^{ij} where $i \neq j$ affects the contribution of the exchange integral K_{ij} to the energy, but such exchange densities must not be included in the sum of exchange densities used to calculate the third property. The unwanted exchange densities may be eliminated by excluding any contributions arising between different spatial configurations.

When an orbital subset contains two electrons, the third property is the bond coupling $U_{\tau_{ij}}$ for this pair of electrons (the expectation value for transposing their spatial coordinates). In general, the third property can be used to obtain the sum of $U_{\tau_{ij}}$'s within and between orbital sets.

Appendix E. Restricted Spin Coupling

This appendix describes the Ni_4 MCSCF wavefunctions in which the *s* electrons are coupled rigorously singlet. Our wavefunctions can ultimately be expanded as a linear combination of Slater determinants. However, the linear degrees of freedom in our calculations are for spin-eigenfunctions (linear combinations of Slater determinants). We use standard spin-eigenfunctions which result from a branching diagram. Consequently, for any standard spin-eigenfunction, the first *N* electrons are coupled into a standard spin-eigenfunction. We wish to use only spin-eigenfunctions which have the *s* orbitals coupled singlet. We place the *s* orbitals before the *d* orbitals so that we can determine precisely how the *s* orbitals are coupled in any spin-eigenfunction. For a given occupation of spatial orbitals, let us now determine which spin-eigenfunctions we shall keep. If there are no singly-occupied *s* orbitals, then we shall keep all of them.

Consider now the case of two singly-occupied *s* orbitals. We shall keep the standard spin-eigenfunctions which couple the first two electrons singlet. Take the total spin to be singlet. For no singly-occupied *d*'s, we keep the one spin-eigenfunction. For two singly-occupied *d*'s, we keep only the 1st of the two. For four singly-occupied *d*'s, we keep only the 1st and 3rd of the five spin-eigenfunctions. Now take the total spin to be triplet. For no singly-occupied *d*'s, we omit the one spin-eigenfunction. For two singly-occupied *d*'s, we keep only the 1st of the three. For four singly-occupied *d*'s, we keep only the 1st, 3rd, and 6th of the nine spin-eigenfunctions. Now take the total spin to be quintet. For two singly-occupied *d*'s, we omit the one spin-eigenfunction. For four singly-occupied *d*'s, we keep only the 1st of the five spin-eigenfunctions.

Consider now the case of four singly-occupied s orbitals. We shall keep the standard spin-eigenfunctions which couple the first four electrons singlet. Take the total spin to be singlet. For no singly-occupied d's, we keep both of the two spin-eigenfunctions. For two singly-occupied d's, we keep only the 1st and 2nd of the five. For four singly-occupied d's, we keep only the 1st, 2nd, 6th, and 7th of the 14 spin-eigenfunctions. Now take the total spin to be triplet. For no singly-occupied d's, we omit all three spin-eigenfunctions. For two singly-occupied d's, we keep only the 1st and 2nd of the nine. For four singly-occupied d's, we keep only the 1st, 2nd, 6th, 7th, 15th, and 16th of the 28 spin-eigenfunctions. Now take the total spin to be quintet. For no singly-occupied d's, we omit the one spin-eigenfunction. For two singly-occupied d's, we omit all five spin-eigenfunctions. For four singly-occupied d's, we keep only the 1st and 2nd of the 20 spin-eigenfunctions.

Appendix I. New Tableau Convention

The standard Young tableau offer a compelling, simple description for two sets of multiplet orbitals coupled low-spin or high-spin. However, any intermediate coupling is awkward to represent, as it requires a linear combination of several tableaux. For example, a single tableau can represent two triplets

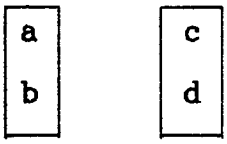

coupled to low-spin (S=0)

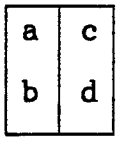

or to high-spin (S=2).

However, the intermediate-spin (S=1) coupling requires the linear combination of two tableaux:

$$\sqrt{\tfrac{2}{3}}$$

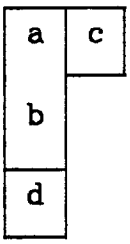

$$+ \quad \sqrt{\tfrac{1}{3}}$$

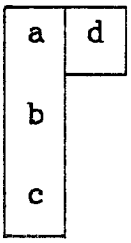

We desire a single diagram to represent this coupling. We want this symbol to have orbitals c and d in the same column to explicitly denote their high-spin coupling, and we want this symbol to accurately represent the total spin for all orbitals. The diagram we have chosen is formally a singlet tableau having blank spaces for "phantom" multiplet electrons:

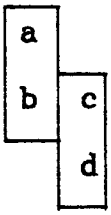

These phantom electrons do not interact with any of our orbitals. They are simply a device to permit a concise representation of our orbital couplings.

Because the phantom electrons are multiplet coupled, our diagram actually represents a linear combination of tableaux in which the phantom electrons are permuted but all orbitals remain in the same positions. To illustrate, we shall assign the phantom electrons spatial coordinates i and j:

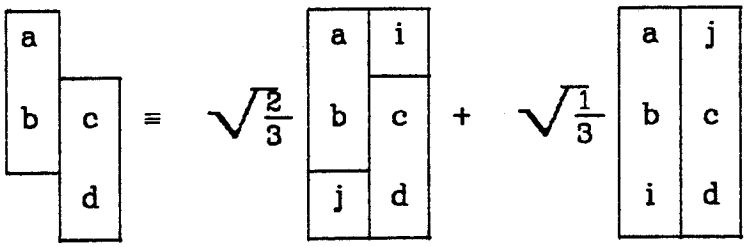

Since the total system including phantom electrons is singlet, the multiplicity of the orbitals equals the multiplicity of the phantom electrons. Hence, the total spin of the orbitals equals half the number of phantom positions.

Our new convention permits a very simple picture of any two tableaux coupled to any allowed total spin. For example, consider the following tableaux:

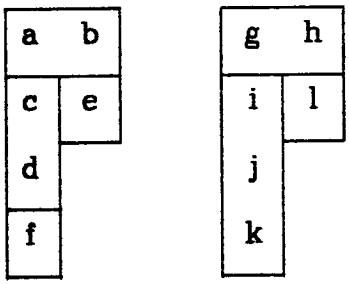

These may be coupled to S=0:

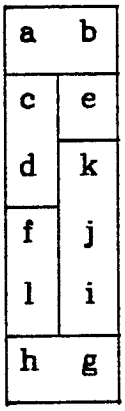

Here we obtain a standard tableau and find that orbitals f and l must be triplet coupled. These tableaux may also be coupled to S=1,

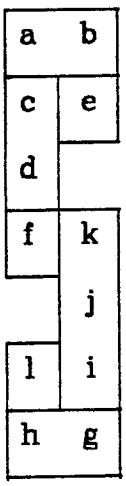

or to S=2.

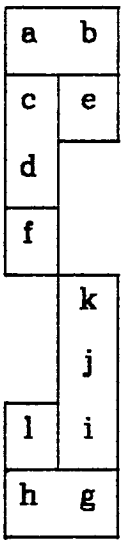

For each of these diagrams, one can evaluate elementary transpositions between the orbitals from top to bottom. Notice that when these diagrams are inverted, they yield precisely the same information. It makes no difference which tableau is written at the top and which is at the bottom. In all cases, the total spin equals half the number of electrons needed to complete a singlet tableau.

Appendix II. Young Tableaux

We interpret our MCSCF wavefunctions as if we have one-electron orbitals, even though our wavefunctions are usually more general than to permit such a simple interpretation. The most general wavefunction with a rigorous one-electron orbital interpretation is the GVB wavefunction. We can represent the permutational symmetry of these orbitals pictorially by placing them in Young tableaux. By Pauli, the spatial and spin permutational symmetries are associate. Thus, we are representing not only the spatial permutational symmetry but also the spin coupling.

We use standard tableaux in this thesis. The orbitals are assigned numerical order, and each Young shape is filled with the orbitals such that the orbital numbers increase to the right in each row and also increase downward in each column. A rectangle is drawn around horizontally or vertically contiguous orbitals. The Pauli principle allows no more than two columns. Two orbitals in a horizontal rectangle are permutationally symmetric, and are singlet coupled. Orbitals in the same vertical rectangle are permutationally antisymmetric and are multiplet coupled. Thus, the rectangles specify the standard tableau and the orbital sequence.

The optimal spin coupling of a GVB wavefunction can be conveniently expressed as a linear combination of standard Young tableaux. These are orthogonal for a specific orbital sequence. However, to obtain a more physical interpretation for some systems, we may choose to use more than one orbital sequence, even though the resulting tableaux may overlap. Note that the orbital sequence for each tableau is specified by the rectangles in that tableau.

Appendix III. U Matrices

$U^{\gamma}_{ij\tau}$ is the ij component of the matrix representing the permutation τ in the γ irreducible representation of the symmetric group. For a GVB wavefunction, we are interested in the permutational symmetry of the one-electron orbitals. This determines the energy of the wavefunction and also specifies the spin coupling. For a GI wavefunction, the matrix element for a permutation τ of the spatial orbitals is

$$\begin{aligned}\langle\tau\rangle &= \langle O^{\gamma}_{ii}\Phi \,|\, \tau \,|\, O^{\gamma}_{ii}\Phi\rangle / \langle O^{\gamma}_{ii}\Phi \,|\, O^{\gamma}_{ii}\Phi\rangle \\ &= U^{\gamma}_{ii\tau}\langle\Phi \,|\, O^{\gamma}_{ii}\Phi\rangle / \langle\Phi \,|\, O^{\gamma}_{ii}\Phi\rangle \\ &= U^{\gamma}_{ii\tau}\end{aligned}$$

Note that we may choose any τ for calculating the energy of this wavefunction, but we must choose $\tau=i$ to calculate a permutation of the spatial orbitals. A ***half*** transformation of the Wigner projection operators is sufficient to calculate the energy of a GVB wavefunction

$$\Psi = \sum_{i=1}^{f^{\gamma}} C_i O^{\gamma}_{ii}\Phi$$

but a ***full*** transformation is required to evaluate the expectation value for a permutation of the spatial orbitals:

$$\Psi = \sum_{i=1}^{f^{\gamma}}\sum_{j=1}^{f^{\gamma}} C_i C_j O^{\gamma}_{ij}\Phi$$

The expectation value for a permutation τ is identical with the U matrix element for that permutation. Because of Pauli's principle, spatial and spin permutational symmetries must be associate:

$$\begin{aligned}\langle\Psi_i \,|\, \tau^{spin} \,|\, \Psi_j\rangle &= \zeta_{\tau}\langle\Psi_j \,|\, \tau^{space} \,|\, \Psi_i\rangle \\ \tilde{U}_{\tau} &= \zeta_{\tau} U_{\tau}\end{aligned}$$

Thus, the expectation value for a permutation of spin coordinates is given by the expectation value for the permutation of spatial coordinates times

the parity of the permutation.

Appendix IV. Bond Couplings

The interaction between two electrons can be bonding or antibonding, depending primarily on the expectation value for transposing the spatial coordinates of the two electrons:

$$\begin{aligned} U_{\tau_{ij}} &= \langle \hat{\tau}_{ij}^{space} \rangle \\ &= -\langle \hat{\tau}_{ij}^{spin} \rangle \\ &= -\tfrac{1}{2} - 2\langle \hat{s}_i \cdot \hat{s}_j \rangle \end{aligned}$$

Symmetric spatial permutational symmetry is bonding, while antisymmetric spatial permutational symmetry is antibonding.

Characteristics of Limiting Values for Bond Couplings				
Interaction	Bond Coupling	$\langle \hat{\tau}_{ij}^{spin} \rangle$	$\langle \hat{s}_i \cdot \hat{s}_j \rangle$	Spin
bonding	+1	-1	$-\frac{3}{4}$	singlet
nonbonding	0	0	$-\frac{1}{4}$	50:50
antibonding	-1	+1	$+\frac{1}{4}$	triplet

To first order in orbital overlaps, the exchange energy between electrons i and j is directly proportional to $U_{\tau_{ij}}$. Thus, the bond energy is approximately the bond coupling ($U_{\tau_{ij}}$) times the coupling constant ($2S_{ij}h_{ij}+K_{ij}$).

Appendix V. Heisenberg Hamiltonian

The energy of a GVB wavefunction is

$$E = \langle\Phi|\hat{H}|O_{ii}^{I}\Phi\rangle / \langle\Phi|O_{ii}^{I}\Phi\rangle$$

where

$$O_{ii}^{I} = \frac{f^{\tau}}{N!}\sum_{\tau} U_{ii\tau}^{I}\tau$$

Including all terms up to first order in orbital overlaps, we obtain the approximate energy as

$$\begin{aligned} E &\approx \langle\Phi|\hat{H}|(U_{\varepsilon}\hat{\varepsilon}+\sum_{i>j}U_{\tau_{ij}}\hat{\tau}_{ij})\Phi\rangle \\ &= \langle\Phi|\hat{H}|\Phi\rangle U_{\varepsilon}+\sum_{i>j}\langle\Phi|\hat{H}|\hat{\tau}_{ij}\Phi\rangle U_{\tau_{ij}} \\ &= E^{Hartree}+\sum_{i>j}J_{ij}\,U_{\tau_{ij}} \end{aligned}$$

where the exchange integral J_{ij} is explicitly $2S_{ij}h_{ij}+K_{ij}$. Using the Pauli principle, $\tilde{U}_{\tau} = \zeta_{\tau}U_{\tau}$, we can write an effective *spin* Hamiltonian to yield the same energy:

$$\hat{H}_{eff} = E^{Hartree}\hat{\varepsilon}-\sum_{i>j}J_{ij}\hat{\tau}_{ij}^{spin}$$

In the space of spin functions,

$$\hat{\tau}_{ij}^{spin} = \tfrac{1}{2}+2\hat{s}_i\cdot\hat{s}_j$$

Making this substitution, we have the *Heisenberg Hamiltonian:*

$$\hat{H}_{eff} = const.-2\sum_{i>j}J_{ij}\hat{s}_i\cdot\hat{s}_j$$

Appendix VI. Heisenberg Coupling

Consider a system of N electrons divided into two weakly interacting high-spin subsystems containing m electrons and n electrons. The total spin S may have values from $|m-n|/2$ to $(m+n)/2$ in unit increments. We seek to evaluate the expectation value for transposing the spatial coordinates of two electrons, one from the m set and the other from the n set. By the Pauli principle, this is equivalent to evaluating the negative of the exchange of the spin coordinates of the two electrons, which is equivalent to the spin operator $-\hat{\tau}_{ij} = -\frac{1}{2}-2\hat{s}_i\cdot\hat{s}_j$. The sum of all exchanges among the $N = m+n$ electrons is

$$\begin{aligned}
\langle\chi(S)|\sum_{i>j}-\hat{\tau}_{ij}|\chi(S)\rangle &= \langle\chi(S)|\sum_{i>j}(-\tfrac{1}{2}-2\hat{s}_i\cdot\hat{s}_j)|\chi(S)\rangle \\
&= \langle\chi(S)|\sum_{i>j}(-\tfrac{1}{2}) + \sum_i(\hat{s}_i^2) - \hat{S}^2|\chi(S)\rangle \\
&= -\tfrac{1}{2}N(N-1)/2 + \tfrac{3}{4}N - S(S+1) \\
&= -N(N-4)/4 - S(S+1)
\end{aligned}$$

The expectation value for transposing the spatial coordinates of two electrons in the same set is -1, while the expectation value for exchanging any one of the m electrons with any one of the n electrons has the same value U for a given total spin S. The sum of all exchanges is

$$(-1)[m(m-1)/2 + n(n-1)/2] + U(S)[mn]$$

Equating the two expressions for the sum of all exchanges leads to

$$U(S) = \frac{1}{mn}[-S(S+1) + \tfrac{1}{2}(m+n) + \tfrac{1}{4}(m-n)^2]$$

Thus, the exchange coupling between two sets of high-spin electrons is a simple function of the total spin S.

We have seen that to first order in orbital overlaps, the energy of a system of electrons is

$$E = E^{Hartree} + \sum_{i>j} J_{ij} U_{\tau_{ij}}$$

where the exchange integral J_{ij} is $2S_{ij}h_{ij}+K_{ij}$. For our system of two high-spin sets of electrons, the spin-dependent contribution to the energy is

$$E(S) = \sum_{i=1}^{m} \sum_{j=1}^{n} J_{ij} U(S)$$

Substituting our value for $U(S)$, we find that the spin-dependent energy is

$$E(S) = -S(S+1)[\frac{1}{mn} \sum_{i=1}^{m} \sum_{j=1}^{n} J_{ij}]$$

Comparison with the equation for a Heisenberg spectrum of states

$$E = const. \; -JS(S+1)$$

shows that the Heisenberg coupling constant J is simply the average of all mn exchange integrals J_{ij}. Thus, J is explicitly

$$J = \frac{1}{mn} \sum_{i=1}^{m} \sum_{j=1}^{n} (2S_{ij}h_{ij} + K_{ij})$$

Appendix VII. Comparison of Projection Operators

We shall compare possible projection operators for use in our approximate method. Consider the homonuclear two-electron bond. We shall consider all two-electron wavefunctions described with an atomic orbital l on the left and an atomic orbital r on the right. The covalent wavefunctions are

$$\Psi_g^{cov} = \frac{lr + rl}{\sqrt{2(1+\bar{S}^2)}}$$
$$\Psi_u^{cov} = \frac{lr - rl}{\sqrt{2(1-\bar{S}^2)}}$$

and the ionic wavefunctions are

$$\Psi_g^{ion} = \frac{ll + rr}{\sqrt{2(1+\bar{S}^2)}}$$
$$\Psi_u^{ion} = \frac{ll - rr}{\sqrt{2(1-\bar{S}^2)}}$$

The two gerade wavefunctions can mix to yield the optimum ground state. The two ungerade wavefunctions cannot mix, since Ψ_u^{cov} is triplet and Ψ_u^{ion} is singlet. The ideal projection operator for correcting the energy of the ionic wavefunctions is

$$C[|\Psi_g^{ion}\rangle\langle\Psi_g^{ion}| + |\Psi_u^{ion}\rangle\langle\Psi_u^{ion}|]$$

This would correct the energy of each ionic wavefunction by C. The energy of the triplet covalent wavefunction would be unaffected, and the energy of the singlet covalent wavefunction would be corrected by $\langle\Psi_g^{cov}|\Psi_g^{ion}\rangle^2 C$. The maximal correction for a mixture of the two gerade wavefunctions is simply C, which is obtained when the mixture has unit overlap with Ψ_g^{ion}.

We desire a projection method which will allow us to modify two-electron integrals prior to optimizing the wavefunction. The integrals J_u

and J_{rr} are each corrected by C. The integrals $(lr\,|\,rr)$ and $(ll\,|\,lr)$ are each corrected by SC. The integral J_{lr} is corrected by $\frac{2S^2}{1+S^2}C$. The integral K_{lr} is corrected by S^2C when evaluated in ionic form $\langle l(1)l(2)\,|\,r(1)r(2)\rangle$ but is corrected by $\frac{2S^2}{1+S^2}C$ when evaluated in covalent form $\langle l(1)r(2)\,|\,r(1)l(2)\rangle$. Since we must choose only one correction for K_{lr}, this ideal projection cannot be performed by modifying the *unique* two-electron integrals.

We have explored a projection operator which is conceptually appealing and can be performed by modifying the *unique* two-electron integrals:

$$C[\,|ll\rangle\langle ll\,| + |rr\rangle\langle rr\,|\,]$$

The integrals J_{ll} and J_{rr} are each corrected by $(1+S^4)C$. The integrals $(lr\,|\,rr)$ and $(ll\,|\,lr)$ are each corrected by $S(1+S^2)C$. The integral J_{lr} is corrected by $2S^2C$. The integral K_{lr} is corrected by $2S^2C$ when evaluated in either ionic or covalent form. Unfortunately, this operator leads to overcorrections for some of the wavefunctions. The energy of Ψ_u^{ion} is corrected by $(1-S^2)C$, which is an undercorrection. However, the energy of Ψ_g^{ion} is corrected by $(1+S^2)C$, which is an overcorrection. The energy of the triplet Ψ_u^{cov} is properly unaffected. The energy of Ψ_g^{cov} is corrected by $\frac{4S^2}{1+S^2}C$. This is an overcorrection, since for $S>.577=1/\sqrt{3}$, the correction is larger than C.

We have settled on a projection operator which has the same conceptual appeal as the previously considered operator, can be performed by modifying the *unique* two-electron integrals, and cannot lead to an overcorrection:

$$C[\,|\overline{ll}\rangle\langle\overline{ll}\,| + |\overline{rr}\rangle\langle\overline{rr}\,|\,]$$

The orbitals $\bar{l}$ and $\bar{r}$ are symmetrically orthogonalized:

$$\bar{l} = \frac{l - \lambda r}{\sqrt{1 - 2S\lambda + \lambda^2}}$$

and

$$\bar{r} = \frac{r - \lambda l}{\sqrt{1 - 2S\lambda + \lambda^2}}$$

where

$$\lambda = \frac{1 - \sqrt{1 - S^2}}{S}$$

The energy of Ψ_u^{ion} is corrected by C, the ideal value. The energy of Ψ_g^{ion} is corrected by $\frac{C}{1+S^2}$, which is less than the ideal value. The energy of the triplet Ψ_u^{cov} is properly unaffected. The energy of Ψ_g^{cov} is corrected by $\frac{S^2}{1+S^2}C$, which is less than the ideal value. The maximal correction for a mixture of the two gerade wavefunctions is C. We symmetrically orthogonalize the ionic and covalent gerade wavefunctions to obtain

$$\bar{\Psi}_g^{ion} = (\bar{l}\bar{l} + \bar{r}\bar{r})/\sqrt{2}$$
$$\alpha\ (\Psi_g^{ion} - S\Psi_g^{cov})$$

and

$$\bar{\Psi}_g^{cov} = (\bar{l}\bar{r} + \bar{r}\bar{l})/\sqrt{2}$$
$$\alpha\ (\Psi_g^{cov} - S\Psi_g^{ion})$$

The purely ionic space is given the full ionic correction of C, and the purely covalent space is given zero correction. This projection operator is equivalent to

$$C[|\bar{\Psi}_g^{ion}\rangle\langle\bar{\Psi}_g^{ion}| + |\Psi_u^{ion}\rangle\langle\Psi_u^{ion}|]$$

Compared with the "ideal" projection operator, this operator chooses an alternative orthogonalization of the overlapping ionic and covalent gerade

spaces. Symmetric orthogonalization is special in that the projection can be applied to the unique two-electron integrals.

We shall now compare the three projection operators we have considered.

Energy Corrections from Projection Operators

Wavefunction	$\Psi_g^{ion}, \Psi_u^{ion}$	$ll, \pi\pi$	$\overline{ll}, \overline{\pi\pi}$
Ψ_u^{cov}	0	0	0
Ψ_u^{ion}	C	$(1-S^2)C$	C
Ψ_g^{ion}	C	$(1+S^2)C$	$\frac{1}{1+S^2}C$
Ψ_g^{cov}	$\frac{4S^2}{(1+S^2)^2}C$	$\frac{4S^2}{1+S^2}C$	$\frac{S^2}{1+S^2}C$